Final Technical Report for NNX16AL31G Title:

“*Further Development Of Aperture: A Precise Extremely Large Reflective Telescope Using Re-Configurable Elements*”

PI Prof. Melville P. Ulmer, Northwestern University

Co-Is: Prof. Victoria Coverstone, Initially at UIUC, now at Univ. of Miami
Profs. Jain Cao and Yip-Wah Chung of Northwestern University

Collaborators: Drs. Ron Shiri (GSFC), David Pappas, C Steve Arnold NIST, Marco Quadrelli JPL, and Ms. Marie-Caroline Corbineau initallay at UIUC, now at CVN, CentraleSupe′lec, INRIA, Universite′ Paris-Saclay

The summary and conclusions report below was prepared primarily by the PI with significant input from Dr. Dr. Turgut Batuhan Baturalp of Texas Tech University.

Summary and Conclusions

1. Original Proposal Summary

One of the pressing needs for space ultraviolet-visible astronomy is a design to allow larger mirrors than the James Webb Space Telescope primary. The diameter of the rocket fairing limits the mirror diameter such that all future missions calling for mirrors up to 16 m in diameter or larger will require a mirror that is deployed post-launch. In response to the deployment requirement, we address the issues of this concept called "A Precise Extremely Large Reflective Telescope Using Reconfigurable Elements (APERTURE) with both hardware experiments and software simulations. APERTURE will use a deployable membrane-like mirror. The mirror figure will be corrected after deployment to bring it into better or equal lambda/20 deviations from the prescribed mirror shape, where lambda (typically 400 nm-1 micron) is the operational wavelength. Instead of using the classical piezoelectric-patch technology, our concept is based on a continuous coating of a Magnetic Smart Material (MSM). We expect that the initially deployed mirror will not have a perfect figure. Thus, our design uses magnetic write head(s) to produce stress in the MSM and improve the figure, post-deployment. This Phase II NIAC proposal is to address two of the tall poles in the concept: (a) Can corrections on a large size be made and retained for a long enough time (> 1 week); (b) Can deployment be done in such a way that the figure corrections are small enough to be correctable via the MSM plus magnetic field, and at the same time, the in-plane [mounting] stresses are small enough to allow the stresses (resulting from the magnetic field injected into the MSM) to make the necessary corrections. Tall pole “a” will be primarily the responsibility of Northwestern University (NU) and “b” of University of Illinois Urbana-Champaign. NU will carry out overall scientific leadership and will coordinate and solicit input from GSFC, JPL, and NIST.

2. Summary of Work

We designed and built several fixtures with O-rings to hold a membrane. We established a coating process to make a membrane that was coated on one side with Cr and the other side with Cr-Terfenol-D-NiCo. The Terfenol-D (T-D hereafter is the MSM we use). We bought and established a procedure for measuring a deformation over time and purchased a Shack Hartmann system from Imagine Optic (https://www.imagine-optic.com). The first substrate we used was DuPont™ Kapton® polyimide film. Due to material creep, we found the stability over a 48-hour period with a Kapton substrate was not a good a desired (> 1 μm). We then switched to CP1 Polyimide. We found the CP1 much more stable to creep, being stable from about 3 hours to 48 hours to within a measurement error to below ~0.1 μm.

We produced a 13 μm maximum deviation on a 50 mm diameter piece of CP1 (25 μm thick). The T-D coating was about 2 μm, and the other layers, about 10 nm. The magnetic field at the base was about 0.1T. We can make the T-D film at least 5 times thicker and the magnetic field at least 5 times stronger, and hence make deformations as much as 25 times larger.

We have a formed a collaboration produced at the NIAC mid-term review with Dr. Ron Shiri of Goddard Space Flight Center (GSFC) to explore making controlled deviations on lambda/14-lambda/20 scales which are required to bring a surface to the diffraction limit. We carried out only preliminary work on Si using a Coordinate Measuring Machine (CMM), which produced deviations on the 1 μm level. We are still working on a program to bring to GSFC a flat enough (radius of curvature > 10 m) coated a Si piece with Cr, T-D, NiCo. Then we plan to carry out tests with an interferometer.

Further, we formed a new collaboration with Prof. Rajan Vaidyanathan of the University of Central Florida to replace the CP1 with a shape memory alloy (SMA). With his collaboration, we acquired new Federal funding outside of NASA to explore the use of SMAs (we use NiTi). Our preliminary results indicate that we can produce deformations > 1 μm on ~100 μm thick. Furthermore we have shown that the NiTi can deploy to better than 1 μm of its set original and then trained shape.

Conclusions

Our tentative conclusions are for CP1-like materials a 200 μm deformation is possible, and is that if we can apply a mirror finish to the NiTi, that this technology could supplant using CP1 or similar substrates for SmalSats/CubeSats. For 16m and larger satellites, however, CP1-like materials remain attractive.

A few (but not complete list of) outstanding lines of investigation are: (a) how to improve a mirror figure, not just changing it; (b) how to deploy the membrane to the best possible figure; (c) how to design and then test a robotic arm with a movable electromagnet.

Below we list citations of the work we have published based on the Kapton, CP1, and Si substrates. Then below the bibliographic listing we provide the papers themselves.

REFERENCES FOR EACH PAPER Published From this Project

Paper 1. M. P. Ulmer, R. Coppejans, M. A. Khreishi, K. Keely, D. B. Buchholz, R. Shiri, L. A. Rodriguez, A. E. O'Donnell, Z. J. Schonfeld, W. H. Reinhardt, L. E. Borgsmiller, T. B. Baturalp, V. L. Coverstone, J. Cao, "**Magnetostrictively deforming the surface of a silicon wafer at two locations**," Proc. SPIE 10761, Adaptive X-Ray Optics V, 107610B (18 September 2018); doi: 10.1117/12.2322511

Event: SPIE Optical Engineering + Applications, 2018, San Diego, California,
SPIE United States

Paper 2. Turgut B. Baturalp, Victoria L. Coverstone, Rocco Coppejans, Jian Cao, YipWah Chung, David B. Buchholz, M. P. Ulmer, "**Membrane mirror evaluation of APERTURE: a precise extremely large reflective telescope using re-configurable elements,**" Proc. SPIE 10698, Space Telescopes and Instrumentation 2018: Optical, Infrared, and Millimeter Wave, 106981K (6 July 2018); doi: 10.1117/12.2309826

Event: SPIE Astronomical Telescopes + Instrumentation, 2018, Austin, Texas,
SPIE United States

Paper 3 R. Coppejans, M. P. Ulmer, D. B. Buchholz, X. Wang, J. Cao, V. L. Coverstone, T. B. Baturalp, K. S. Condron, A. E. O'Donnell, B. E. Harpt, W. H. Reinhardt, M. E. Johnson, "**APERTURE, a precise extremely-large reflective telescope using re-configurable element: a progress report,**" Proc. SPIE 10398, UV/Optical/IR Space Telescopes and Instruments: Innovative Technologies and Concepts VIII, 103980N (5 September 2017); doi: 10.1117/12.2274278
Event: SPIE Optical Engineering + Applications, 2017, San Diego, California,
SPIE United States

Paper 4. Turgut B. Baturalp, Victoria L. Coverstone, Rocco Coppejans, Jian Cao, YipWah Chung, Xiaoli Wang, David B. Buchholz, and Melville P. Ulmer. "**Deployment Design of APERTURE: a precise extremely large reflective telescope using re-configurable elements**", AIAA SPACE and Astronautics Forum and Exposition, AIAA SPACE Forum, (AIAA 2017-5378)

Paper 5. M. P. Ulmer, V. L. Coverstone, J. Cao, Y.-W. Chung, M.-C. Corbineau, A. Case, B. Murchison, C. Lorenz, G. Luo, J. Pekosh, J. Sepulveda, A. Schneider, X. Yan, S. Ye, "APERTURE: a precise extremely large reflective telescope using re-configurable elements," Proc. SPIE 9904, Space Telescopes and Instrumentation 2016: Optical, Infrared, and Millimeter Wave, 99041I (29 July 2016); doi: 10.1117/12.2231679

Copies of the papers follow:

Magnetostrictively deforming the surface of a Silicon wafer at two locations

M. P. Ulmer[a], R. Coppejans[a], M. A. Khreishi[b], K. Keely[b], D. B. Buchholz[c], R. Shiri[b], L. A.
Rodriguez[d], A. E. O'Donnell[e], Z. J. Shonfeld[e], W. H. Reinhardt[f], L. E.
Borgsmiller[g], T. B. Baturalp[h], V. L. Coverstone[d], and J. Cao[e]

[a]Center for Interdisciplinary Exploration and Research in Astrophysics (CIERA)
and
Department of Physics and Astronomy, Northwestern University, 2145 Sheridan Road,
Evanston, IL, 60208, USA
[b]NASA / Goddard Space Flight Center, Optics Branch, 8800 Greenbelt Road, Greenbelt, MD
20770, USA
[c]Materials Research Science and Engineering Center, Northwestern University, Technological
Institute, 2145 Sheridan Rd., K111 Evanston, IL, 60208, USA
[d]Department of Mechanical and Aerospace Engineering, University of Miami, Miami, FL,
33146, USA
[e]Department of Mechanical Engineering, 2145 Sheridan Road, Northwestern University,
Evanston, IL, 60208, USA
[f]Department of Electrical Engineering, 2145 Sheridan Road, Northwestern University,
Evanston, IL, 60208, USA
[g]Department of Materials Science and Engineering, 2220 Campus Drive, Northwestern
University, Evanston, IL 60208
[h]Department of Mechanical Engineering, Texas Tech University, Lubbock, TX, 79409, USA

ABSTRACT

The only way to increase the sensitivity of X-ray telescopes without significantly increasing their size (compared to existing telescopes) is to use thinner mirror shells. However, to maintain the figure of thin mirror shells, their shape will need to be adjusted after they are mounted and/or actively controlled during flight. Here we describe progress toward developing a method that can be used to do both. The core of the concept is to coat thin ($< 500\mu$m) X-ray mirrors with a $\sim 10\mu$m layer of magnetic smart material (MSM). When an external magnetic field is applied to the MSM layer it will expand or contract, changing the shape of the mirror. We have previously demonstrated that this method can be used to generate a single localized deformation on the surface of a test sample. Here we present work to study how two deformations affect each other. The first deformation that we created has a height of $\sim 5\mu$m. The second deformation, generated by applying a magnetic field to the sample 4mm from the first position, has a height of $\sim 1\mu$m. It is likely that the second deformation is smaller than the first because the two areas where the magnetic field was applied were close to each other. This could have caused the MSM to already be partially expanded in the second area when the field was applied there. **Keywords:** X-ray optics, magnetic smart materials, grazing incidence optics, Silicon

1. INTRODUCTION

At the moment there is no technology readiness level (TRL) six or above method to fabricate mirrors for X-ray telescopes that has a significantly larger mirror surface area than, and similar angular resolution, mass and mirror assembly dimensions to the Chandra X-ray Observatory. These requirements have, however, been the baseline for the next flagship X-ray astronomy mission (Lynx[1]). In particular in[2–4] the authors stress the importance of developing methods to manufacture lower-mass per unit area mirrors than those of Chandra. Here we report on progress toward developing a method that has the potential to meet these requirements.

The core of the concept is to use magnetostriction to shape and/or actively control the figure of thin ($< 500\mu$m) X-ray optics. Magnetostriction is the phenomenon whereby a ferro-magnetic material expands or contracts under the influence of an external magnetic field. Materials which have a very large change in dimensions compared to other ferro-magnetic materials when a magnetic field is applied to them are known as magnetic smart materials (MSMs). Our concept is to coat X-ray optics with a MSM. When an external magnetic field is applied to the mirror (by an electromagnet), the MSM will expand or contract. The expansion or contractions applies a local stress to a small area of the mirror, changing the shape of the reflecting surface. The amount by which a MSM expands or contracts is proportional to the field strength. In principle, the shape of the mirror can therefore be controlled by changing the field strength. Most MSMs relax when the external magnetic field is removed. If, however, the mirror is coated with a separate magnetic hard material (that has a relatively large coercivity and remanence), the magnetic hard material will retain a fraction of the external magnetic field after it has been removed. This residual field will prevent the MSM from relaxing, causing the shape change to be retained.

A specific advantage of the concept is that unlike static processes, such as ion-beam stress implantation or stress induced film deposition e.g.[5] the concept allows for both preflight and post-launch corrections. Post-launch correction with electromagnets requires that the mirror nesting design has gaps large enough to accommodate an electromagnet that fits between the mirror shells. While such gaps could decrease the collecting area, the magnetic write heads developed for computers hard drives are only $\sim$ 1mm thick. The necessary gaps can, therefore, be achieved without a significant loss in collecting area. Furthermore, while post-launch corrections and active control of the mirror may not be required for Lynx, post-launch corrections will almost certainly be required for future missions with larger collecting areas and higher angular resolutions, which is necessary to beat the confusion limit.

Further author information: (Send correspondence to M.P.U.)
M.P.U.: E-mail: m-ulmer2@northwestern.edu

Adaptive X-Ray Optics V, edited by Daniele Spiga, Hidekazu Mimura, Proc. of SPIE Vol. 10761, 107610B · © 2018 SPIE · CCC code: 0277-786X/18/$18 · doi: 10.1117/12.2322511

Additional reasons why our concept is intriguing is: (1) The concept does not require wires to be attached to the substrate, and thus, in situ corrections in space will allow a scale up for a next generation mission beyond Lynx; (2) The concept can be applied to both full or partial shells and corrections can be applied to a mirror after mounting; (3) Companies exist that could carry out large scale MSM film deposition via direct current (DC) magnetron sputtering, plus small magnetic write heads and motion stages exist. Hence moving from a proof of concept to realization of a full system is quite feasible; (4) If a surface finish of 0.3nm could be achieved when electroforming a magnetic hard material such as NiCo, electroforming can be used as a full shell substrate which would also hold in the magnetic field. Full shells have the advantage of reducing the number of mirror pieces needed for a full telescope (and the related error budget propagation) by a factor of about 10.

The advantages of our approach over other active control methods such as lead zirconate titanate (PZT) in-plane actuators and micro-electro-mechanical system (MEMS) actuators are: (1) When moving to larger diameters, the number of actuators becomes unfeasibly large. Our concept, however, only requires a few electromagnets, allowing it to be easily scaled up. (2) In our concept the magnetic field that re-shapes the mirror is exerted outside of the mirror. The non-contact application of an external magnetic field avoids the step of depositing the actuators on the backside of the mirror, decreasing the complexity of manufacturing the mirror. (3) Our concept does not require active control, whereas actuators require fixed wires and constant power to prevent them from relaxing. (4) With PZT and MEMs actuators, deformation can only be applied at the location of an actuator. In our concept a deformation can be applied at any position on the mirror. (5) Unlike MEMS actuators, our concept does not suffer from print-through: the effect where depositing the actuators increases the RMS surface error of the mirror. (6) In our concept, the area over which the deformation is created is determined by the area over which the magnetic field is applied. Thus, by changing the design of the poles of the electromagnet, the pixel size of the deformation can be optimized for the specific mission requirements.

Comparing our concept to static process, such as ion-beam stress implantation, stress induced film deposition and polishing monocrystalline Si e.g.[5] and,[6] we already noted that these methods do not allow post-launch corrections, which will be required if telescopes with angular resolutions smaller than 0.1^{00} are desired. These methods also do not allow the mirror to be corrected after it has been mounted in the telescope. Therefore these static processes leave no way of correcting the mirror shape if it is distorted by mounting stress. Polishing monocrystalline Si will also require approximately 20,000 pieces to be polished for Lynx.[7] This is not only very time consuming, but also requires a very complex mounting scheme.[7] In addition, for optics in which the launch loads are not so great as to require post-launch re-shaping, our process does not need any active control after the shape of the mirror has been corrected prior to launch. If it can be advanced to a high enough TRL, our concept therefore has the potential to produce a paradigm shift in the shape control of X-ray mirrors.

In Ref 8 we demonstrated that we can generate a $\sim 1\mu$m deformation which can be retained for as much as 60hours. In this publication we report a test in which we study how two deformations generated close to each other affect each other. In Sections §2 and §3 we describe the sample and methodology. The results of the test are given and discussed in Sections §4 and §5. A summary and conclusion are given in §6.

2. SAMPLE DESCRIPTION

The sample used in the test is composed of four layers: a substrate, an adhesion layer (Cr), a MSM (Terfenol-D) and a magnetic hard material (NiCo). The substrate is a semi-rectangular piece of 100μm thick (100) Si. The long edges are 50mm, while the maximum width is $\sim$ 20mm at the center, decreasing to $\sim$ 10mm at the edges. The latter is because the Si piece was cut from the edge of a larger wafer.

The Cr, Terfenol-D and NiCo layers were deposited onto the Si via DC magnetron sputtering using an AJA ST20 sputtering head. A detailed description of the sputtering system is given in Ref 8. Prior to depositing the Terfenol-D, we deposited a 58nm Cr adhesion layer which bonds the Terfenol-D to the Si. The Terfenol-D layer is 2.2μm thick and was deposited at a bias voltage of -200V and an Ar pressure of 28mTorr (see Ref 8). The Terfenol-D layer was over coated with 65nm NiCo to both prevent oxidation and provide a magnetic hard layer to hold in the magnetic field.

After completing the deposition we measured the composition of the Terfenol-D layer on a 5 × 20mm Si witness sample. The witness sample was placed next to the main sample only during the Terfenol-D deposition. The composition was measured using Wavelength Dispersive Spectroscopy (WDS) with a Hitachi S-3400N-II scanning electron microscope. We found a composition of 71.3 at. % Fe, 7.2 at. % Tb and 21.4 at. % Dy. The sample is therefore 5.3 at. % heavy in Fe, 3.8 at. % light in Tb and 1.6 at. % light in Dy compared to the ideal composition of Terfenol-D.

3. METHODOLOGY

The test was carried out on 26 July, 2018 at the National Aeronautics and Space Administrations (NASA) Goddard Space Flight Center (GSFC) with the Optics Branches Hexagon Leitz PMM-C 700 non-contact Coordinate Configuration Machine (CMM) using a Percitec LSP-S4-LR sensor head. The test setup, shown in Figure 1, consists of four primary components the: CMM, sample, sample holder and an electromagnet. The sample is mounted horizontally and held in place by two aluminum clamps along the two edges of the sample that are parallel to the y-axis. Foam tape was placed on both sides of the clamps. During the experiment a magnetic field is applied to the sample using a custom built electromagnet manufactured by International Electro-Magnetics, Inc. At the magnetic face of the electromagnet, the poles are 10mm apart and 15mm wide. The poles taper upward and inward to a final pole length of 6mm and a 2mm separation. When a 20A current is run through the electromagnet, the field strength initially peaks at $\sim$ 4500G. The peak (likely caused by transient currents) lasts for about two seconds after which the it decreases to a steady state vale of $\sim$ 2500G.

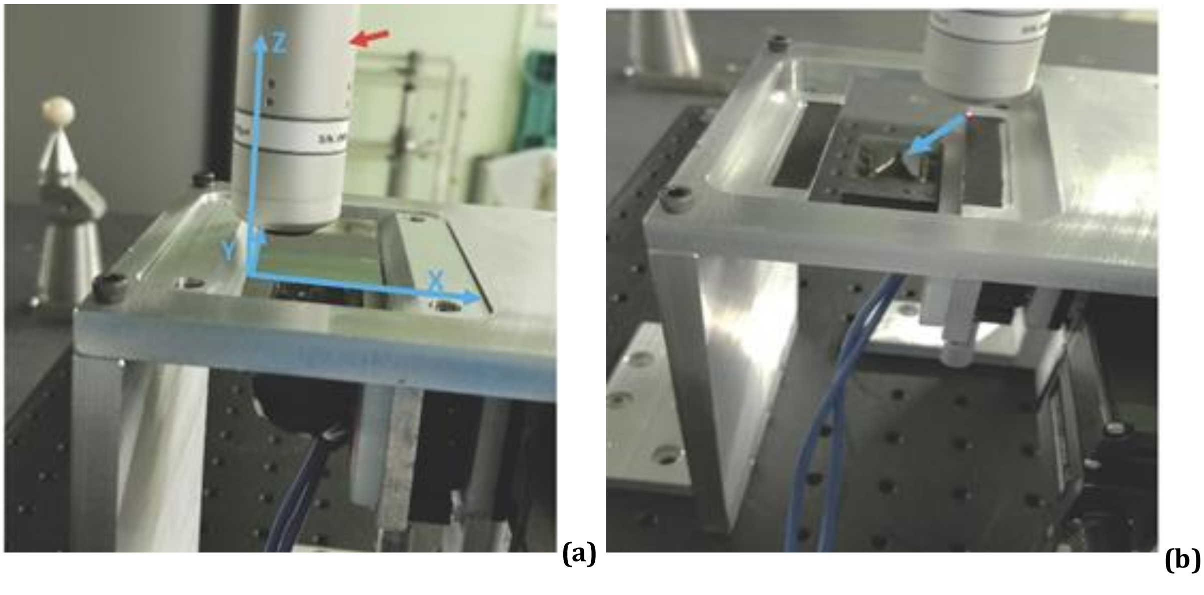

Figure 1. Two images showing the experimental setup. (a) The setup with a sample and clamps in place. Note that the sample is difficult to see because of how reflective it is. The CMM sensor head is indicated by the red arrow. The coordinate system used in the test is also indicated on the image. (b) The setup without a sample and the top parts of the clamps removed. The black foam strips on which the sample rests are visible and the poles of the electromagnet are indicated by a blue arrow.

The CMM took images of the surface of the sample by measuring the height of the sample 90,000 times in a 300 × 300 grid across a 21 × 21mm area. Since we only imaged the central area of the sample, there is ~ 8mm between the edges of the imaged area and where the sample is clamped on either side. The test was done by: (1) Degaussing the sample using a Proton 1100 Degausser Wand. (2) Placing the sample in the holder such that the uncoated side of the silicon is at the top (facing toward the CMM) and the MSM coated side is facing down, toward the electromagnet. (3) Taking an initial (zero) image of the sample, shown in Figure 2 and 3, using the CMM. (4) Applying a magnetic field near the center of the area imaged in the previous step by first raising the poles of the magnets to within ~ 1.5mm of the bottom surface of the sample. Then, using a Volteq Programmable DC Power Supply HY3030EP, a steady state 20A current is then run through the electromagnet for ~ 10s. (5) Taking a second image of the same area of the sample as in step 3. (6) Moving the electromagnet 4mm downward parallel to the y-axis. (7) Applying a magnetic field to the sample at the new position in the same way as in step 4. (8) Taking a third image of the same area of the sample as in steps 3 and 5. (9) Imaging the deformations created by subtracting the image in step 3 from the images in steps 5 (hereafter referred to as the first deformation) and 8 (hereafter referred to as the second deformation).

4. RESULTS

In Figure 3 the initial image is shown. The complex shape of the surface is caused by: (1) The films deposited on the substrate have non-zero stress. The majority of this stress is from the Terfenol-D film, which is more than thirty times as thick as the other two films. (2) The clamps exert a nonuniform stress on the sample, and possibly titling the surface relative to the CMM.

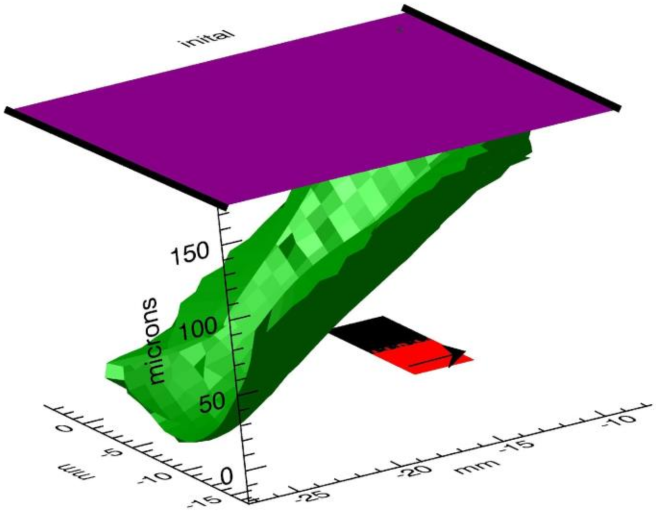

Figure 2. A graphical illustration of the test setup. The area over which the CCM measurement was taken is shown as a purple plane and the initial image of the sample is shown in green. The location where the sample

is clamped is indicated by the black lines at the edges of the purple plane. The approximate locations of the electromagnet is depicted by the black (first position) and red (second position) squares. The arrow in the red square indicates the direction of the magnetic field for both positions.

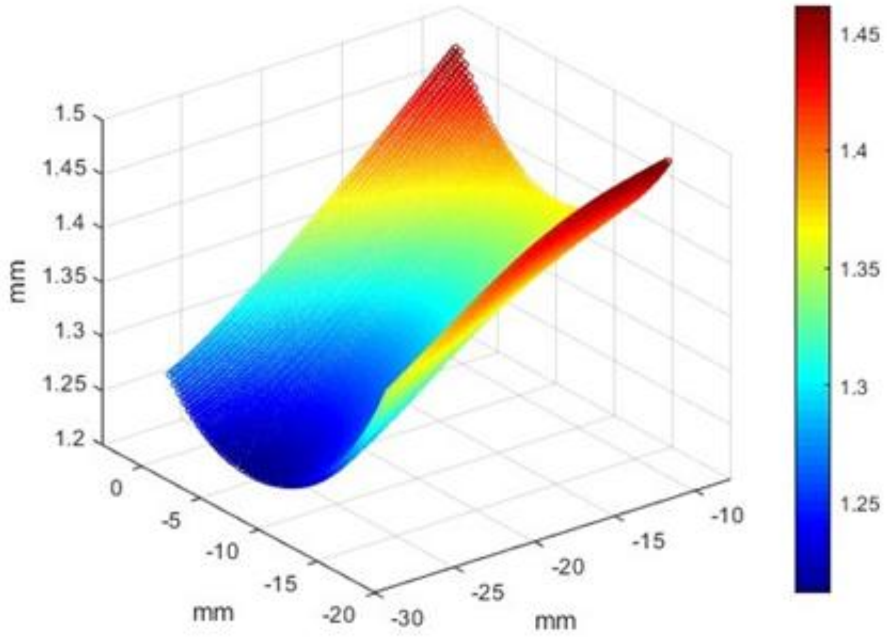

Figure 3. The initial (zero) image.

The right side of the initial image, the image taken after the electromagnet was switched on the first time (the image in step 5 in Section 3) and the image taken after the electromagnet was switched on the second time (the image in step 8 in Section 3) are shown in Figure 4. From these images it can be seen that even without subtracting the initial image from the other two images, the shape of the sample was changed by the magnetic field.

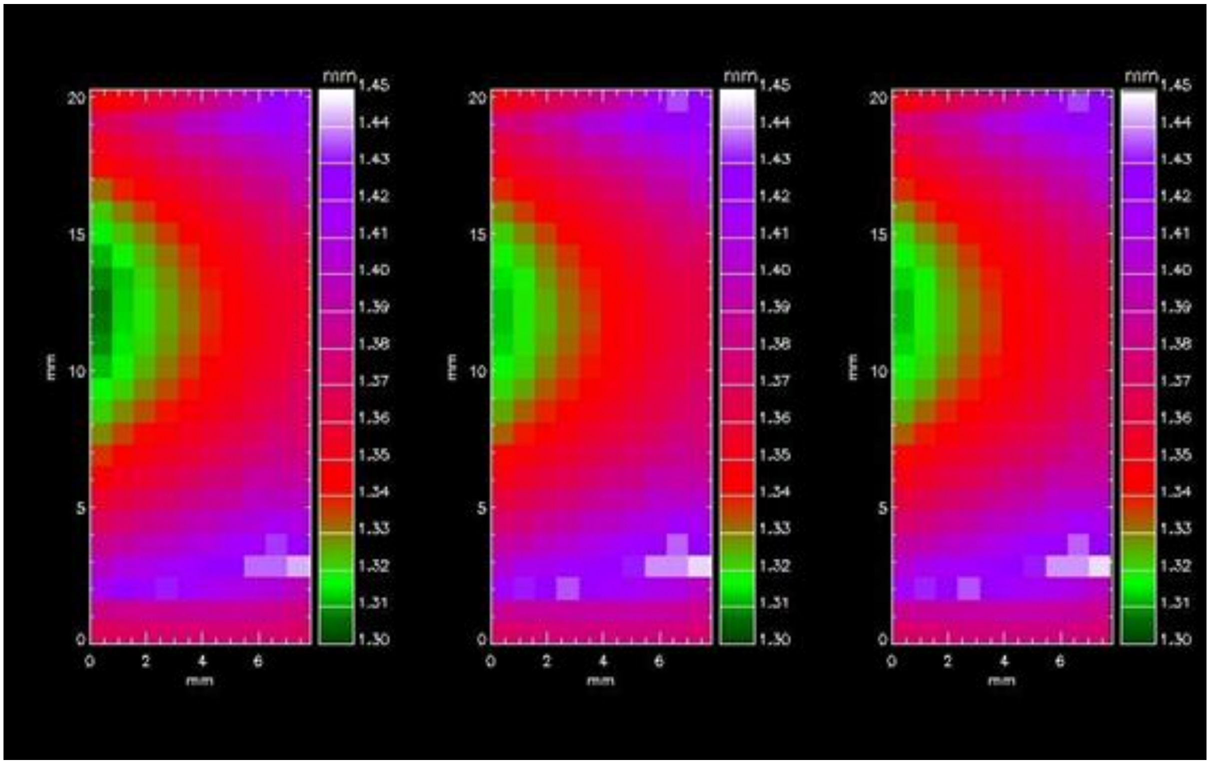

Figure 4. From left to right, the initial image, the image taken after the electromagnet was switched on the first time and the image taken after the electromagnet was switched on the second time. The color bars in all three images have the same range so that the images can be compared directly. Only the right hand portion of the images are shown here for easy of comparison.

The two deformation images are shown in Figure 5. A difference image made by subtracting the two deformations images from each other are also shown in the figure. Based on visual inspection we believe that there is a $\sim 5\mu$m deformation in the first deformation image and that the size of the combined deformation was changed by $\sim 1\mu$m by the second deformation. Since the maximum height change of both deformations are located on or beyond the edge of the images these value are lower limits.

5. DISCUSSION

From Figure 5 (a) it is evident that the first deformation is not located at the center of the image, directly above the electromagnet, as might be expected. We believe that the peak of the deformation was likely shifted away from the center by the non-uniform stress exerted on the sample by the clamps and the sample not being clamped along two of its edges. To address this problem we are currently investigating ways of mounting the sample with uniform stress along all four edges.

Figures 5 (a) and (b) are very similar with only a $\sim 1\mu$m height difference between them (Figure 5 (c)). The electromagnet pole tips are 6mm long and the two places where the field was applied are only separated 4mm in the direction parallel to the long axis of the poles. The difference in height between the deformations may therefore have been caused by the magnetic footprint of the poles being larger than their physical dimension.

This could have caused the Terfenol-D to already be partially expanded in the second area when the field was applied there.

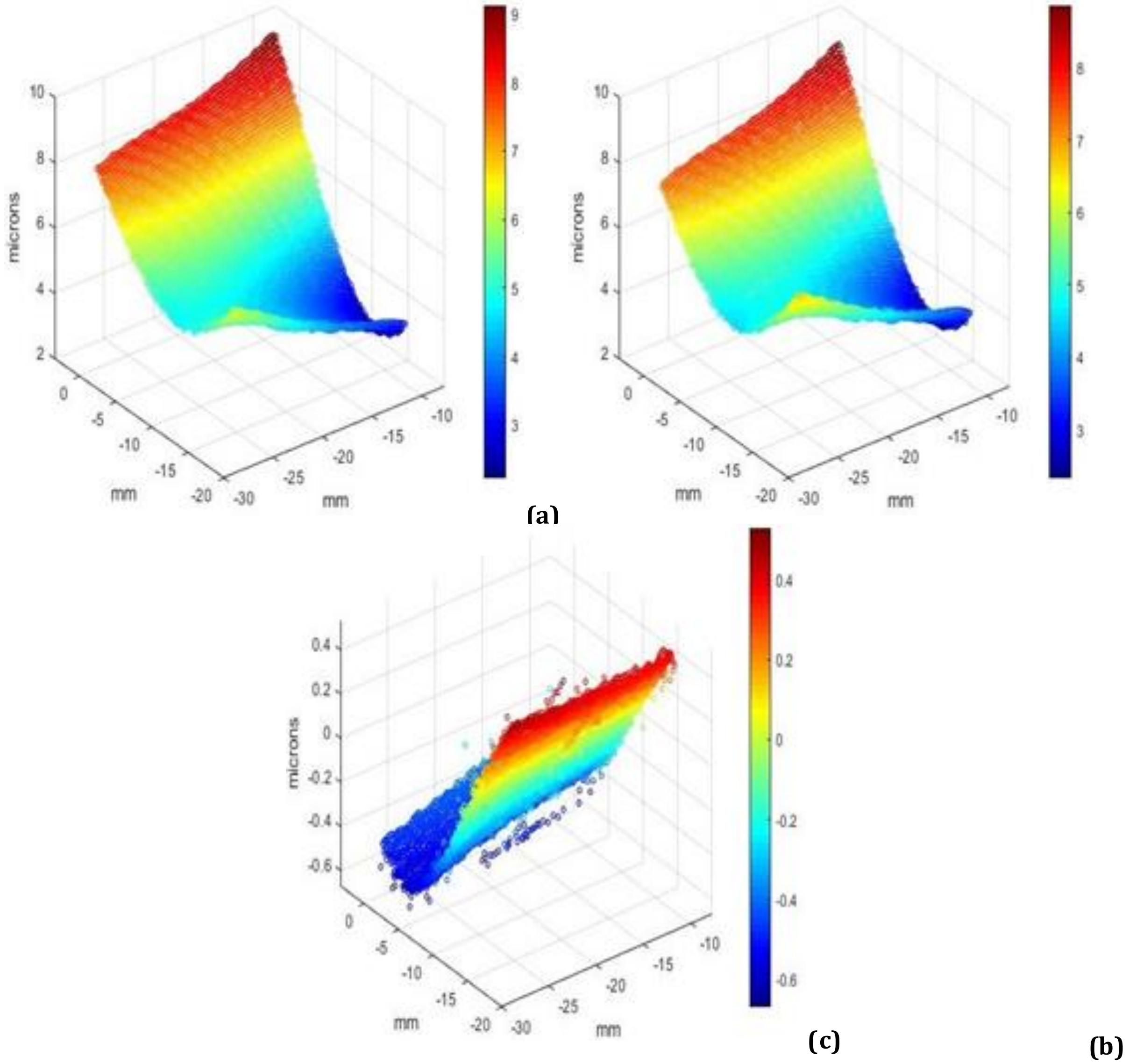

Figure 5. (a) The first and (b) second deformation images. (c) The difference between the first and second deformation images.

5.1 Positional Offset Check

If there is a position offset between two images subtracted from each other, the subtracted image will have a non zero height variation, which could be confused with a deformation. To test for this we took a series of images of the sample without changing anything between the images. The result of subtracting two representative images from this set is shown in Figure 6. While there is a noise spike in the corner of the image, which causes the peak-to-valley (PV) height variation in the image to reach $\sim 2\mu$m, the PV of the majority of the image is only $\sim$ 300nm. We therefore do not believe that position offsets between images are a problem. We remark that to smooth these images, we fitted the surface data with a fifth order polynomial.

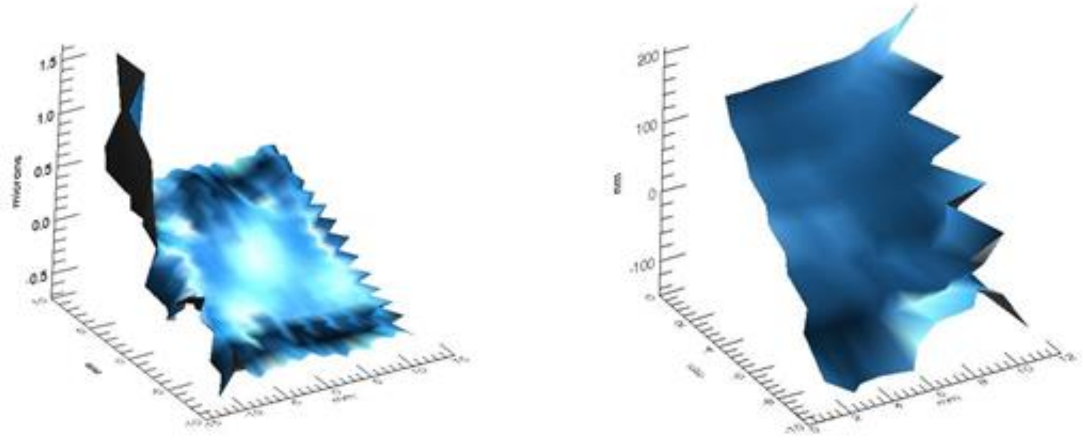

(a) **(b)**

Figure 6. (a) A difference image made by subtracting two images taken after each other without changing anything between the images. (b) The same as (a), but with the corner noise spike removed.

6. SUMMARY AND CONCLUSION

In this publication, we report on progress toward developing thin X-ray mirrors that can be actively controlled using a layer of magnetostrictive material and an electromagnet. Using DC magnetron sputtering we fabricated a sample consisting of 100μm Si coated with 58nm Cr, 2.2μm Terfenol-D and 65nm NiCo. Using a custom built electromagnet and the non-contact Coordinate Configuration Machine at NASA GSFC we generated and imaged two deformations in the sample. The first deformation has a height of $\sim 5\mu$m, while the second deformation, which was generated by moving the electromagnet 4mm away from the first position, has a height of $\sim 1\mu$m. It is therefore likely that the second deformation was smaller than the first because the Terfenol-D was already partially expanded in the second area when the field was applied there. We are currently working on developing models to predict the height and shape of deformations and studying the amount of control that we have over the height of the deformation by varying the field strength.

ACKNOWLEDGMENTS

This work was supported primarily by an adaptive X-ray optics NASA grant (Grant NNX16AL31G) plus support from a NASA NIAC grant (NX15AL89G). We also thank the ISEN center at Northwestern University for providing funds for purchasing additional sputtering guns. This work made use of the EPIC facility of Northwestern Universitys NUANCE Center, which has received support from the Soft and Hybrid Nanotechnology Experimental (SHyNE) Resource (NSF ECCS-1542205); the MRSEC program (NSF DMR-1121262) at the Materials Research Center; the International Institute for Nanotechnology (IIN); the Keck Foundation; and the State of Illinois, through the IIN. We thank Yip-Wah Chung for advice on coating, materials, and magnetics. Special acknowledgement and thanks is extended to the Illinois Space Grant Consortium for providing support via the

Northwestern Summer University Undergraduate Research Program to Z.J.S and W.H.R

REFERENCES

[1] Vikhlinin, A., *Lynx X-ray Observatory* (2016).

[2] Ulmer, M. P., Wang, X., Cao, J., Graham, M. E., and Vaynman, S., "Update to an application using magnetic smart materials to modify the shape of an x-ray telescope mirror," in [*Society of Photo-Optical Instrumentation Engineers (SPIE) Conference Series*], *Society of Photo-Optical Instrumentation Engineers (SPIE) Conference Series* **8861** (Sept. 2013).

[3] O'Dell, S. L., Allured, R., Ames, A. O., Biskach, M. P., Broadway, D. M., Bruni, R. J., Burrows, D. N., Cao, J., Chalifoux, B. D., Chan, K.-W., Chung, Y.-W., Cotroneo, V., Elsner, R. F., Gaskin, J. A., Gubarev, M. V., Heilmann, R. K., Hertz, E., Jackson, T. N., Kilaru, K., Kolodziejczak, J. J., McClelland, R. S., Ramsey, B. D., Reid, P. B., Riveros, R. E., Roche, J. M., Romaine, S. E., Saha, T. T., Schattenburg, M. L., Schwartz, D. A., Schwartz, E. D., Solly, P. M., Trolier-McKinstry, S., Ulmer, M. P., Vikhlinin, A., Wallace, M. L., Wang, X., Windt, D. L., Yao, Y., Ye, S., Zhang, W. W., and Zuo, H., "Toward large-area sub-arcsecond x-ray telescopes II," in [*Society of Photo-Optical Instrumentation Engineers (SPIE) Conference Series*], *Proc. SPIE* **9965**, 996507 (Sept. 2016).

[4] Wang, X., Yao, Y., Ye, S., Liu, T., Assoufid, L., Cao, J., and Ulmer, M. P., "Shaping Si, NiCo, and glass substrates via stresses in the coatings," in [*Society of Photo-Optical Instrumentation Engineers (SPIE) Conference Series*], *Proc. SPIE* **9965**, 99650D (Sept. 2016).

[5] Chalifoux, B., Sung, E., Heilmann, R. K., and Schattenburg, M. L., "High-precision figure correction of x-ray telescope optics using ion implantation," in [*Optics for EUV, X-Ray, and Gamma-Ray Astronomy VI*], *Proc. SPIE* **8861**, 88610T (Sept. 2013).

[6] Riveros, R. E., Biskach, M. P., Allgood, K. D., Kearney, J. D., Hlinka, M., and Zhang, W. W., "Progress on the fabrication of lightweight single-crystal silicon x-ray mirrors," in [*Society of Photo-Optical Instrumentation Engineers (SPIE) Conference Series*], *Society of Photo-Optical Instrumentation Engineers (SPIE) Conference Series* **10399**, 103990T (Aug. 2017).

[7] Riveros, R. E., Biskach, M. P., Allgood, K. D., Mazzarella, J. R., Sharpe, M. V., and Zhang, W. W., "Progress on the fabrication of high resolution and lightweight monocrystalline silicon x-ray mirrors," in [*Space Telescopes and Instrumentation 2016: Ultraviolet to Gamma Ray*], *Proceeding SPIE* **9905**, 990521 (July 2016).

[8] Ulmer, M. P., Coppejans, R., Buchholz, D. B., Cao, J., Wang, X., Mercado, A. M., Qian, J., Assoufid, L., O'Donnell, A. E., Condron, K. S., and Harpt, B. E., "Controlling the shapes of coated silicon substrates via magnetic fields, a progress report," in [*Society of Photo-Optical Instrumentation Engineers (SPIE) Conference Series*], *Society of Photo-Optical Instrumentation Engineers (SPIE) Conference Series* **10399**, 103991N (Aug. 2017).

Membrane Mirror Evaluation of APERTURE: A Precise Extremely large Reflective Telescope Using Re-configurable Elements

Turgut B. Baturalp[a], Victoria L. Coverstone[b], Rocco Coppejans[c], Jian Cao[d], YipWah Chung[e], David B. Buchholz[f], and M. P. Ulmer[c]

[a]Department of Mechanical Engineering, Texas Tech University, 7th and Boston Ave.,
Lubbock, TX, USA
[b]Department of Mechanical and Aerospace Engineering, University of Miami, 1251 Memorial
Drive, Miami, FL, USA
[c]Center for Interdisciplinary Exploration and Research in Astrophysics (CIERA) and
Department of Physics and Astronomy, Northwestern University, 2145 Sheridan Road,
Evanston, IL, USA
[d]Department of Mechanical Engineering, Northwestern University, 2145 Sheridan Road,
Evanston, IL, USA
[e]Department of Materials Science and Engineering, Northwestern University, 2145 Sheridan
Road, Evanston, IL, USA
[f]Materials Research Science and Engineering Center, Northwestern University, Technological
Institute, 2145 Sheridan Road, Evanston, IL, USA

ABSTRACT

Larger mirrors are needed to satisfy the requirements of the next generation of UV-Vis space telescopes. Our NASA-NIAC funded project, titled A Precise Extremely large Reflective Telescope Using Reconfigurable Elements (APERTURE), attempts to meet this requirement. The aim of the project is to demonstrate technology that would deploy a large, continuous, high figure accuracy membrane mirror. The figure of the membrane mirror is corrected after deployment using a contiguous coating of a Magnetic Smart Material (MSM) and a magnetic field. The MSM is a magnetostrictive material which is driven by magnetic write head(s) (MWH), locally imposed on the non-reflective side of the membrane mirror. In this proceeding we report the figure accuracy of the MSM coated membrane mirror under various conditions using a Shack-Hartmann surface profiler. The figure accuracy and magnetostrictive performance of the membrane mirror is found to be significantly dependent on ambient temperature fluctuations, the tension load on the membrane, time, magnetic writing head orientation and magnetic field strength. The results and reproducibility of the surface profiling experiments under various conditions are introduced and discussed.

Keywords: Magnetic Smart Materials, Membrane Mirrors, Deployable Optics, Post Deployment Correction, Space Mirrors, Space Telescopes, Magnetostriction

1. INTRODUCTION

1.1 Need for the Concept and Current Solutions

For future UV-Vis space telescopes, mirrors that are larger than those that can be accommodated in current launch vehicle fairings[1] are required. This goal can be achievable by replacing traditional thick telescope mirrors with foldable thinner mirrors that are <1 mm thick. Another major advantage of using thinner primary mirrors is the possibility of significant decrease the satellite weight and correspondingly the mission cost compared to satellites with similar size conventional mirrors. Due to the required figure accuracy of UV-Vis mirrors, post deployment corrections of the membrane mirror figure will be required. We are motivated to explore our concept because previous membrane mirror concepts, which proposed using piezoelectric[2,3] or electrostatic[4–6] actuators to correct the mirror figure after deployment, have not yet been successful. Some of the problems with these actuators are that: (1) When moving to larger diameters, the number of actuators becomes unfeasibly large. (2) They need to be deposited on the backside of the mirror, increasing the complexity of the manufacturing the mirror. (3) The actuators require fixed wires and constant power to prevent them from relaxing. (4) A deformation can only be applied at the location of an actuator.

1.2 The APERTURE Concept

Our NASA Innovative Advanced Concepts (NIAC) funded project, which is called A Precise Extremely large Reflective Telescope Using Reconfigurable Elements (APERTURE), endeavors to find a way to deploy a large, continuous, high figure accuracy membrane mirror for space telescopes (for more detail see[7–9]). In our concept the membrane mirror is composed of three or more different layers: (1) A reflective layer such as gold for the IR, (2) A substrate that provides the structural component of the mirror, and (3) A layer of Magnetic Smart Material (MSM). Our aim is to achieve a figure accuracy of $\lambda/20$ at visible wavelengths ($\lambda \approx 600$ nm). To decrease the figure error below $\lambda/20$, the mirror figure is corrected after deployment. The figure correction approach is the novel part of this study. We use a contiguous coating of MSM instead of using classical piezoelectric-patches or electrostatic actuators. The MSM is a magnetostrictive material which contracts or elongates under the influence of a magnetic field. The post deployment corrections are applied by a magnetic write head (MWH) which moves along the non-reflective side of the membrane mirror and the corrections are held in place by a magnetically hard material. Fig. 1 is a video demonstration of the APERTURE concept and its operating principles.

In this proceeding we measure the figure accuracy and magnetostrictive performance of the membrane mirror under various conditions using a tailored experimental setup. The membrane mirror sample that was used, experimental setup and the results of conducted experiments are presented and explained.

Further author information: (Send correspondence to M.P.U. or T.B.B.)
M.P.U.: E-mail: m-ulmer2@northwestern.edu
T.B.B.: E-mail: b.baturalp@ttu.edu

Space Telescopes and Instrumentation 2018: Optical, Infrared, and Millimeter Wave, edited by Makenzie Lystrup, Howard A. MacEwen, Giovanni G. Fazio, Proc. of SPIE Vol. 10698, 106981K
© 2018 SPIE · CCC code: 0277-786X/18/$18 · doi: 10.1117/12.2309826

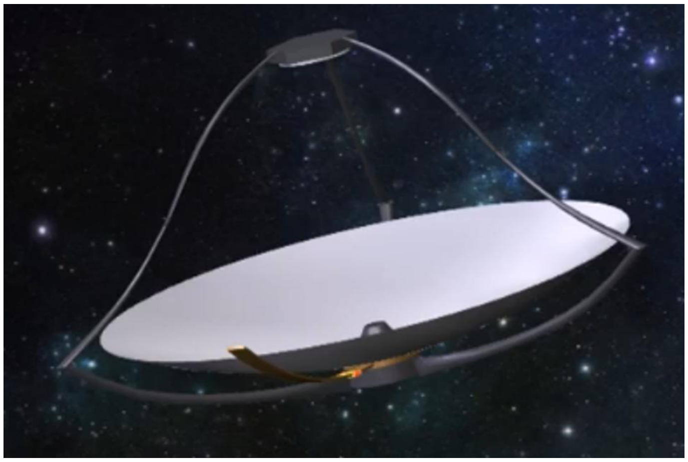

Figure 1. APERTURE_VIDEO.wmv, The video explains the APERTURE concept and its operating principles, in detail:

http://dx.doi.org/10.1117/12.2309826

2. MATERIALS AND METHODS

In this section we describe the membrane mirror sample and how it was prepared. Additionally, the experimental setup and procedure are reported.

2.1 The Magnetic Smart Material: Terfenol-D

A detailed review of MSMs can be found in.[10] All ferromagnetic materials expand or contract when an external magnetic field is applied to them. The magnetic structure of ferromagnetic materials are composed of domains of uniform magnetic polarization. When a magnetic field is applied, the domains will rotate to orientate themselves parallel to the field. This rotation changes the crystal structure of the material, causing a strain as different crystal structures have different lengths. Materials with a positive magnetostriction experience a tensile strain and materials with negative magnetostriction experience a compressive strain parallel to the field.

Increasing the applied field strength causes more domains to align. The resulting strains increase almost linearly until the material approaches saturation, when all of the domains are aligned with the field. In general, magnetostriction is a reversible exchange of energy between the magnetic and the mechanical forms of the material. Once the external field is removed, the material relaxes (strain reverts to almost zero) nearly instantaneously. For our application, relaxation is prevented by coating the mirror with a magnetic hard material such as NiCo. The NiCo locks in a fraction of the externally applied magnetic field. When the external field is removed, this locked in field prevents the material from completely relaxing.

In the 1970's the Naval Ordinance Laboratory developed a material, Terfenol-D ^{R}, that has a very large change in dimensions compared to other ferromagnetic materials when a magnetic field is applied to it. Terfenol-D ^{R} was the first MSM and is a three elements alloy: $Tb_xDy_{1-x}Fe_y$ where 0.27 $< x <$ 0.30 and 1.9 $< y <$ 2.0. TerfenolD ^{R} is a positive magnetostriction material with typical magnetostrictive strains of 0.1 − 0.2% and saturates at a field strength of ∼ 1T.[10] We have previously used Terfenol-D ^{R} as its properties are well known,[11–13] it is commercially available with an affordable price and has a large magnetostrictive strain.

Terfenol-D ^{R}, like all MSMs, has a magnetic anisotropy in which it is easier to line up the domains in a certain direction, called the easy axis. The saturation field strength is therefore lower along the easy axis compared to other directions. The easy direction is strongly influenced by the external stress placed on a MSM film.[14] In MSMs with positive magnetostriction under tensile stress, the easy axis lies in the film plane, while under compressive stress the easy axis is perpendicular to the film plane.[15] This is caused by the magneto-elastic coupling energy, which causes MSMs to respond to external stress with a rotation of the spins.[16]

The magnetic anisotropy of the Terfenol-D^R is examined by changing the orientation angle of the MWH, allowing the easy axis of the sample to be constrained. Moreover, the locking performance of the NiCo coating is observed in the surface profiling measurements by conducting long duration tests.

2.2 Making Samples

The preparation and characteristics of the sample are described in detail in previous work.[9] In brief, the sample was prepared by deposing 0.029μm Cr, 0.984μm Terfenol-D^R and 0.047μm Nickel-Cobalt (NiCo) by direct current (DC) magnetron sputtering on Aluminized Dunmore DE340 Kapton^R. The Kapton^R substrate is 127μm thick and coated with 300˚A aluminum. Using a Hitachi S-3400N-II scanning electron microscope, we measured the mass percentage composition of the Terfenol-D^R as 17% Tb, 36% Dy and 47% Fe. The outer diameter of the sample is approximately 8 cm, where the MSM coated portion has a diameter of 5 cm.

2.3 Experimental Setup

The experiments were conducted in an enclosed system to create a temperature controlled and dust/AC blow protected environment. The main components of the experimental setup are: a Shack-Hartmann wavefront sensor with optical accessories (HASO4 RFlex50, Imagine Optics Inc.), a vibration isolated optical table, a temperature controller/heater, a MWH with power-supply, a membrane holder, and a 2 × 2 × 4 feet enclosure with an adjustable height ceiling for creating smaller spaces. Detailed information about the design process of the experimental setup can be found in.[8]

Figure 2(a) shows the whole experimental setup with the sliding door open. All of the components were placed on the optical table including the power-supply of the MWH and the computer used for data acquisition from the wavefront sensor. Fig. 2(a) also shows the overall size of the enclosure. For measurements taken in this study the ceiling height was adjusted to 1 foot. Figure 2(b) is a close-up picture of the vertical optical path which consists of height and yaw/pitch alignment stages, a wavefront sensor, and the membrane mirror sample with its holder.

Although the wavefront sensor is not effected by small temperature fluctuations, the membrane mirror samples are laminated with different materials, thus temperature fluctuations might be a problem for the samples. We are aware of the coefficient of thermal expansion considerations for space application materials, but we neglect it in this early proof of concept phase of the project. A Proportional, Integral, Derivative (PID) temperature controller (48VFL13, Extech Instruments Inc.) (Fig. 2(c)) with a heating strap and Resistance Temperature Detector (RTD) probe was used to stabilize the temperature in the enclosure. Temperature fluctuations of ± 0.3° F was observed around the set point temperature.

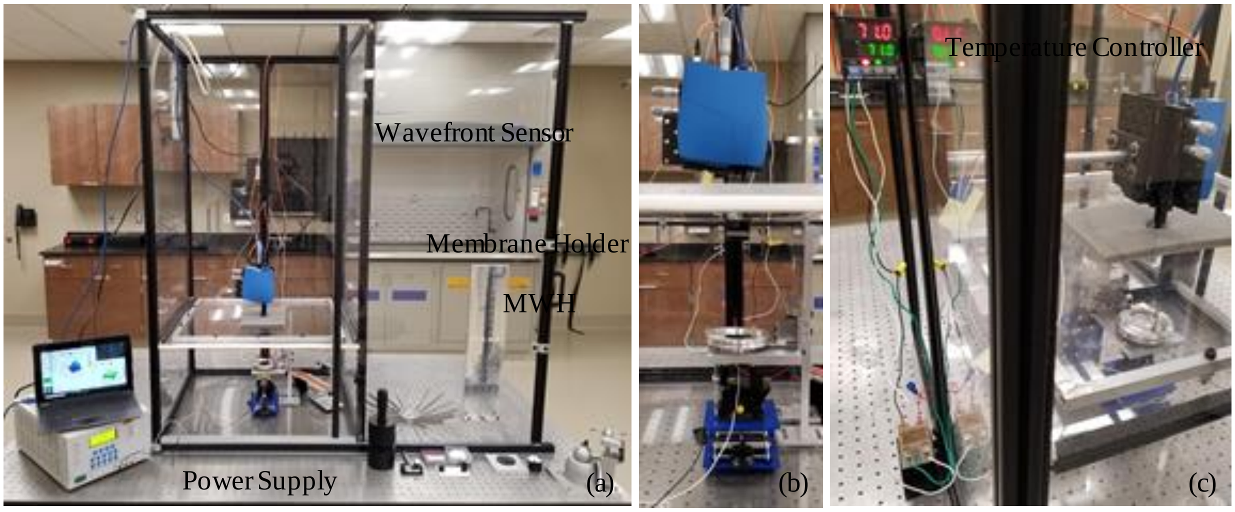

Figure 2. Experimental Setup: (a) Picture of the entire experimental setup, (b) close-up picture of the optical path and (c) the PID temperature controller.

2.3.1 Magnetic Writing Head (MWH)

Electromagnets were chosen over permanent magnets to demonstrate the magnetostrictivity of the membrane samples due to the ability to control the field strength; which essentially means control of the membrane figure correction. After a wide survey of electromagnet vendors, MWHs came to the forefront with their smaller sizes and high magnetic flux capabilities. The selected MWH (World Magnetics Inc., Model 10095) has outer dimensions of 0.99 × 0.94 × 0.8in. The poles are made of HiCo 5000 with a pole gap and length of 0.002 in and 0.5 in, respectively. Additionally, a programmable high current power-supply was used to drive the MHW and a gaussmeter was used to measure its performance. During the performance tests, the maximum field strength that can be generated by the MWH without melting the insulation of its wiring (max applied current was 5 A) was determined to be ~ 0.1T. The maximum magnetic field strength was observed at the center of the pole gap at a distance less than 1 mm from the top of the poles. All of the experiments were done at a field strength slightly lower than 0.1 T.

2.3.2 Membrane Holder

Because of the nature of the MSM based shape correction approach, a trade-off between structurally supporting and magnetically controlling the shape of membrane mirror has emerged. This trade-off between the required flexibility (low enough in-plane stress) for the MSM corrections and low initial post deployment figure error requires a membrane holder design which can be adjusted to a low-tension load/high figure accuracy state. To meet these requirements a membrane holder which consists of two rings was designed and prototyped (see Fig. 3). Similar designs can be found in the literature.[6,17] The purpose of the rings are: (1) The outer ring is utilized for mounting/clamping the membrane, providing a coarse tension load (pre-straining), and making co-planarity adjustments by changing the height of the ring; (2) The inner ring is employed to avoid wrinkles on the boundary and compartmentalization of the holder. Figure 3(a) shows the cross-sectional view of the membrane holder.

The outer ring is equipped with an o-ring groove and an o-ring to keep the membrane in place when applying tension using the inner ring. The height of outer ring can be adjusted with a translational stage so that the tension can be applied by the inner ring. Figure 3(b) is a picture of the membrane holder, placed in the setup with a membrane in tension.

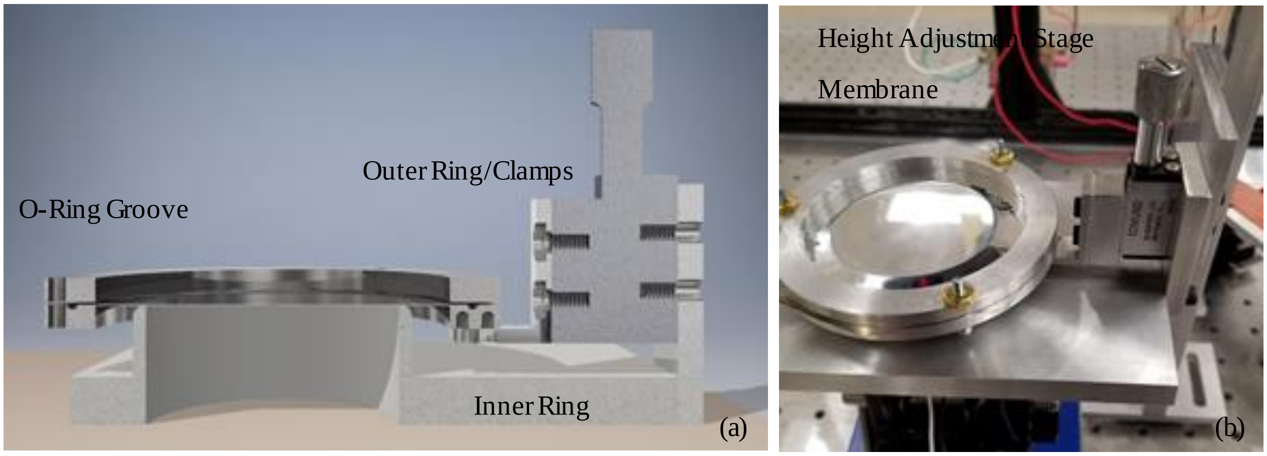

Figure 3. Membrane Holder: (a) a cross-sectional drawing and (b) a picture of the actual membrane holder.

3. RESULTS

In this section we discuss our experimental procedure, the results of surface measurements done under various conditions, and post-processing.

3.1 Experimental Procedure

The Terfenol-D coated membrane mirror sample was placed in the membrane holder. The MWH was placed in a non-magnetic vise which was in turn placed on a lifting platform. This allowed the gap between the membrane and MWH to be adjusted. After each experiment, the membrane was degaussed using a commercial degausser (TDM-1, TTC Inc.) to remove the magnetic field captured by the NiCo, thereby resetting the membrane. At the start of each experiment, an alignment procedure was performed using the yaw/tilt stages on the ShackHartmann wavefront sensor to straighten the optical path. Additionally, the MWH was centered on the surface profiling measurement area of 5×7 mm and the gap between the MHW and the membrane was set to ~ 1 mm. The surface profiling experiments were performed by taking an initial image after which images were taken at the following times with respect to the initial image: 1, 2, 3, 4, 5, 10, 20, 30, 40, 50 and 60 minutes, and 3, 6, 12, 24, and 48 hours. The wavefront and intensity maps were exported to text files for further analysis.

3.2 Zernike Polynomial Wavefront Reconstruction

Zernike polynomials were used to reconstruct the wavefront image to compensate for the tip/tilt drift of the membrane and smooth the image. There are three wavefront reconstruction modes in the Waveview software (Imagine Optics Inc.): zonal, Zernike and Legendre. The main advantage of zonal reconstruction is that it can be adapted to all types of pupil shapes since it uses a local slope signal integration concept.[18] This reconstruction method was, however, found to be noisy by the manufacturer. It is stated that the reconstructed wavefront is sensitive to any noise present on a local slope. The noise level was measured using a flat reference mirror (BB211E02, Thorlabs Inc.) which has a surface flatness of $\lambda/10$ at 632.8 nm and surface quality of 10-5 Scratch-Dig. The noise was measured by taking 12 measurements at various times. The average peak to valley surface figure was 0.072μm with an upper limit of 0.083μm and a lower limit of 0.063μm. The Zernike wavefront reconstruction method is considered a much better method not only for noise reduction, but also because it allows the effects of optical aberrations such as tip, tilt and focus to be removed. Additionally, Zernike polynomials are often used

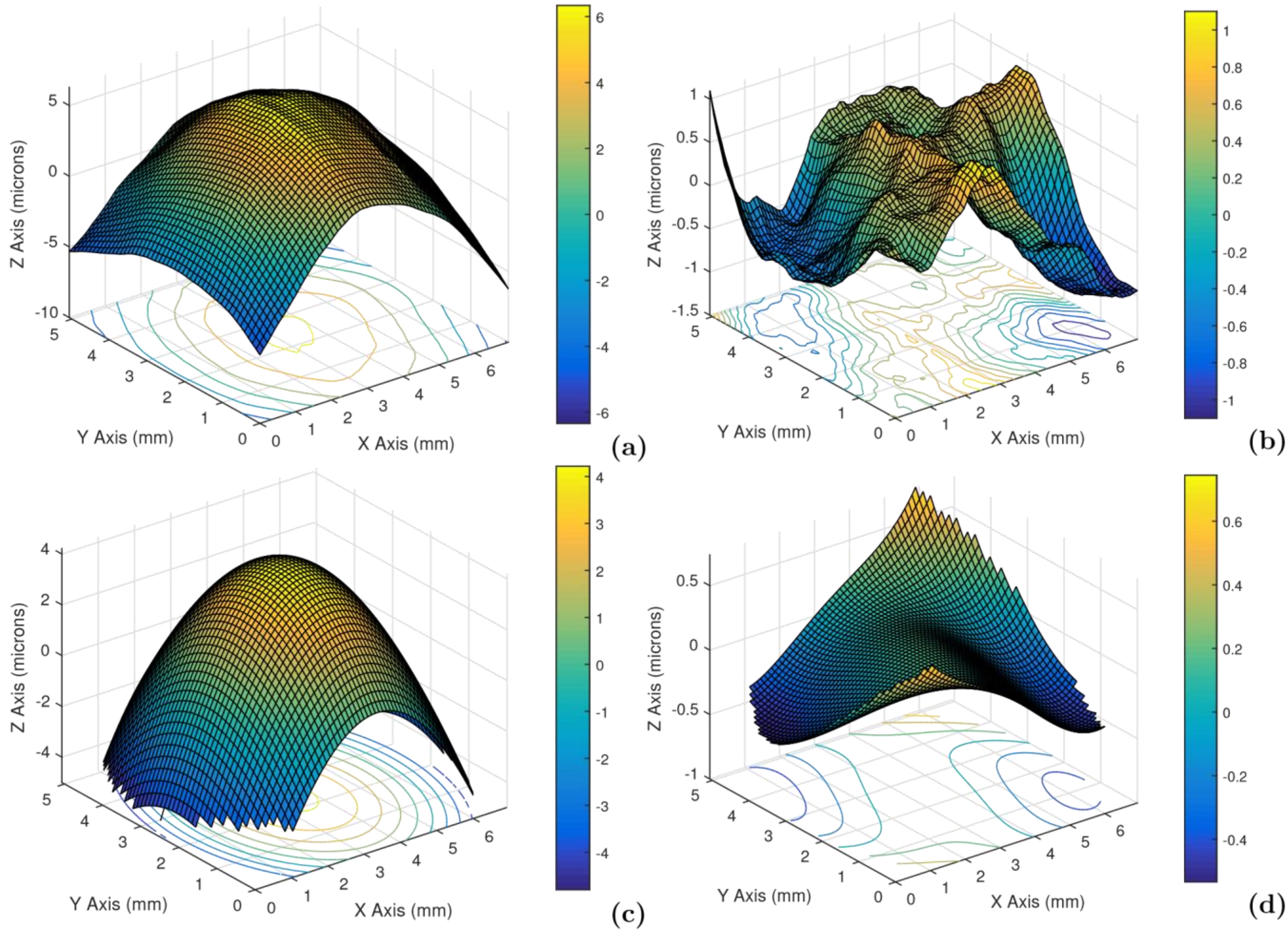

Figure 4. Zonal and Zernike wavefront reconstruction images of the membrane sample: (a) a raw zonal wavefront image, (b) a tip/tilt and focus removed zonal wavefront image, (c) a raw Zernike wavefront image and, (d) a tip/tilt and focus removed Zernike wavefront image. The scale of the Z axis and color-bar is μm, while XY units are in mm.

in the field of optical metrology and adaptive optics. A Zernike polynomial of eight coefficients (excluding the piston) was found to be sufficient to represent the surface of our sample. The tip, tilt and focus components were removed due to drifting and distortion that they cause. Figure 4 shows the improvement of the wavefront reconstruction of a flat membrane sample measurement by the above methodology. In the figure the XY plane is the 5 × 7 mm measurement area and the Z axis represents the height values in μm. In Fig. 4, (a) is a raw zonal wavefront reconstructed image, (b) is a tip/tilt and focus compensated zonal wavefront reconstructed image, (c) is a raw Zernike wavefront reconstructed image and (d) is a tip/tilt and focus compensated Zernike wavefront reconstructed image. The (a) and (b) images were reconstructed using the zonal method, where (c) and (d) were reconstructed by Zernike polynomials. To illustrate how the focus aberration dominates in zonal and Zernike reconstruction, both aberration filtered (Fig. 4(b) and (d)) and raw images (Fig. 4(a) and (c)) are shown. When tip/tilt and focus aberrations are removed for the wavefront reconstruction images were more realistic as can be seen in Fig. 4(b) and (d) for both zonal and Zernike reconstructions. Moreover, the noise introduced by zonal wavefront reconstruction can be seen in Fig. 4(b) and noise reduced Zernike wavefront reconstructed image in Fig. 4(d). The final aberration and noise filtered wavefront image can be seen in Fig. 4(d). The scale of the colorbar in Fig. 4(d) is lower than Fig. 4(b) due to the rectangular pupil area corners of the zonal reconstruction are not included in the Zernike polynomial fits since Zernike polynomials are circular.

3.3 Tensile Loading Measurements

To see the effect of the applied tension on the figure of the membrane a set of surface profiling measurements were conducted using the membrane holder shown in Fig. 3. The membrane holder is equipped with a z axis precision linear stage to apply and adjust the tension. The travel per knob rotation of the stage is 2.9 mm. Four measurement points were taken with half knob rotation increments (1.45 mm), starting with the inner ring slightly touching the membrane. Figure 5 shows the effect of increasing the tension on the membrane. As the tension increases the height variations decrease, i.e. the membrane figure accuracy increases. Figure 5(a) shows the membrane figure when the inner ring only lightly touches the membrane. In this image some parts of the wavefront could not be reconstructed due to the beam scattering from wrinkles on the membrane. After increasing the tension by lowering the outer ring 1.45 mm (Fig. 5(b)), the size of the wrinkles decreased. This resulted in most of the wavefront being reconstructed. Figures 5(c) and (d) shows the images of the reconstructed wavefronts at 2.9 and 4.35 mm inner ring penetrations. Note that the saddle shape is changed in (d) with the increasing tension. Table 1 shows the root mean square (RMS)

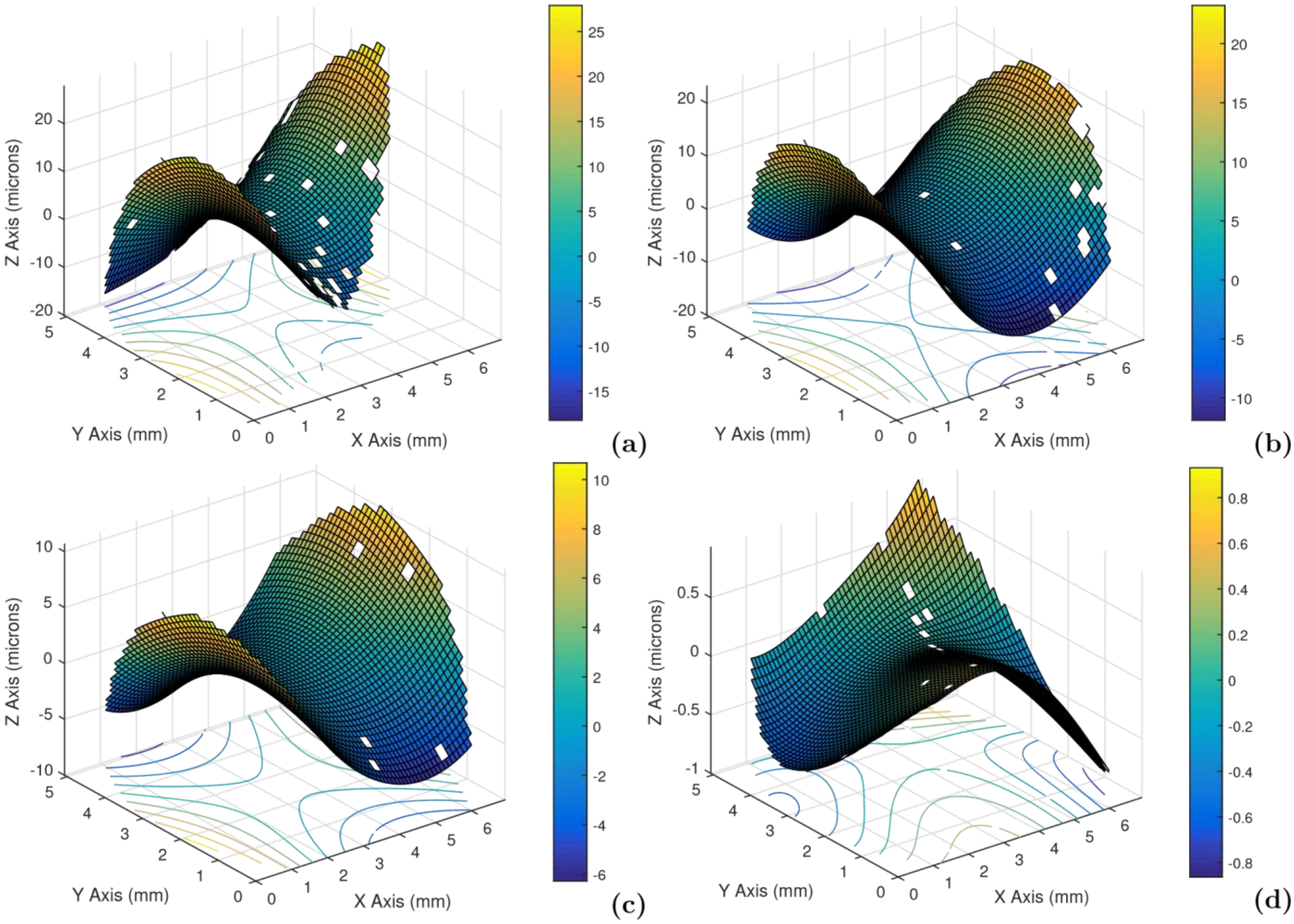

Figure 5. Wavefront reconstruction images under different inner ring penetration values (tensile loadings): (a) 0 mm, (b) 1.45 mm, (c) 2.90 mm, (d) 4.35 mm. The scale of the Z axis and color-bar is μm, while XY units are in mm.

and peak to valley (PV) values for each measurement. The table clearly shows that figure accuracy increases with increasing inner ring penetration (tension loading).

Table 1. RMS and PV values of the tension loading experiments.

Inner Ring Penetration (mm)	RMS (μm)	Peak to Valley (μm)
0	8.96	46.11
1.45	7.37	35.10
2.90	3.47	16.95
4.35	0.31	1.79

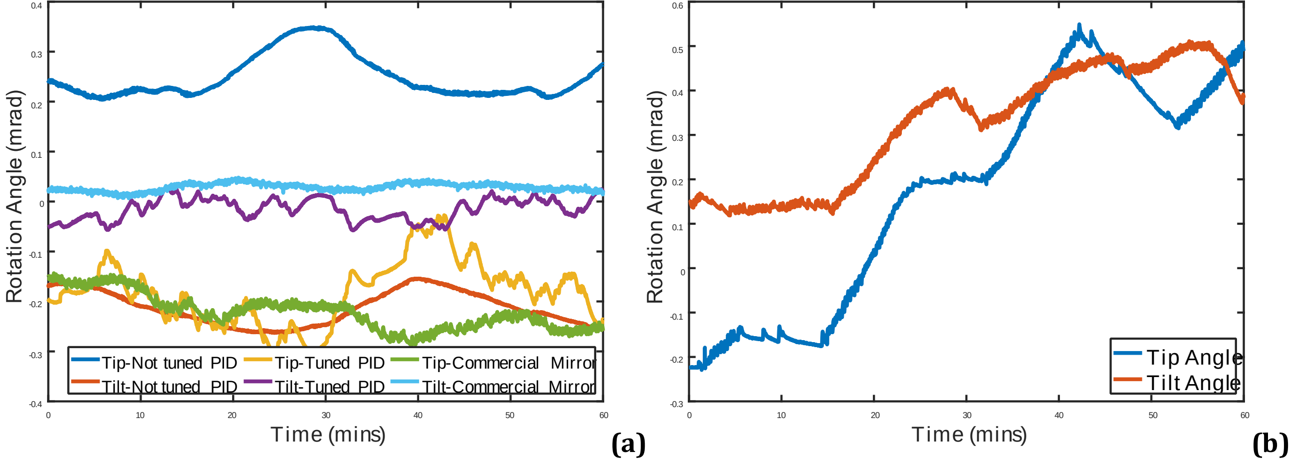

Figure 6. Tip/tilt angles in the temperature controlled experiments: (a) the effect of PID tunning and comparison with a commercial Zerodur ^{R} mirror, (b) the tip/tilt angle sensitivity to increasing the chamber temperature from 70° F to 75° F.

3.4 Temperature Controlled Measurements

The effect of temperature changes is also examined in this study. A direct correlation between the tip/tilt values and temperature was found. This issue was overcome by compensating for the drift using Zernike coefficients and keeping the temperature constant (± 0.3° F) in the experimental chamber. In this section, two different set of measurements were conducted: (1) Tuning the PID coefficients of the temperature controller and testing the results by comparing the membrane sample with a commercial reference flat mirror while keeping the temperature constant at 75° F, (2) The temperature is increased from 70 to 75° F in the chamber to study the temperature sensitivity of the experimental setup. Figure 6(a) is a 60 minutes long experiment plot that shows the effect of PID tunning. The membrane mirror sample was compared to a commercial flat reference mirror (BB211-E02, Thorlabs Inc.) made of Zerodur ^{R}, which has a extremely low coefficient of thermal expansion. The PID tuning of the temperature controller improved the temperature stability from ± 0.5° F to ± 0.3° F and also decreased the response time of the controller significantly (see Fig. 6(a)). After PID tuning, the frequency of the tip/tilt angle changes increased, while the amplitude of their variations decreased. A comparison with the Zerodur ^{R} mirror was conducted after PID tunning to study the thermal expansion performance of the membrane mirror when the temperature was stabilized to ± 0.3° F. The tip/tilt angle deviation of the membrane mirror was reasonably close to that of the Zerodur ^{R} reference flat mirror. Hence the temperature control of the experimental setup is sufficient. Another experiment was conducted to study the sensitivity of the membrane mirror's tip/tilt angle on temperature variations. In Fig. 6(b), the temperature of the chamber was ramped from 70° F to 75° F over a period of 60 minutes while tracking the tip/tilt angles. This experiment showed that the tip/tilt angles are highly sensitive to temperature changes. Temperature changes may therefore be one of the major causes of the tip/tilt drifting issue.

3.5 Magnetic Anisotropy Test of the Membrane Mirror

The magnetic anisotropy of the MSM (Terfenol-D^{R}) was explained in Subsection 2.1. To determine the direction of the easy axis, images were taken with different orientation angles of the MWH with respect to the membrane mirror sample. Four different MWH orientation angles were selected for this study (see Fig.7): (a) the MWH parallel to the X axis, (b) the MWH parallel to the Y axis, (c) the MWH diagonal to X and Y axes towards positive X direction and (d) the MWH diagonal to X and Y axes towards negative X direction. Figure 7 shows the magnetostriction performance of the membrane sample for these four MWH orientations. The magnetostriction performance was measured by subtracting wavefront reconstruction image taken before the MWH was switched on to an image taken one minute after the MWH was switched on. These subtracted images are shown in Fig.7 ((a)-(d)). The highest deformation was measured when the MWH was oriented diagonal to X and Y axes towards negative X direction (-45° angle, if the vertical (Y) axis assumed to be 0° angle). The diagonal axis at -45° angle was therefore identified as being closest to the easy axis. The MWH was consequently placed at a -45° angle for

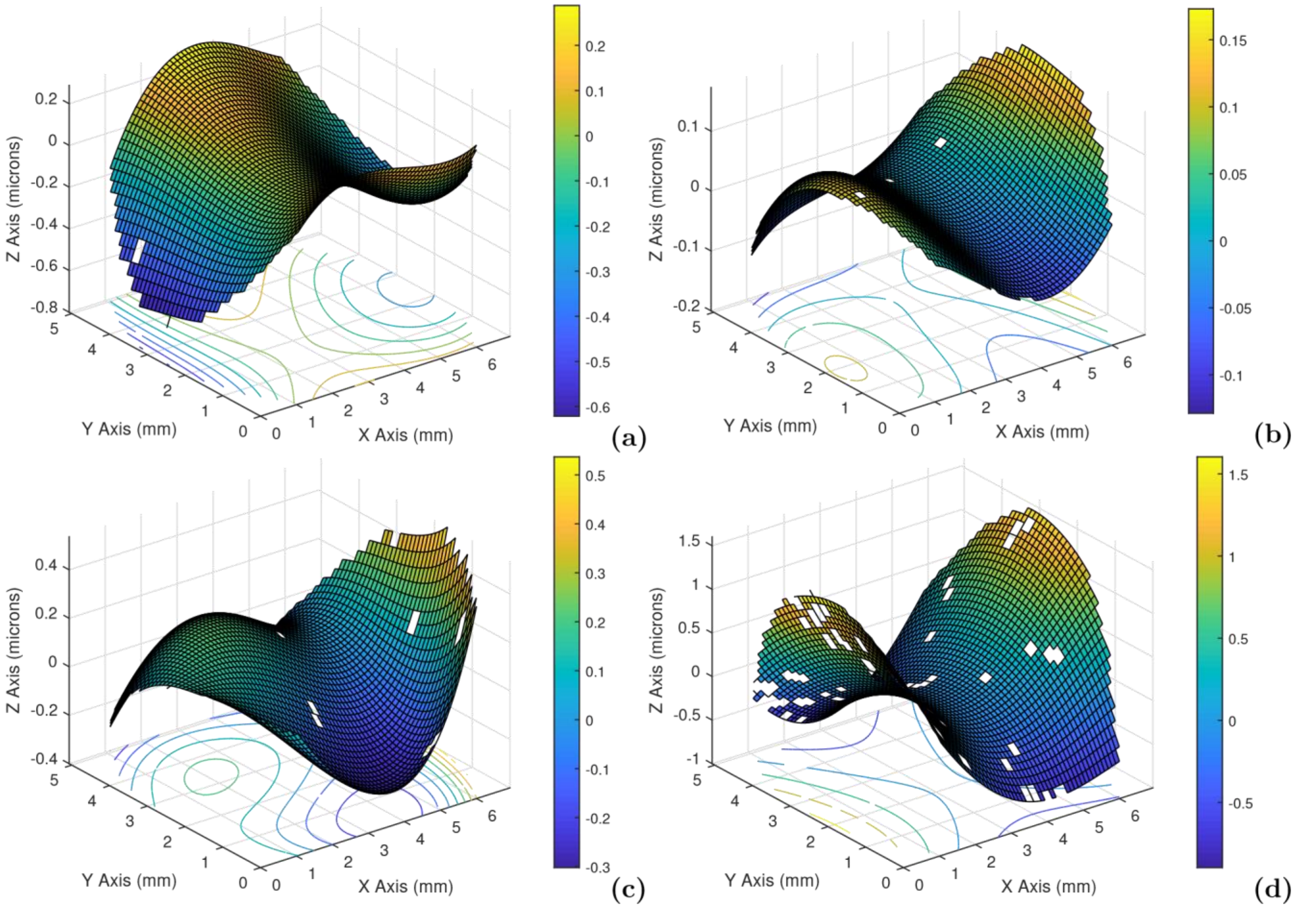

Figure 7. Magnetic anisotropy test of the membrane mirror in four different MWH orientations: (a) the MWH parallel to the X axis, (b) the MWH parallel to the Y axis, (c) the MWH diagonal to X and Y axes towards positive X direction (d) the MWH diagonal to X and Y axes towards negative X direction. The scale of the Z axis and color-bar is μm, while XY units are in mm.

the magnetostriction performance (Section 3.6) and reproducibility studies (Section 3.7). The RMS and PV of the 45° subtracted wavefront reconstruction image is 0.55 μm and $\sim$ 2.50μm, respectively.

3.6 Magnetostriction Performance of the Membrane Mirror

The magnetostriction performance of the membrane mirror is demonstrated with the MWH placed at a -45° angle in this section. The deformation images in this section were generated in the same way, was as those in Section 3.5. The applied magnetic flux density was < 0.1 T and the MWH was turned on for less than 10 seconds to prevent it from over heating. The deformation images were taken 1 minute after the MWH was turned on and has a RMS of 0.55 μm and PV of $\sim$ 2.50μm. This points out a clear deflection that lasted in a decreasing tendency as long as 12 hours. Moreover, the locking performance of the NiCo coating is observed in the surface profiling measurements by conducting long duration tests (see Fig. 8 (a)-(d)). Although the magnetic hard material (NiCo) was preserving the deformation at some level, the height of the deformation decreased during the long duration tests. Table 2 shows the measured RMS and PV values from reconstructed subtraction images displayed in Fig. 8. The relaxation of the membrane can be seen clearly along the lower X axis of Fig. 8 (c) and (d).

3.7 Reproducibility Test of the Membrane Mirror's Magnetostrictive Performance

The reproducibility of the deformation generated 1 minute after the MWH was turned on (Section 3.6) was also examined. To better illustrate the results, a cross-section of the images were taken at Y equals to 2.5 mm (see Fig. 9 (a)). The cross-section at $Y = 2.5$ mm has one of the highest PV values of all of the possible

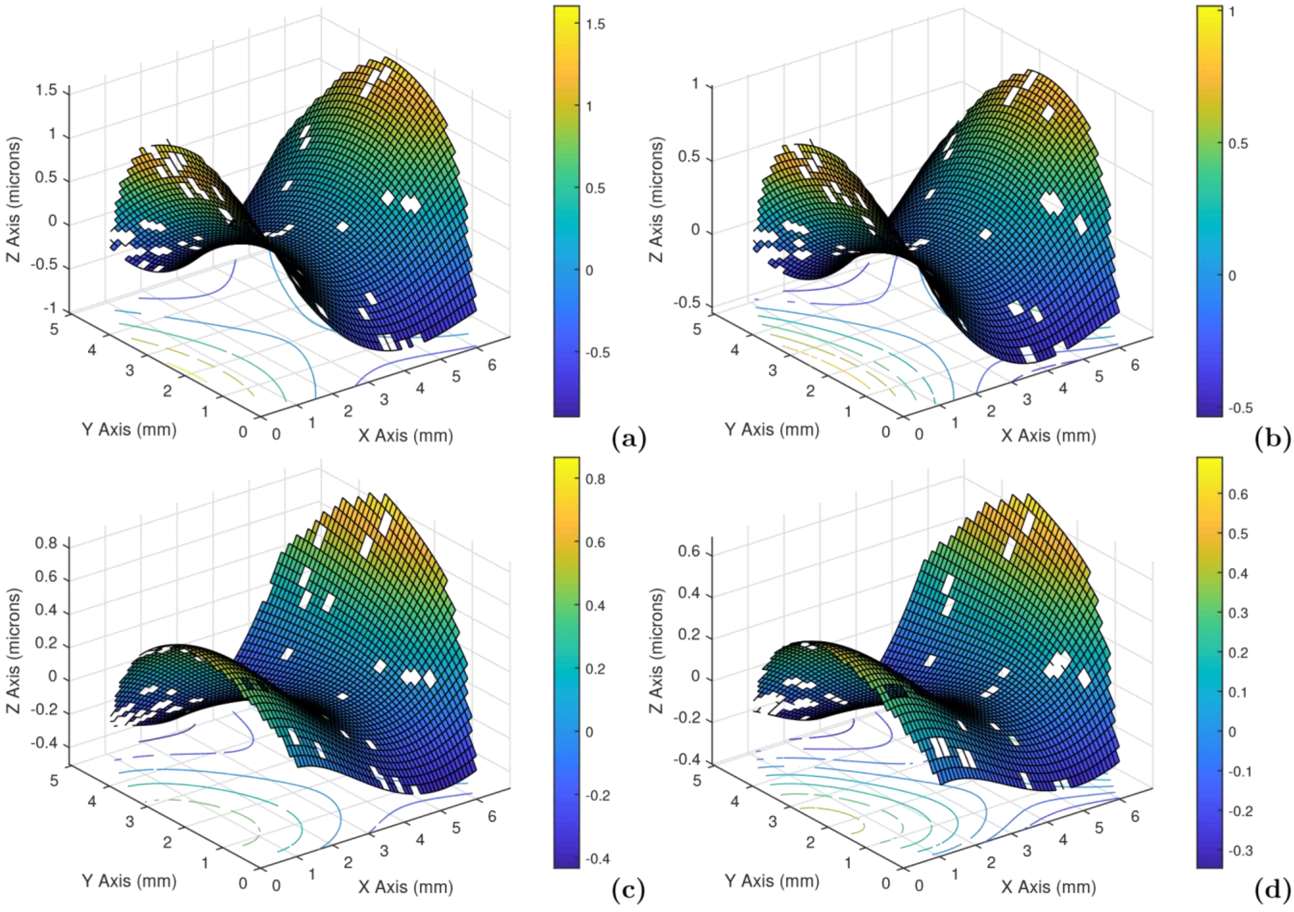

Figure 8. Magnetostriction performance of the membrane mirror:(a) 1 minute after MWH application, (b) 10 minutes after MWH application, (c) 6 hours after MWH application, (d) 12 hours after MWH application. The Z axis and color-bar units scale is in μm, while XY units are in mm.

Table 2. RMS and PV values in the long duration magnetostriction performance test.

Elapsed time after MWH activation	RMS (μm)	Peak to Valley (μm)
1 minute	0.55	~ 2.50
10 minutes	0.34	~ 1.55
6 hours	0.27	~ 1.30
12 hours	0.22	~ 1.04

cross-sections. Three different measurements were taken while keeping all the experimental parameters constant. A comparison of the three measurements at the selected cross-sectional plane is shown in Fig. 9 (b). The measurement presented in Subsection 3.6 is shown as the first measurement in the figure. Figure 9 (b) shows that the generated deformations are reproducible and consistent with each other when keeping the experimental parameters constant.

4. SUMMARY AND CONCLUSION

In this proceeding, we introduce an experimental setup for surface profiling a membrane mirror sample which is composed of a membrane substrate that has been coated with a MSM and a magnetically hard material (NiCo). Additionally, we conducted experiments to characterize the membrane mirror sample under various conditions such as ambient temperature fluctuations or pre-tensioning (fixing tension load) of the membrane. The results

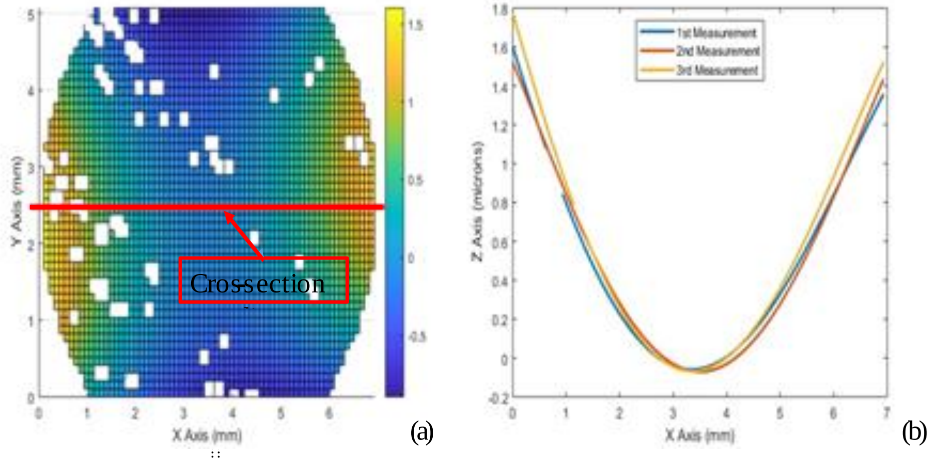

Figure9.Reproducibility test of magnetostriction performance of the membrane mirror:(a) a representation of the cross-section viewed from the top,(b)the cross-section of the three measurements.

showed that temperature changes are causing tip/tilt angle drifting during measurements and the figure accuracy of the membrane is significantly influenced by the tension load. Moreover, the magnetostrictive performance of the MSM material was tested by generating deformations, measuring the magnetic anisotropy, and investigating the reproducibility of the deformations. The easy axis of the MSM material was identified as being close to -45°, where the vertical (Y) axis is defined as 0°, since the highest measured deformation occurred at this MWH orientation. A deformation was generated at this orientation that has a RMS of 0.55 μm and a PV of ~ 2.50μm 1 minute after MWH activation. The deformation results were found to be reproducible when using the same experimental parameters. The performance of the magnetically hard material was also found to be reasonable since the deformation has a RMS of 0.22 μm and a PV of $\sim 1.04\mu$m 12 hours after MWH activation.

4.1 Future Work

Improvements are being considered for the membrane holder to better distribute and measure the tension load. Two possible different membrane holder designs are being considered: (1) A design that consists of two vacuum chambers, one inside the inner ring to form a spherical shape mirrors and one between the inner and outer rings (annulus chamber) to provide precise and measurable control on the membrane pre-strain (tension load); (2) The second membrane holder design is based on the current design but improving on it using a precision vertical stage and a load cell instead of the current linear stage, allowing the membrane tension load to be measured and applied accurately.

A beam expander will also be added by adding a commercial achromatic lens to expand the measurement area from 5×7 mm to a circular area with a diameter of 50 mm, which is the size of current membrane mirror sample. The beam expander will be used for further surface profiling measurements, allowing the whole membrane mirror sample to be measured during experiments. The capability of measuring the whole sample, with the addition of the beam expander, will expand our horizon for exploring our technology's controllability and effects on different length scales. In this study, the largest generated deflection was $\sim 2.50\mu$m over a measured area of 5×7 mm, however being enable to measure the whole sample area will show us over what length scale we cause the deflection. Moreover, the fine scale control of our technology can be investigated with full size measurements, since we can measure the effect of the generated deflection on contiguous areas.

As mentioned in Subsection 2.1, although the MSM material's saturation field strength is $\sim$ 1T, we applied a maximum of just less than 0.1 T in this study due to MWHs limitations. A custom designed and manufactured electromagnet which can generate >0.5 T, has therefore been ordered.

Membrane mirror improvements on the coatings and substrate are also being considered. We are continuously working on advancing our coating quality and exploring new membrane substrates which are more resistant to pre-strain (tension load).

ACKNOWLEDGMENTS

This work was supported by NASA NIAC grant number NNX15AL89G. The authors would also like to thank David Pappas, Dr. Marco Quadrelli, Dr. Peter Takacs, Dr. Ron Shiri, Drs. Steve Arnold and Drs. William W. Zhang for advice and support. We thank Giovanni Pareschi for suggesting working with MSM films in the first place.

REFERENCES

[1] GUIDE, P. P., "DELTA IV PAYLOAD PLANNERS GUIDE," (1998).

[2] Hill, J. R., Wang, K. W., Fang, H., and Quijano, U., "Actuator grouping optimization on flexible space reflectors," in [*Active and Passive Smart Structures and Integrated Systems 2011*], **7977**, 797725, International Society for Optics and Photonics (2011).

[3] Lan, L., Jiang, S., Zhou, Y., Fang, H., Wu, Z., and Du, J., "An experimental study on reflector wavefront error correction using PZT actuators," in [*Active and Passive Smart Structures and Integrated Systems 2016*], **9799**, 97990G, International Society for Optics and Photonics (2016).

[4] Duan, B., Gao, F., Du, J., and Zhang, S., "Optimization and experiment of an electrostatic forming membrane reflector in space," *Journal of Mechanical Science and Technology* **29**(4), 1355–1360 (2015).

[5] Liu, C. and Shi, Y., "Comprehensive structural analysis and optimization of the electrostatic forming membrane reflector deployable antenna," *Aerospace Science and Technology* **53**, 267–279 (2016).

[6] Moore, J. D., Patrick, B., Gierow, P. A., and Troy, E., "Design, test, and evaluation of an electrostatically figured membrane mirror," in [*UV/Optical/IR Space Telescopes: Innovative Technologies and Concepts*], **5166**, 188–197, International Society for Optics and Photonics (2004).

[7] Ulmer, M. P., Coverstone, V. L., Cao, J., Chung, Y.-W., Corbineau, M.-C., Case, A., Murchison, B., Lorenz, C., Luo, G., and Pekosh, J., "APERTURE: a precise extremely large reflective telescope using re-configurable elements," in [*Space Telescopes and Instrumentation 2016: Optical, Infrared, and Millimeter Wave*], **9904**, 99041I, International Society for Optics and Photonics (2016).

[8] Baturalp, T. B., Coverstone, V. L., Coppejans, R., Cao, J., Chung, Y., Wang, X., Buchholz, D. B., and Ulmer, M. P., "Deployment Design of APERTURE: a precise extremely large reflective telescope using re-configurable elements," in [*AIAA SPACE and Astronautics Forum and Exposition*], 5378 (2017).

[9] Coppejans, R., Ulmer, M. P., Buchholz, D. B., Wang, X., Cao, J., Coverstone, V. L., Baturalp, T. B., Condron, K. S., O'Donnell, A. E., and Harpt, B. E., "APERTURE, a precise extremely-large reflective telescope using re-configurable element: a progress report," in [*UV/Optical/IR Space Telescopes and Instruments: Innovative Technologies and Concepts VIII*], **10398**, 103980N, International Society for Optics and Photonics (2017).

[10] Olabi, A.-G. and Grunwald, A., "Design and application of magnetostrictive materials," *Materials & Design* **29**(2), 469–483 (2008).

[11] Wang, X., Yao, Y., Liu, T., Liu, C., Ulmer, M. P., and Cao, J., "Deformation of rectangular thin glass plate coated with magnetostrictive material," *Smart Materials and Structures* **25**(8), 85038 (2016).

[12] Wang, X., Yao, Y., Ye, S., Liu, T., Assoufid, L., Cao, J., and Ulmer, M. P., "Shaping Si, NiCo, and glass substrates via stresses in the coatings," in [*Adaptive X-Ray Optics IV*], **9965**, 99650D, International Society for Optics and Photonics (2016).

[13] Ulmer, M. P., Wang, X., Cao, J., Buchholz, D. B., Assoufid, L., Coppejans, R., Condron, K. S., Harpt, B. E., Mercado, A. M., Qian, J., and O'Donnell, A. E., "Controlling the shapes of coated silicon substrates via magnetic fields, a progress report," in [*Optics for EUV, X-Ray, and Gamma-Ray Astronomy VIII*], Pareschi, G. and O'Dell, S. L., eds., **10399**, 59, SPIE (aug 2017).

[14] Mohanchandra, K. P., Prikhodko, S. V., Wetzlar, K. P., Sun, W. Y., Nordeen, P., and Carman, G. P., "Sputter deposited Terfenol-D thin films for multiferroic applications," *AIP Advances* **5**(9), 97119 (2015).

[15] Speliotis, A. and Niarchos, D., "Magnetostrictive properties of amorphous and crystalline TbDyFe thin films," *Sensors and Actuators A: Physical* **106**(1-3), 298–301 (2003).

[16] Schatz, F., Hirscher, M., Schnell, M., Flik, G., and Kronmüller, H., "Magnetic anisotropy and giant magnetostriction of amorphous TbDyFe films," *Journal of applied physics* **76**(9), 5380–5382 (1994).

[17] Marker, D. K., Rotge, J. R., Carreras, R. A., Duneman, D. C., and Wilkes, J. M., "Minimum strain requirements for optical membranes," in [*High-Resolution Wavefront Control: Methods, Devices, and Applications*], **3760**, 224–232, International Society for Optics and Photonics (1999).

[18] Southwell, W., "Wave-front estimation from wave-front slope measurements," *J. Opt. Soc. Am.* **70**, 998– 1006 (Aug 1980).

APERTURE–a precise extremely-large reflective telescope using re-configurable element: a progress report

R. Coppejans[a], M. P. Ulmer[a], D. B. Buchholz[b], X. Wang[c,d], J. Cao[c], V. L. Coverstone[e], T. B. Baturalp[e], K. S. Condron[a], A. E. O'Donnell[c], B. E. Harpt[f], W. H. Reinhardt[g], and M. E. Johnson[h]

[a]Center for Interdisciplinary Exploration and Research in Astrophysics (CIERA) and
Department of Physics and Astronomy, Northwestern University, 2145 Sheridan Road,
Evanston, IL, 60208, USA
[b]Materials Research Science and Engineering Center, Northwestern University, Technological
Institute, 2145 Sheridan Rd., K111 Evanston, IL, 60208, USA
[c]Department of Mechanical Engineering, 2145 Sheridan Road, Northwestern University,
Evanston, IL, 60208, USA
[d]School of Automotive Engineering, Wuhan University of Technology, 205 Luoshi Road,
Wuhan, 430070, China
[e]Department of Mechanical Engineering, Texas Tech University, Lubbock, TX, 79409, USA
[f]Department of Physics, Massachusetts Institute of Technology, 77 Massachusetts Ave,
Cambridge, MA 02139, USA
[g]Department of Electrical Engineering, 2145 Sheridan Road, Northwestern University,
Evanston, IL, 60208, USA
[h]Department of Electrical Engineering and Computer Science, Northwestern University, 2145
Sheridan Road, Evanston, IL, 60208, USA

7. ABSTRACT

One of the pressing needs for the UV-Vis is an affordable design that allows larger mirrors than the JWST primary. In this publication we report the results of the first year of a NASA Innovative Advanced Concepts Phase II study. Our project is called A Precise Extremely large Reflective Telescope Using Reconfigurable Elements (APERTURE). The concept is to deploy a continuous membrane-like mirror. The mirror figure will be corrected after deployment, causing the figure error to decrease below $\lambda/20$. While the basic concept is not new, our innovation lies in a different approach to correcting the residual figure errors from the classical piezoelectric patch technology.

Instead, our concept is based on a contiguous coating of a magnetic smart material (MSM). After deployment, a magnetic write head will move along the non-reflecting side of the mirror. The magnetic field will produce a stress in the MSM which then corrects the mirror shape. This publication summarizes the results of minimizing the MSM deposition stress as well as the size and stability of the deformation, which is maintained by a magnetically hard material.

Keywords: Deformable, Deployable, Membrane, Space Mirrors, Magnetostriction, Magnetic Smart Materials

8. 1. INTRODUCTION

The following reports our efforts to demonstrate the viability of using magnetic smart materials (MSMs) to correct a deployed membrane.[1] Our NASA Innovative Advanced Concepts (NIAC) funded project is to demonstrate the feasibility of using magnetostriction to correct a deployed membrane mirror. To accomplish this, we used the magnetostrictive stress of applying an external magnetic field to the MSM Terfenol-D^{R} combined with a magnetically hard coating of nickel-cobalt (NiCo). With these corrections the goal is to achieve a deployed figure with RMS figure error below $\lambda/20$ at visible wavelengths (λ = 600nm).

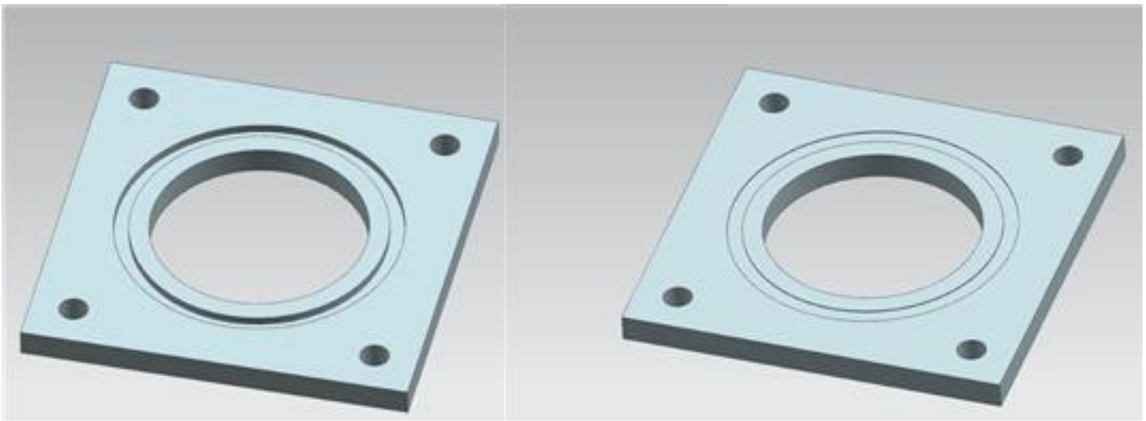
(a) (b)

Figure 1. Illustration of the bottom (a) and top (b) halves of the aluminum membrane fixture.

In Ulmer et al.,[1] we described how this concept would be applied to large (∼ 16 m diameter) space telescope mirrors, and why membrane mirror deployment is needed. Although the original idea for the technique was patented,[2] until our work, no implementation of this concept has been published. Therefore, before addressing the technical hurdles that need to be overcome, we needed to demonstrate the basic concept works well enough to develop further.

Further author information: (Send correspondence to M.P.U. or R.C.)
M.P.U.: E-mail: m-ulmer2@northwestern.edu
R.C.: E-mail: rocco.coppejans@northwestern.edu

UV/Optical/IR Space Telescopes and Instruments: Innovative Technologies
and Concepts VIII edited by Howard A. MacEwen, James B. Breckinridge,
Proc. of SPIE Vol. 10398, 103980N
· doi: 10.1117/12.2274278

We demonstrate below (see also previous work Ref 3) that when an external magnetic field was applied to a Terfenol-D^{R} and NiCo coated Kapton^{R} membrane, a shape deflection was produced on order 2μm over ~ 9mm. Although we show the deflection was present 18hours after the external magnetic field was removed, there are issues that need to be addressed. While the concept produced favorable results, it is in need of maturation.

In this proceeding, we provide the details of this work.

9. 2. METHODOLOGY

In this section we describe how the samples were prepared and measurements taken.

9.1 2.1 Sample preparation

Two different substrates were used: (1) Aluminized Dunmore DE340 Kapton^{R}, comprised of 127μm Kapton^{R} coated with 300˚A aluminum and (2) $5 \times 20 \times 0.2$mm (100) silicon coupons.

For coating and measurement, the Kapton^{R} (membrane) sample was placed in an aluminum fixture shown in Fig. 1. The fixture has a 5cm diameter hole at the center. An o-ring is placed in the guiding groove (depth of 0.3mm) on the top plate (Fig. 1b), then the Kapton is placed on the o-ring, and finally the bottom plate (Fig. 1a) is placed on the Kapton. The plates are held together by four bolts, one at each corner, which can be tightened to increase the in-plane stress of the sample. This forces the o-ring, and the membrane below it, into the deep groove (depth of 2mm) on the bottom plate.

Before coating, the membrane substrate were cleaned with a mild detergent, rinsed with deionized water, blow-dried and placed in the membrane holder. The membrane was placed in the holder such that the Kapton^{R} (non-aluminized) side of the substrate would be deposited upon. Silicon substrates were cleaned by ultrasonically agitating in acetone for 15minutes, ultrasonically agitating in isopropanol for 15minutes, rinsing with isopropanol, rinsing with deionized water and blow-drying.

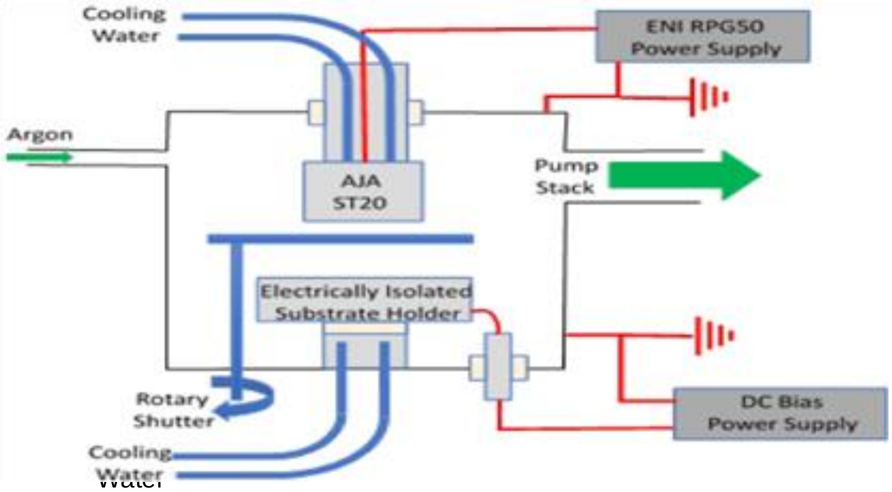

Figure 2. A schematic of the deposition chamber.

In all cases, thin films were deposited on the substrates via direct current (DC) magnetron sputtering, which used an AJAST20 sputtering head and an ENIRPG50 power source (see Fig. 2). In the setup, the sputter chamber was grounded, and the substrate mount was isolated from the chamber so it could be grounded or biased. A target-substrate separation of 70mm was used throughout. Argon was used as the sputtering gas. For the membrane target, Terfenol-D^{R} was deposited at 50W, 17mTorr argon pressure and -100V substrate bias (see Sec. 3). NiCo was always deposited at 100W and 14mTorr argon pressure with the substrate grounded. Similarly, Cr was always deposited at 50W and 17mTorr argon pressure with the substrate grounded. All targets were of the material to be deposited and 5.08cm in diameter. The chamber was fitted with a shutter and all targets pre-sputtered for 10minutes prior to film deposition.

Membrane substrates were coated with a tri-layer of chrome, Terfenol-D^{R} and NiCo. The chrome is an adhesion layer between the Kapton^{R} and Terfenol-D^{R}, while the NiCo serves to hold in the magnetic field and prevents the Terfenol-D^{R} from oxidizing. During coating, a silicon test coupon was fixed with copper tape on top of the fixture and next to the opening. The coupon was used to measure film thickness and radii of curvature. The copper tape holds the coupon in place and defines a step edge for measuring thickness. Each material in the tri-layer was deposited in a separate step, breaking vacuum between each step. The coupons were changed before each layer, and therefore, provided a reliable measurement of each layer's thickness.

9.2 2.2 Measurement and analysis procedure

All measurements were done using a Zygo New View™ 7300 White Light Interferometer (WLI) which has a

0.1nm resolution in the z-direction and 2.21μm in the x- and y-directions. Using a 10× objective

and a zoom of 0.5, the WLI can capture an area of 1.41 × 1.06mm in a single image. Larger areas

were captured by stitching images together using a 25% overlap.

2.2.1 Silicon Samples

For the silicon samples, the film thickness' were measured by using the instrument software to calculate the height of the step edge from a captured image. The values reported in this publication are the average values of measuring six different locations along the step edge. The samples' radii of curvature were measured by scanning an area of 10.96×2.65mm (a 10×3 stitch) centered on the sample. A radius of curvature parallel to the samples long axis was calculated using the instrument software.

The convention used in this study assigned a positive radius of curvature to films that were convex when viewed from the film side (i.e. the film is under compression and exerts a tensile force) and a negative radius to films that were concave as viewed from the film side (i.e. the film is under tension and exerts a compressive force), see Fig. 3.

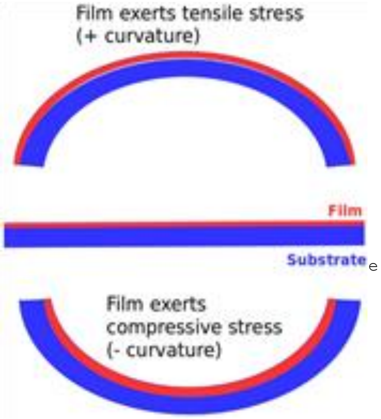

Figure 3. Radius of curvature convention.

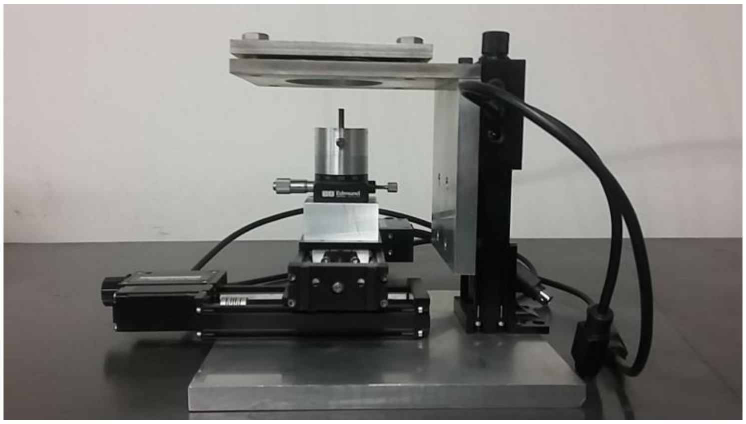

Figure 4. Experimental setup to measure the membrane samples.

2.2.2 Membrane Samples

Membrane samples were measured by placing them in the holder, which was then secured to a set of three computer controlled linear stages (Fig. 4). The setup contained a pair of permanent magnets, 3.175mm in diameter and 25.40mm in height, with a peak field strength of 0.11T.

Because the rim of the membrane was clamped and the inner area exposed, the membrane responded like a drum to mechanical and acoustic vibrations. Vibrations added to the noise of the images. The WLI was unable to image the sample if the amplitude of the vibrations was too large. Therefore, vibrations needed to be minimized. The WLI is mounted on a vibration isolation table, however, the sample could not be left completely loose as mechanical vibrations were noticeably transmitted through it. In addition, acoustic vibrations could be a significant problem. To minimize the effect of vibrations, measurements were only taken after normal work hours. The membrane's in-plane stress was increased by tightening the bolts until a good image was obtained. Most of the time, this only required the bolts to be finger tightened.

Measurements were done in the following way: (1) Three images of a 8.84 × 6.63mm area (a 8 × 8 stitch) of the sample were taken with the magnets as far away as possible. (2) The magnets were moved as close as possible to the sample (< 1mm) and directly below the area imaged in step (1). (3) The magnets were moved as far away as possible from the sample and three more images were taken. (4) Additional sets of images were taken as long as possible after step (2) within the constraints of the WLI's availability.

Typically, it takes about 20minutes to acquire each stitched image. Therefore, the final image in step (3) finished about an hour after the magnets were removed. After each image, the instrument software subtracted a planar fit from it. This removed the arbitrary instrumental offsets between the images and the slope of the sample due to it not being perfectly horizontal. Each image is then exported to text format and read into IDL ^{R}.

To image the deformation caused by applying the magnetic field to the membrane, an image taken before the field was applied (a zero image) was subtracted from each of the images taken after the field had been applied. After subtraction, the images were smoothed using the IDL ^{R} Gaussian smoothing algorithm GAUSS SMOOTH with a six sigma standard deviation value. The image noise was calculated by subtracting the three images that were taken before the magnets were applied from each other, smoothing the images and calculated the standard deviation between the pixel values of the subtraction images.

10. 3. STRESS MINIMIZATION

The deposition parameters affect the properties, specifically the stress, of the deposited film. Films with higher stress have smaller responses. Therefore, before coating membranes we investigated the deposition parameters under which the film stress is minimized using silicon samples coated only with chrome and Terfenol-D ^{R}.

Deposition parameters that affect the film stress include deposition pressure,[4,5] sputtering power[67] and substrate bias.[8] These three variables were studied for their effect on Terfenol-D ^{R} stress, as well as how to minimize it. The goal was to minimize the stress in the deposited film. For a thin film deposited on a substrate, the film stress is proportional to the radius of curvature. For a substrate of a given thickness (t_s), Youngs modulus (Y_s) and Poisons ratio (ν_s), the stress of the film (σ_f) of a given thickness (t_f) is related to the radius of curvature of the film-substrate pair (r) by Stoneys equation:

$$\sigma_f = \left(\frac{Y_s}{1-\nu_s} \right) \frac{t_s^2}{6rt_f}. \tag{1}$$

For the analysis, silicon coupons and values of $t_s = 200\mu$m, $Y_s = 150$GPa, $\nu_s = 0.27$, were used. The film thickness and radii of curvature were measured as explained in Sec. 2.2 and the stress computed with Eq. 1. For the chrome and NiCo films, the thickness and radii of curvature was measurement but the effect of deposition conditions on the film stress was not studied. These films were thin, 10-50nm, relative to the Terfenol-D ^{R} film, $\sim$ 1000nm, and the stress from these films resulted in relatively little strain (curvature) in the final film-substrate materials stack.

The effect of deposition pressure, sputtering power and substrate bias are shown in Fig. 5. The argon sputter pressure, Fig. 5a, and the sputter power, Fig. 5b, have a relatively minor effect on the film stress. The bias voltage, however, has a large effect on the film stress and crosses from positive to negative stress as the bias is made more negative. In Fig. 5c the four points at -50V are significantly different from the trend, which indicates there is noise in the system that we are currently investigating.

The same processing parameters that affect film stress can affect the sputter rate. A very low sputter rate would make the film deposition impractical. Therefore, the sputter rate was studied as a function of the same process parameters used to study film stress. The effect of deposition pressure, sputtering power and substrate bias on the sputter rate are shown in Fig. 6a-c, respectively. All three parameters had a significant effect on the sputter rate, although, with the exception of a deposition power of 25W, all deposition rates were deemed sufficient for use in the Kapton ^{R} studies.

For the film depositions used in the Kapton ^{R} film studies, several considerations went into the decision of deposition parameters. An argon deposition pressure of 17mTorr was chosen based on the film sputter rates and the relative insensitivity of film stress to this parameter. A sputter power of 50W was chosen for multiple reasons. First, the film stress was relatively insensitive to the sputter power. Secondly, the qualitative judgment was that less substrate heating occurred at lower sputter power; therefore, the decision was to minimize heating of the Kapton ^{R} substrate. Finally, the sputter rate was deemed to be sufficient at this power. A substrate bias voltage of -100V was chosen to minimize the film stress. Using these parameters, and despite the previously mentioned noise, we have been able to produce low stress films on Kapton ^{R}.

For X-ray applications, iridium is often used as a reflective coating. However, iridium films have notoriously high stress (on the order of gigapascals[9]), which deforms the mirror substrate. In the past, a number of solutions

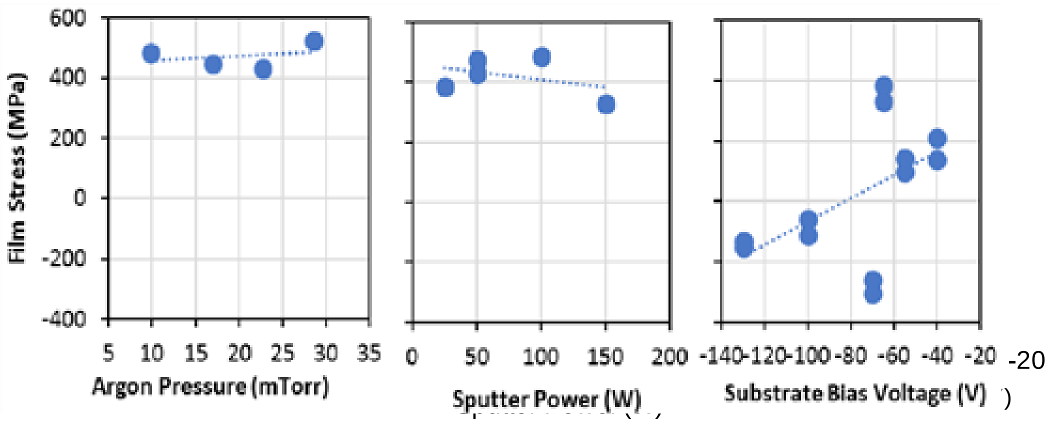

(a) (b) (c)

Figure 5. The effect of a) argon sputter pressure (sputter power 100W, substrate bias voltage -55V) b) sputter power (argon pressure 17mTorr, substrate bias voltage -130V), and c) substrate bias voltage (argon pressure 14mTorr, sputter power 50W) on the stress in Terfenol-D^{R} film stress.

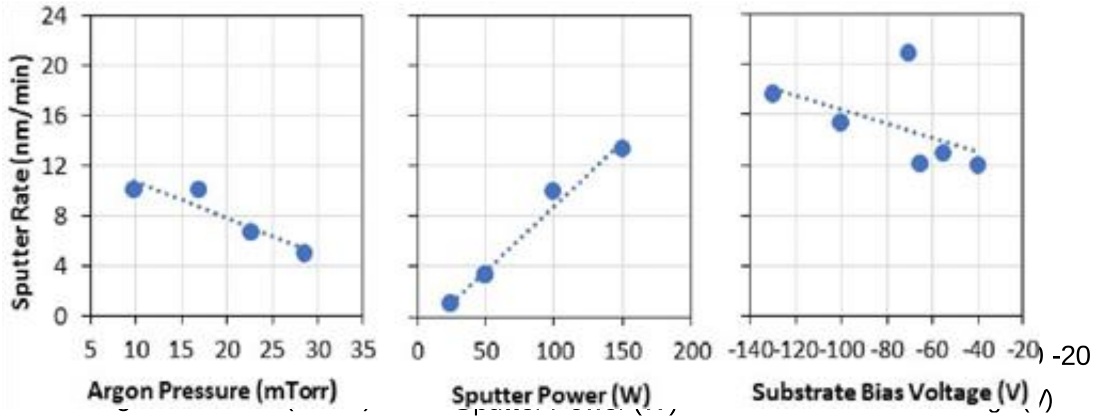

(a) (b) (c)

Figure 6. The effect of a) argon sputter pressure (sputter power 100W, substrate bias voltage -55V) b) sputter power (argon pressure 17mTorr, substrate bias voltage -130V), and c) substrate bias voltage (argon pressure 14mTorr, sputter power 50W) on the sputter rate of Terfenol-D^{R}.

have been explored, including depositing a second film with opposite stress to the iridium coating and depositing the coating on both sides of the substrate.[9] Despite these efforts, a solution to this problem is still needed. The work in this section is important as, using a similar methodology, it is likely that the stress in these coatings can be reduced to allow thinner mirror substrates to be used.

11. 4. MEMBRANE MEASUREMENT

The membrane was manufactured, measured taken and analyzed as described in Sec. 2. The chrome, Terfenol-

D^{R} and NiCo films have average thicknesses over the six measurement of different areas of the step edge of 0.029, 0.984 and 0.047μm, respectively. The radii of curvature in the long dimension of the chrome, Terfenol-D^{R} and NiCo test coupon were measured as -67.3, 23.4m and -49.2m, respectively. The chemical composition of Terfenol-D^{R} is $Tb_xDy_{1-x}Fe_2$ with $x \sim 0.3$. By mass, there is 18% Tb, 42% Dy and 41% Fe in Terfenol-D^{R}. Using the Terfenol-D^{R} test coupon and a Hitachi S-3400N-II scanning electron microscope, we measured the mass percentage of the elements to be 17% Tb, 36% Dy and 47% Fe in the membrane.

During the measurement, the magnets were aligned parallel to the x-axis, with the WLI measuring the coated side of the membrane. After the magnetic field had been applied to the sample, the magnets were moved away from the sample. The magnets were moved 20.6mm in the z-direction and 39.5mm in the xy-plane to give a total separation of 44.5mm between the center of the image and the magnets. Three sets of three images were taken after the magnets had been removed from the sample. The first set was taken immediately after the magnets had been removed, the second was started three hours after and the third was started 19 hours after. All of the images were taken on the same day except the final set of images. We will refer to the images as e.g. image 2-3, where the first number indicates the image set and the second the number of the image in that set.

Subtracting the three images that were taken before the magnetic field was applied from each other, three difference images were generated. These images have median values of 3, 4 and 6nm, respectively, and standard deviations between the image pixels of 65, 39 and 41nm. Based on this, the pixel uncertainty was set to 65nm for all images. As all three of these image are extremely similar, the first was arbitrarily chosen as the subtraction image for all subsequent images taken after the magnetic field had been applied to the sample.

Two example images taken after the application of the magnetic field are shown in Fig. 7. In previous work using NiCo and glass substrates, we also obtained convex deformations.[3,10,11] To determine the size of the deformation in each image, we averaged the central 30 rows (1% of the total rows) of the images together and plotted the data as illustrated in Fig. 8. In both Fig. 7 and Fig. 8 there is no indication that the slope of the deformation is decreasing near the edge of the image. We therefore conclude that the deformation is larger than the imaged area of 8.84 × 6.63mm.

The surface profiles from averaging the central 30 rows together were fitted with a parabola of the form

$$y = \frac{(x-b)^2}{2R} + c \tag{2}$$

using a linear least-squares fitting routine. The surface profiles and fits are shown in Fig. 8. In the equation, c is a constant, b is the x-value of the vertex of the parabola and R is the radius of curvature of the parabola at the vertex. The maximum difference between the peak of the fitted parabola and the edge of the image was calculated (Tab. 1). The linear distance of the measurement was also calculated. Using these two values and the small angle approximation, the angular size of the deformation was calculated and is shown in Tab. 1. A plot of the deformation size and the angular deformation as a function of time is shown in Fig. 9. The uncertainties of the deformation sizes calculated using standard error propagation are very small (between 1 and 2nm), and therefore underestimated. For the reasons discussed later in the section, we elected to conservatively set the uncertainty on the deformation size to 0.5μm. Because the deformation is larger than the imaged area, the values in Tab. 1 are lower limits.

Comparing the values of image 3-1 in Tab. 1 to those of images 3-2 and 3-3, it is clear that image 3-1 is significantly different from images 3-2 and 3-3. While images 3-2 and 3-3 have very similar convex shapes similar to all of the other images, image 3-1 has a central ridge parallel to the y-axis. We believe that image 3-1 (which

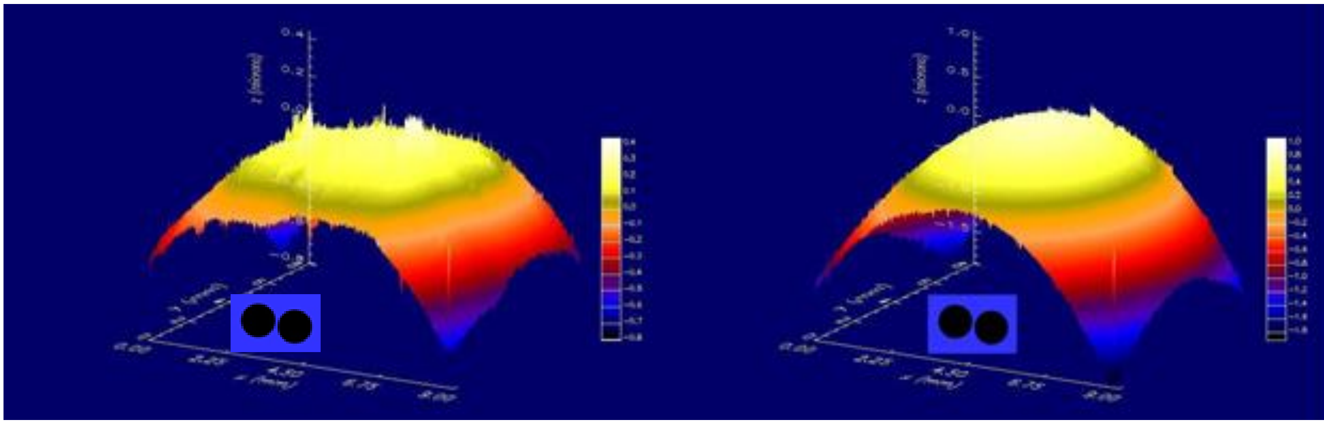

(a) (b)

Figure 7. Example images of the deformation. (a) Image 2-2 taken approximately three and a half hours after the magnets were removed and (b) image 3-3 taken approximately 20 hours after the magnets were removed. The orientation of the magnets (not to scale) are indicated by the black circles.

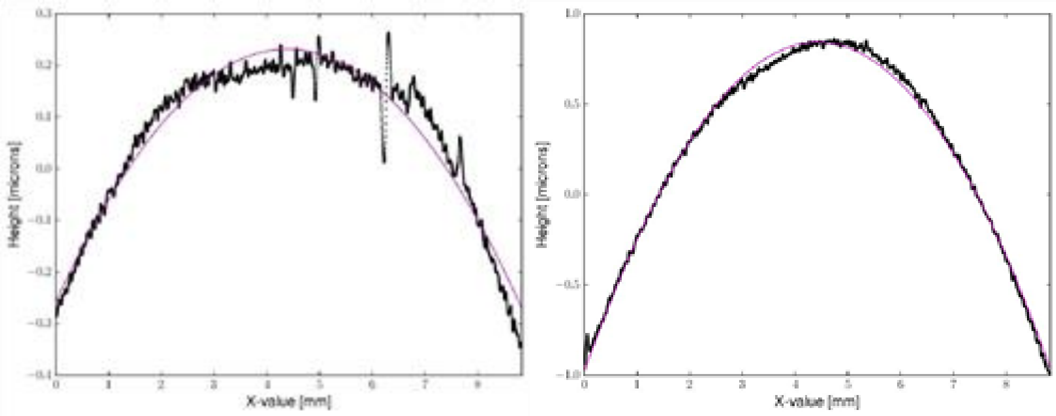

(a) (b)

Figure 8. Example of two line cuts through the centers of (a) image 2-2 and (b) image 3-3. In both images the cut is shown in black and the parabola fitted to it as a magenta line. Note that (a) appears more noisy than (b) due to the scale of the y-axis differing.

Table 1. Size of the deformation.

Image	Deformation Size [μm]	Angular Deformation [arcsec]
1-1	0.248 ± 0.5	10.17 ± 20.48
1-2	0.349 ± 0.5	15.38 ± 22.06
1-3	0.391 ± 0.5	17.16 ± 21.93
2-1	0.328 ± 0.5	15.05 ± 22.95
2-2	0.501 ± 0.5	23.27 ± 23.20
2-3	0.898 ± 0.5	41.43 ± 23.06
3-1	0.583 ± 0.5	26.57 ± 22.78
3-2	1.559 ± 0.5	72.59 ± 23.29
3-3	1.822 0.5	84.84 23.29

± ±

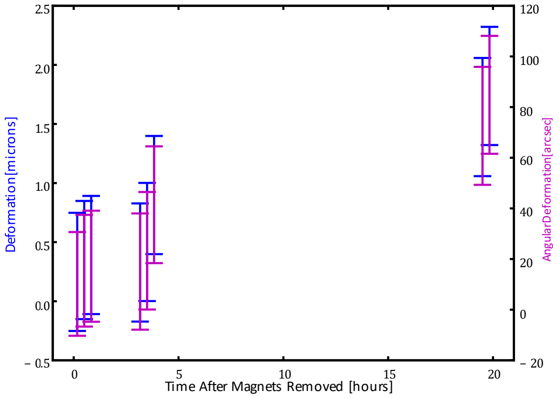

Figure 9. The deformation size and the angular deformation plotted as a function of time. The values for image 3-3 were not included for the reasons explained in the text.

was the first image taken on the second day) is different because of noise or an error in this image, and discount this image in further analysis.

From Figs. 7 and 8 and Tab. 1, it is clear that the shape of the deformation changes between images. The size of the deformation increases between images in a within a set and between image sets. In Wang et al.[3] our group measured a $50 \times 50 \times 0.05$mm NiCo substrate coated with 2μm Terfenol-D ^{R} using the same setup and procedure described in Sec. 2. Three measurements were done 9, 23 and 71hours after the magnetic field had been removed. In their experiment, the deformation did not change between the three epochs within the measurement noise of $\pm 0.3\mu$m.[3] It is likely that the reason why we see the average size of the deformation increasing between image sets in this study, but not in Wang et al.,[3] is due to the different substrates in the two studies.

Tests of the experimental setup indicates that there could have been thermal variations in the system of $\sim 3^{o}$C between the three images in the second and third image sets. Further measurements on the membrane that did not include varying the magnetic field indicated that the temperature variations could produce deflections of $\sim 1\mu$m in the opposite direction of those shown in Figs. 7 and 8. Thus, most of ($> 50\%$), if not all, the deflection in Figs. 7 and 8 and Tab. 1 are most likely due to magnetostriction. This conclusion is consistent (in terms of magnitude of the deflection and the direction of the deflection) with previous work,[3] where the expected defection was estimated from an application of Stoneys equation using a magnetic field of ~ 300G (~ 0.03T) that extended from NiCo film into the Terfenol-D^{R}. While we do not expect that this problem affects the first image set, we none the less increased the uncertainty on the deflection size to 0.5μm for all three image sets.

This temperature sensitivity indicates that: (a) In the future we need to control the environmental temperature to 1^{o}C or better and/or (b) choose a substrate that has a closer coefficient of thermal expansion to Terfenol-D^{R}.

From Tab. 1 and Eq. 2, the deformation in image 3-3 has a radius of curvature of 5.383 ± 0.005m. Using Eq. 1, we can calculate the magnetostrictive stress using $t_s = 127\mu$m, $t_f = 0.984\mu$m, $Y_s = 2.5$GPa and $\nu_s = 0.3$. From this, the uniaxial magnetostrictive stress ($\nu_s = 0$) is 1.27MPa and the equi-biaxial stress is 1.81MPa.

In the technical information on Kapton^{R}, the manufacturer (Dupont™) indicates that 25.4μm Kapton^{R} placed under 6.5MPa of tensile stress at 26^{o}C will creep. The creep stabilizes at a material elongation of 0.2% after a period of 2-17hours.[12] Since we used 127μm Kapton^{R} at a lower stress, we do not expect that the deformation not stabilizing is a result of the Kapton^{R} irreversible deforming. Kapton^{R} is also known to be sensitive to humidity changes.[12] Once again, we do not expect that this is the reason for the deformation not stabilizing since the Kapton^{R} is sealed from the environment on both sides. However, the possibility cannot be completely ruled out.

While the size of the deformation changing may, at first glance, appear problematic we note that: (1) The purpose of the experiment was to show that a deformation could be generated and held in place after the external magnetic field had been removed. (2) Additional measurements will in future be done over a longer time period to determine how long it takes the deformation to stabilize. (3) As noted in Sect. 5 we are currently examining methods of increasing the size of the deformation. Among other things, this includes using a thicker layer of Terfenol-D^{R}, which would increase the Young's modulus of the composite and likely decrease the relaxation time. (4) We are also investigating replacing Kapton^{R} with another substrate.

Despite the problems with the stability of the deformation and that there are a lot of parameters that can be changed to increase the size of the deformation (see Sec. 5), we did manage to achieve a deformation of between 0.25 and 1.82μm, or an angular deformation of between 10 and 85arcsec. As the imaging area is smaller than the deformation, these values are lower limits. We conclude that there is promising evidence that magnetostriction can be used to change the shape of a membrane mirror.

11.1 5. SUMMARY AND CONCLUSION

In this publication, we report on work that we have done towards developing deployable membrane mirrors composed of a membrane substrate (such as Kapton ^{R}) that has been coated with a MSM and a magnetically hard material (NiCo). The MSM and NiCo thin films are deposited via DC magnetron sputtering. We discussed work done to minimize the stress in the coatings and showed that by changing the bias voltage of the substrate the stress in the coating can be changed from compressive to tensile. We further found there is a bias voltage (near -100V) where the stress in the coating is minimized. We also found that the two other processing parameters that were studied, argon pressure and sputter power, do not significantly affect the film stress. Using this method, we have successfully coated low stress films.

We also showed that by applying an in-plane external magnetic field of 0.11T to the composite, the magnetostrictive stress from the MSM generates a deflection in the membrane surface. We measured the size of the deflection 0, 3 and 19hours after the external field was applied and found it to increase from 0.25 to 1.82μm over the maximum measurement dimension of 8.84mm. In Wang et al.[3] our group measured a 50 × 50 × 0.05mm NiCo sample coated with 2μm Terfenol-D $_{R}$ using the same setup and procedure. During this experiment, three measurements were done 9, 23 and 71hours after the magnetic field had been removed. The authors found that the deformation did not change between the three epochs within the measurement noise of ±0.3μm.[3] It is likely that the reason why we see the average size of the deformation increasing between image sets in this study, but not in Wang et al.,[3] is due to the different substrates in the two studies.

We additionally found that the size of the deflection varied between the three images taken at each epoch. Further measurements on the membrane that did not include varying the magnetic field indicated this was caused by a $\sim 3^{o}$C thermal variation of the sample. Environmental temperature control of 1^{o}C or better is therefore required in future experiments, and we will investigate substrates that has a closer coefficient of thermal expansion to Terfenol-D ^{R}. In future experiments, we will also determine the time needed for the deflection to stabilize and study ways of minimizing this problem. If a solution cannot be found, the Kapton ^{R} membrane will be replaced with another substrate for which this is not a problem.

Despite the change in the size of the deflection, we did manage to achieve a deflection as large as 1.82μm or an angular deformation of 85arcsec. As the imaging area is smaller than the deflection, these values are lower limits. We conclude that there is promising evidence that magnetostriction can be used to change the shape of a membrane mirror.

5.1 Future work

We are currently investigating methods of increasing the size of the deformation. This includes increasing the thickness of the Terfenol-D ^{R}, increasing the strength of the external magnetic field applied to the samples, annealing the membrane to decrease film stress and annealing the membrane in an external magnetic field to set the easy direction. Preliminary results indicate this increases the size of the deformation. We are also working on re-designing our linear stage setup to allow the use of electromagnets, which will allow us to increase the strength of the field applied to the membrane and determine the amount of figure control. The later will be done by creating a deformation before determining the minimum amount by which we can change it by changing the field strength.

11.2 ACKNOWLEDGMENTS

This work was supported primarily by NASA NIAC grant number NNX15AL89G as well as synergistic work for adaptive X-ray optics supported NASA (Grant NNX16AL31G). The authors would like to thank Dr. Lahsen Assoufid at Argonne National Laboratory for providing silicon substrate samples. The authors would also like to thank David Pappas, Dr. Marco Quadrelli, Dr. Peter Takacs, Dr. Ron Shiri, Drs. Steve Arnold and Drs. William W. Zhang for advice and support. We thank Giovanni Pareschi for suggesting working with MSM films in the first place. We also thank the ISEN center at Northwestern University for providing funds for purchasing additional sputtering guns that were used for a portion of the coating work done here. This work made use of the EPIC facility of Northwestern Universitys NUANCE Center, which has received support from the Soft and Hybrid Nanotechnology Experimental (SHyNE) Resource (NSF ECCS-1542205); the MRSEC program (NSF DMR-1121262) at the Materials Research Center; the International Institute for Nanotechnology (IIN); the Keck Foundation; and the State of Illinois, through the IIN. We thank Yip-Wah Chung for advice on coating, materials, and magnetics. BH was supported by an Illinois Space Grant summer research scholarship and AO was supported part both by an Illinois Space Grant summer research scholarship and a Northwestern University Undergraduate Research grant.

11.3 REFERENCES

[1] Ulmer, M. P., Coverstone, V. L., Cao, J., Chung, Y.-W., Corbineau, M.-C., Case, A., Murchison, B., Lorenz, C., Luo, G., Pekosh, J., Sepulveda, J., Schneider, A., Yan, X., and Ye, S., "APERTURE: a precise extremely large reflective telescope using re-configurable elements," in [*Space Telescopes and Instrumentation 2016: Optical, Infrared, and Millimeter Wave*], *Proc. SPIE* **9904**, 99041I (July 2016).

[2] Racz, L. and Joshi, C., "Magnetostrictive thin film actuator," (July 31 2007). US Patent 7,250,839.

[3] Wang, X., Yao, Y., Ye, S., Liu, T., Assoufid, L., Cao, J., and Ulmer, M. P., "Shaping Si, NiCo, and glass substrates via stresses in the coatings," in [*Society of Photo-Optical Instrumentation Engineers (SPIE) Conference Series*], *Proc. SPIE* **9965**, 99650D (Sept. 2016).

[4] Chinmulgund, M., "Effect of Ar gas pressure on growth, structure, and mechanical properties of sputtered Ti, Al, TiAl, and Ti3Al films," *Thin Solid Films* **270**, 260–263 (Dec. 1995).

[5] El Khakani, M. A., Chaker, M., and Le Drogoff, B., "Iridium thin films deposited by radio-frequency magnetron sputtering," *Journal of Vacuum Science Technology* **16**, 885–888 (Mar. 1998).

[6] Rizzo, A., "Structural and optical properties of silver thin films deposited by RF magnetron sputtering," *Thin Solid Films* **396**, 29–35 (Sept. 2001).

[7] Kola, R. R., Celler, G. K., Frackoviak, J., Jurgensen, C. W., and Trimble, L. E., "Stable low-stress tungsten absorber technology for sub-half-micron x-ray lithography," *Journal of Vacuum Science Technology B: Microelectronics and Nanometer Structures* **9**, 3301–3305 (Nov. 1991).

[8] Kim, S., "A study on the crystallographic orientation with residual stress and electrical property of Al films deposited by sputtering," *Thin Solid Films* **322**, 298–302 (June 1998).

[9] Chan, K.-W., Zhang, W. W., Windt, D., Hong, M.-L., Saha, T., McClelland, R., Sharpe, M., and Dwivedi, V. H., "Reflective coating for lightweight x-ray optics," in [*Space Telescopes and Instrumentation 2012: Ultraviolet to Gamma Ray*], *Proc. SPIE* **8443**, 84433S (Sept. 2012).

[10] Wang, X., Yao, Y., Liu, T., Liu, C., Ulmer, M. P., and Cao, J., "Deformation of rectangular thin glass plate coated with magnetostrictive material," *Smart Material Structures* **25**, 085038 (Aug. 2016).

[11] Wang, X., Yao, Y., Cao, J., Vaynman, S., Graham, M. E., Liu, T., and Ulmer, M. P., "Investigation of magnetically smart films applied to correct the surface profile of light weight X-ray optics

in two directions," in [*Society of Photo-Optical Instrumentation Engineers (SPIE) Conference Series*], *Proc. SPIE* **9603**, 96031O (Sept. 2015).

[12] "Dupont™ Kapton ^{R} summary of properties." http://www.dupont.com/content/dam/dupont/products-and-services/membranes-and-films/polyimde-films/documents/ DEC-Kapton-summary-of-properties.pdf. Accessed: 2017-07-24.

Deployment Design of APERTURE: A precise extremely large reflective telescope using re-configurable elements

Turgut B. Baturalp[1], Victoria L. Coverstone[2]
Texas Tech University, Lubbock, Texas, 79409, USA

Rocco Coppejans[3], Jian Cao[4], Yip Wah Chung[5], Xiaoli Wang[6], David B. Buchholz[7], Melville P. Ulmer[8]
Northwestern University, Evanston, Illinois, 60208, USA

Larger mirrors, even than the primary mirror of the JWST, is a necessity for the UV-Vis design to go further. Our NASA Innovative Advanced Concepts (NIAC) funded project is called A Precise Extremely large Reflective Telescope Using Reconfigurable Elements (APERTURE). The project is based on the idea of deploying a large, continuous, flexible membrane mirror and correcting the mirror shape after deployment to within λ/20 deviations. The main contribution of this study is executing the corrections using a contiguous coating of a Magnetic Smart Material (MSM) instead of using classical piezoelectric-patch or electrostatic actuation technology. The corrections are applied by a magnetic write head which will move on the non-reflective side of the membrane mirror. In this paper, selection and design process of the deployment mechanism, and the design of the experimental setup for surface measurements is discussed. The design process of the deployment mechanism for the flexible membrane mirror is presented, lessons learned from it, and future work that needs to be done.

12. Nomenclature

λ = wavelength
R_F = allowable minimum radius of curvature
ω = allowable deflection
t = thickness of the material
E = young's modulus of the material
H = plasticity model constant
n = strain hardening exponent
λ_{min} = shortest operating wavelength
ϵ = strain
σ = stress
f = focal length
D = outer diameter of the mirror

---

[1] Postdoctoral Research Associate, Department of Mechanical Engineering, 7th & Boston Ave., Mail Stop 1021, Member.

[2] Professor, Department of Mechanical Engineering, 7th & Boston Ave., Mail Stop 1021, Fellow.

[3] Postdoctoral Research Associate, Center for Interdisciplinary Exploration and Research in Astrophysics (CIERA) and Department of Physics and Astronomy, 2145 Sheridan Road.

[4] Professor, Department of Mechanical Engineering, 2145 Sheridan Road.

[5] Professor, Department of Materials Science and Engineering, 2145 Sheridan Road.

[6] Postdoctoral Research Associate, Department of Mechanical Engineering, 2145 Sheridan Road.

[7] Pulsed Laser Deposition Facility Manager, Materials Research Science and Engineering Center, 2145 Sheridan Road.

[8] Professor, Center for Interdisciplinary Exploration and Research in Astrophysics (CIERA) and Department of Physics and Astronomy, 2145 Sheridan Road.

I. Introduction

DEVELOPING large size, lightweight, and precise reflectors is an on-going problem in the field of space telescopes. The size of the primary mirror is an essential driver for ultraviolet-visible telescope designs; however, there are some physical limitations on the size of the primary mirror such as weight, folded volume and reflective surface accuracy. The well-known space telescopes of the ultraviolet-visible type Hubble Space Telescope and the near-infrared James Webb Space Telescope (JWST) have a diameter of 2.4 m and 6.5 m, respectively. However, the Delta Heavy IV[1] rocket fairing limits the payload to a diameter of 4.6 m and a height less than 17 m. As a result, the cylindrical cargo shape can carry larger mirrors, if the stowed configuration of the mirror compliances with the cylindrical shape. One approach to investigate this, is a deployable mirror design. Within this category, there are segmented mirrors like JWST. A preliminary conservative approach of scaling up JWST by unfolding rigid segments would yield a design with a maximum diameter of ~ 12 m [2]. Another approach to deployable space optics is the MOIRE[3] optic design supported by DARPA. The MOIRE concept uses diffraction, rather than reflection or refraction, and is therefore only sensitive to a very small range of wavelengths. The concept is, therefore, not competitive with the traditional broadband mirrors of the same size. Our concept is to achieve reflecting space mirrors that are larger than 12 m diameter using deployable membrane optics.

Our project develops the idea of deploying a large (≥16 m diameter), continuous, and flexible membrane mirror. After the initial surface is set during the deployment, the surface is corrected to an accuracy of $\lambda/20$, where λ is 600 nm. In literature, the prominent methodologies for membrane mirror correction are using piezoelectric-patch[4] and electrostatic actuation[5] technologies. The main difference of APERTURE from these methods, is the use of coating as an actuating material so that the correction actuation is not localized anymore. Corrections can, therefore, be made any location on the membrane mirror, while it can only be done on the patch locations for the other methods. The corrections are applied by a magnetic write head which moves on the non-reflective side of the membrane mirror. The magnetic write head moves along the non-reflective side of the mirror and generates a magnetic field that produces a stress in the MSM that corrects the mirror shape. Fig. 1 demonstrates the conceptual representation of the membrane mirror and the magnetic write head in deployed and stowed configurations.

Because of the nature of the novel MSM based shape correction approach, a tradeoff between structurally supporting and magnetically controlling the shape of membrane mirror has emerged. This tradeoff and the need of high figure accuracy after deployment requires a modified solution other than those previously studied and used such as the Tracking and Data Relay Satellites (TDRS)[6] or the AstroMesh™ design[7]. The problem with these approaches is that they have yet to achieve sufficient figure accuracy required at S, Ku and Ka-band wavelengths (respectively ≈ 150 mm, ≈ 20 mm, ≈ 11 mm). If one assumes a Strelh ratio of 90%, then the Ka-band wavelength corresponds to a figure Root Mean Square (RMS) error of about 11 mm/20. Since APERTURE is meant to be used for UV-Vis observations, a similar Strelh ratio would lead to a RMS of (400 nm)/20 (or better for the deep UV). Hence, if a deployed membrane mirror is to be employed, post deployment corrections will need to be applied. What is novel about our concept is that the corrections will be applied to a contiguous film that has been deposited on a monolithic membrane.

Figure 1. Conceptual views of the APERTURE telescope in fully deployed configuration (left side) and in stowed configuration (right side) (For simplicity only one magnetic write head is shown).

The aim for the diameter size is ≥ 16 m and the desired shape of the membrane mirror is chosen as a concave parabolic shape with a focal length to diameter ratio of the f/D = 1. This f/D ratio enables the placement of the secondary mirror at the tip of the stowed configuration of the membrane as shown in Fig. 1 and to fit in the Delta Heavy IV rocket fairing. The closeness to this desired parabolic shape right after deployment is crucial for the project, since the required time for post deployment shape correction is directly related to the figure error. If the time during which the MSM holds its shape is shorter than the time needed to correct the figure after deployment, the design would not be feasible.

In this proceeding, various issues in a membrane mirror telescope deployment design, such as micro-yielding, selection process of deployment mechanism, design of the experimental setup for surface accuracy measurements, and membrane preparation for deployment is discussed and presented. In Ulmer et al.,[8] the application of this concept to large (~ 16 m diameter) space telescope mirrors is explained in detail. But first, the concept should be shown to be feasible, thus it is necessary to demonstrate the performance of membrane mirrors on scaled down samples. We provide initial details of the scaled down deployment and experimental setup designs in this work.

II. Methodology

Although the ultimate goal of this project is to apply our concept to large parabolic shape space telescope mirrors, the concept should first be proven on scaled down spherical prototypes for feasibility purposes. Thus, the design and prototyping effort on this phase of the project is based on a 30 cm diameter spherical mirror. In this chapter, the conditions of micro-yield (and how it effects our maximum allowable deflection), design and development of the experimental setup, deployment mechanism and preparing the membrane for mechanism assembly is addressed.

A. Micro-Yield Condition

One design parameter that influences deployment is membrane thickness and risk of micro-yield. Given the dimensions of the desired rocket fairing, if a mirror is monolithic then it needs to be flexible. Moreover, the thinner a membrane is, the easier it is to make corrections with a magnetic write head. However, a thin membrane would not be able to hold a parabolic shape without stiffeners.

Micro-yield (microscopic plastic deformations) also needs to be taken into account in the calculation of the membrane thickness. While it is necessary to make sure that the membrane can be folded without being damaged, there is a minimum radius of curvature allowable before producing micro-yields in the structure. The minimum radius of curvature depends on the materials that are used to make the membrane. Kapton^{TM} and Mylar^{TM} substrate membrane materials were selected for the mirror due to their variety of commercially available thicknesses. A micro-yielding analysis was conducted in our previous work[8]. The flexibility of a material, or allowable minimum radius of curvature

(R_F), can be computed according to the analytic approach of Domber and Peterson[9]. Usually, the criterion of the elastic "0.2%" yield stress is chosen, but for optical components even small residual strains should be considered. The calculation of R_F is given by Eq. (1).

$$R_F \approx \left(\frac{\omega t}{\pi^2}\left(\frac{2H}{tE}\right)^{\frac{1}{n}}\right)^{\frac{n}{2n-1}} \tag{1}$$

Here the variable ω is the allowable deflection, t is the thickness of the material, E is the Young's modulus of the material, H is the plasticity model constant, and n is the strain hardening exponent. The length of the curved surface has been approximated as $2\pi R_F$ [10] which is true for localized curvature (i.e. our deployment concept). The main hypothesis behind this formula is that, for very small deformations, the plastic term in the Ramberg-Osgood model (Eq. 2) can be neglected with regards to the elastic term.

$$\epsilon = \frac{\sigma}{E}\left(\frac{\sigma}{H}\right)^{\frac{1}{n}} \tag{2}$$

The plastic parameter H and the exponent n can be found using the Ramberg-Osgood model for one-dimensional yield. The strain-stress curve of a material can be approximated by the model represented by Eq. 2. A least-squares approximation, applied to the 23°C strain-stress curve for Kapton™, leads to n_{KAPTON}=0.238 and H_{KAPTON}=0.249 GPa. The same method is applied to Galfenol[11]. The exponent n takes a value between 0 and 1. The smaller n is, the more plastic the material is. For aluminum Al 2014-T6, the value for H and n have been found in the literature[9]: H = 0.68 GPa, n = 0.06. To compute R_F using Eq. 1, a value for the deflection ω must be chosen. Usually, the maximal deflection allowed for a mirror is expressed as a fraction of the shortest operating wavelength of the reflector[10] (Eq. 3).

$$\omega_{max} \leq \lambda_{min}/20 \tag{3}$$

For APERTURE, λ_{min} is about 200 nm for the UV and the lower limit value is chosen as 1/20. Thus, $\omega_{max} \leq$10nm. However, APERTURE will use post deployment corrections. Hence, it is reasonable to take a higher value for the maximal deflection, such as 1 micron.

B. Experimental Setup Design for Surface Profiling.

The initial scaled down deployment prototypes will have a diameter of 30 cm and their surface accuracy will be measured using a surface profiler to check if the post deployment surface accuracy is within reasonable limits. The design of the experimental setup was started with the selection of a suitable surface profiler. There are various technologies in the market for surface profiling such as interferometry, contact stylus, confocal microscopy, photogrammetry and shack-hartmann setups. The flexible nature of the membrane mirror ruled out the contact stylus surface profilers. Also, confocal microscopy is eliminated because the lack of capability on measuring large samples. Many vendors were contacted for interferometry, photogrammetry and shack-hartmann setups. The following specifications were sought out:

- Capability of large surface sample measurement (up to 50 cm diameter).
- The ability to measure a f/D=1 parabolic or spherical mirror with a 30 to 50 cm diameter without stitching surface measurements (Stitching requires the sample or measuring device to be moved which decreases the accuracy of the measurements since the concept is based on flexible components).
- A large dynamic range.
- Cost efficiency.
- System flexibility. The system should be easily re-configured for various work pieces that have different dimensions since the aim is to use larger prototypes later in the project.
- A resolution of at least 0.5 microns in z direction.
- The spatial resolution should be less than 5 mm in x and y directions.
- Quasi-static measurement rate will be sufficient.
- A partial area (%20-25) at the center can be ignored.
- Insensitivity to vibration.

Based on these specifications, interferometers with the capability of measuring large surfaces were found costly and the resolution of most photogrammetry devices were found lower than that required. Shack-hartmann setups, therefore, came forward with their versatility, broad dynamic range, cost efficiency and insensitivity to environmental effects such as vibration and temperature fluctuations. We contacted numerous shack-hartmann setup vendors and finally selected HASO4 RFlex50 from Imagine Optics Inc. due to its compact solution, broad dynamic range, 50 x 68 spatial points, and standard accuracy of λ/100, λ/200 in double pass configurations.

The next aspect of the experimental setup design was developing a protected environment for the tests. Design parameters of the experimental setup enclosure are: temperature controlled environment, dust/AC blow protection, ease of reach and height adjustability for different diameter samples. The CAD design of the experimental setup is shown on the left-hand side, while the actual setup is shown on the right-hand side of Fig. 2. The main components and dimensions of the experimental setup is indicated on the CAD design figure on the left of Fig. 2.

Although the shack-hartmann setup is immune to temperature fluctuations, the membrane mirror samples are laminated with different materials, thus temperature fluctuations might be a problem for the samples. The team is aware of the coefficient of thermal expansion considerations for the space application materials, but it's neglected in this early proof of concept phase of the project. Therefore, this issue is addressed by stabilizing the temperature in the experimental setup. A commercial PID temperature controller which is equipped with a RTD Probe for Air (accuracy of ±0.2°C) and a heat sheet is used to control the temperature in the enclosure.

The enclosure is sealed for not only temperature stabilization, but also protection of the flexible samples from dust or air currents originating from the air conditioning system or people. As shown in Fig. 2, the conflict between sealing and ease of reach is solved by using a sliding panel door secured by a latch. The structural components of the experimental setup enclosure are acrylic panels and t-slotted black anodized aluminum framing. The use of t-slotted frames enabled height adjustability for the shack-hartmann profiler which is required to be able to work on different diameter samples. The experimental setup enclosure was designed in dimensions of 2x2 feet base and 4 feet height. These dimensions were chosen based on the desired sample size range (30-50 cm diameter) and related height of the surface profiler (twice the sample diameter).

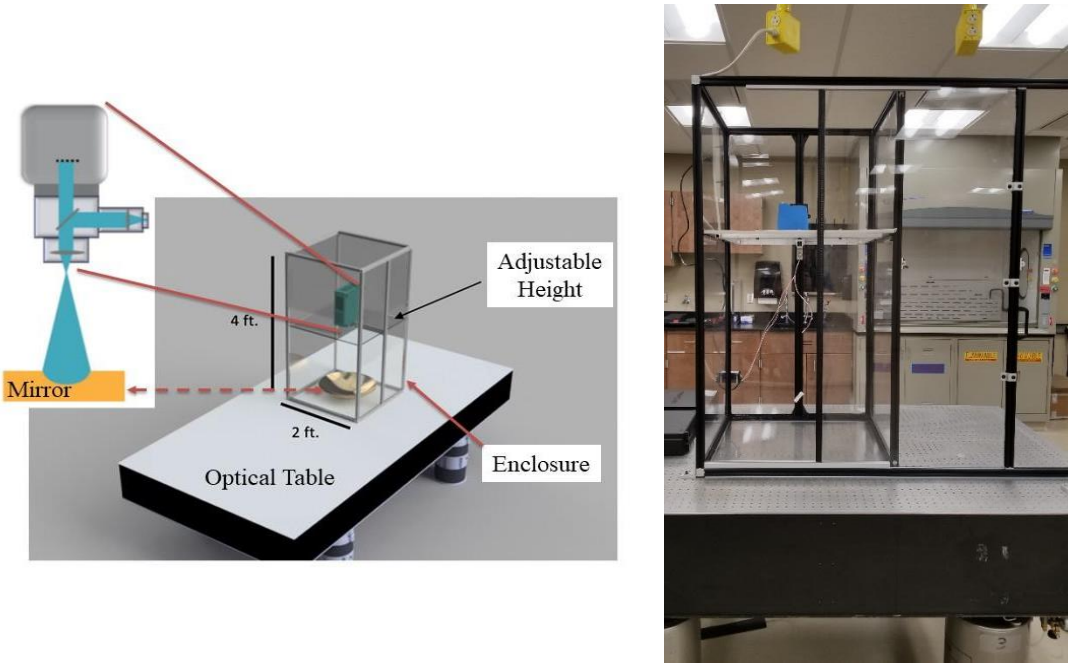

Figure 2. Design of the experimental setup (left side), a picture of the actual experimental setup (right side)

The vibration isolation is provided by a pneumatically damped optical table.

C. Design Process of the Deployment Mechanisms

A wide literature survey was conducted at the start of the deployment mechanism design, it has been seen that the major necessary differentiation in this concept is the tradeoff between required flexibility (low enough in-plane stress) for MSM corrections and low initial post deployment figure error. Most of the designs in the literature are focused on rigid high surface accuracy mirror surfaces since shape correction is not included or driven by more rigid structural elements like piezo electric actuators or tension wires. Two of the main criteria of our deployment concept are: (1) the ability to stow the primary mirror into a Delta IV Heavy rocket fairing without damaging the surface, and (2) deploying the mirror in space while assuring that the final shape is precise enough to be corrected by magnetostriction. Other relevant parameters are the stowed volume efficiency, the stability, and the launch mass.

There are articulated and expandable mast structures in the literature for space structures but demanding high surface accuracy of visible range telescopes eliminated this option. Other common deployment methods such as taco shell, tension mesh, segmented architecture, and inflatable structures are also not preferred due to the need of flexibility. Therefore, the tradeoff between flexibility of the membrane for MSM correction and having a close enough shape to the desired membrane shape, can be carried out by using fan-fold or umbrella-rib deployment designs since they offer both. In other words, the in-plane stress of the membrane should be as low as possible (relaxed state which occurs between the ribs) so that it can be corrected by a magnetic write head and at the same time the surface accuracy of the membrane mirror should be high (occurs on the ribs) enough for the functionality of the telescope. The ribs are reference surfaces for high surface accuracy.

The deployment mechanism design was based on a 30 cm outer diameter, spherical shaped mirror with f/D equals to 1. The inner circle with 6 cm diameter was considered as a hole. The first design iteration is pictured in Fig. 3 in stowed (left) and deployed (right) configurations. A disadvantage of the first iteration is that it has wide ribs which makes manufacturing difficult due to the top-bottom and side-side curved spherical surfaces, and also the lack of additional reference surfaces such as an outer ring which assists and drives the deployment movement of the membrane.

Figure 3. First iteration of deployment mechanism design in the stowed (left) and deployed (right) configurations.

Additional outer ring reference surfaces were added in the second and third iteration deployment designs which are shown in Fig. 4 in the deployed configuration. The outer ring reference surfaces were designed to fold downwards during the stowing action. It has been found in the preliminary mechanism analysis that the downward folding action was impossible due to the shift of rotation planes during the folding action. We have concluded that the number of degrees of freedom of the outer ring reference arms (blue and red parts in Fig. 4) was not enough to complete the downward folding action. In other words, the axis of the holes, where the two upper reference arms connect does not stay in line during the folding action.

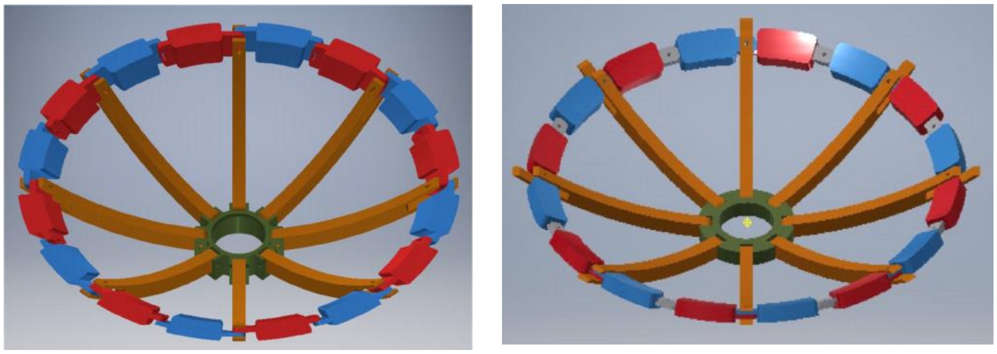

Figure 4. Second and third iterations of the downward folding deployment mechanism designs.

The degrees of freedom of the outer ring reference arms were increased in the third iteration by allowing the outer ring tabs to rotate where the connecting holes are located. This additional degree of freedom was provided by the gray parts in between the blue and red outer ring reference surfaces (see right side of Fig. 4). With the rotating tabs, the mechanism was able to move toward the stowed position, and the connecting holes on the rotating tabs of the two reference arms stayed aligned. Despite solving this problem, the third iteration, it was judged to be overcomplicated and also creates unwanted stresses on the membrane in the stowed configuration since it's folded downwards. The stretching action of the downward folding on the membrane might cause micro-yielding and permanent wrinkles. Therefore, the downward folding deployment mechanism idea was put aside.

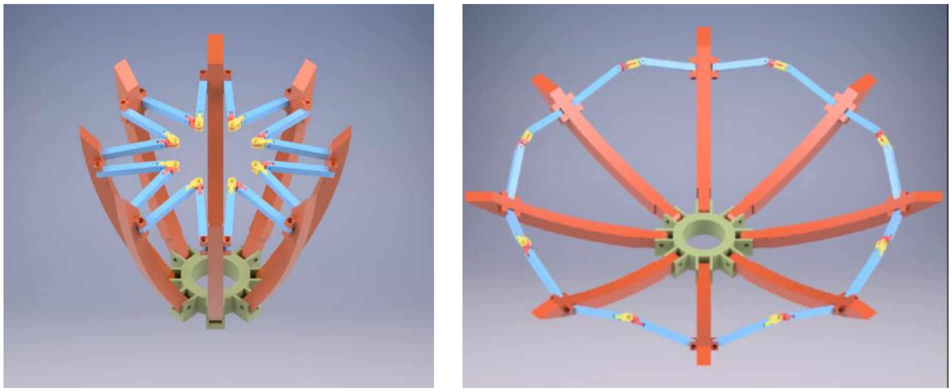

Figure 5. Isometric view of the forth iteration radial folding deployment mechanism design in the stowed (left) and deployed (right) configuration.

We next investigated a radial folding deployment mechanism. This has the advantage of a lower risk of wrinkling and a simpler mechanism. Although it also required an extra degree of freedom (similar to the downward folding design; provided by the yellow and red parts in Fig. 5 and Fig. 6), the movement range of these parts were much more smaller than downward folding mechanism. It is, therefore, considered as less complex. Another advantage of this deployment method was a smaller radius of curvature requirement on the folded configuration which means less risk of micro-yielding. The isometric and top views of the stowed (left side) and deployed (right side) configurations of the radial folding deployment mechanism is shown in Fig. 5 and Fig. 6, respectively.

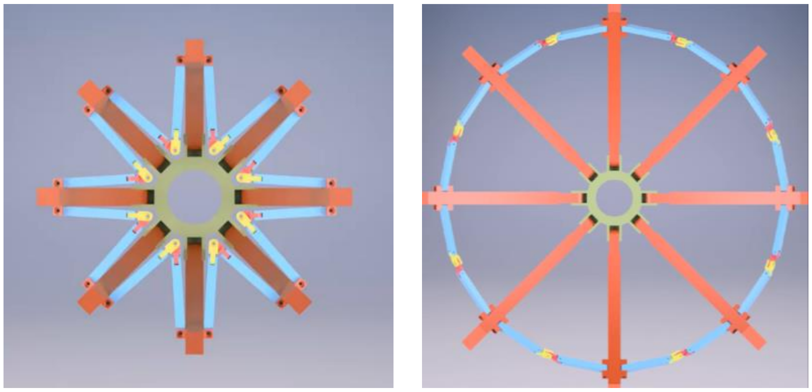

Figure 6. **Top view of the forth iteration radial folding deployment mechanism design in the stowed (left) and deployed (right) configuration.**

A preliminary mechanism analysis was conducted on the design and it was found to be operating smoothly. Therefore, a 3D printed prototype was decided to be produced for the proof of concept. Two different 3D printers were used. While bigger parts were printed by an ABS plastic based printer (the black parts in Fig. 7), the smaller parts were printed by a PLA based printer (the transparent parts at the center of Fig. 7). The radial arms were printed in side to side configuration to obtain better surface accuracy and as a result, additional surfaces were created on the sides of the radial arms for bedding purposes. Fig. 7 demonstrates the 3D printed and moving parts (bearings and shafts) of the prototyped radial folding deployment mechanism. A bearing (McMaster #57155K341) and shaft (McMaster #1263K16) combination was used at all revolute joints of the mechanism except the joint in between smaller tabs (transparent parts) and outer ring arms (blue parts in Fig. 6). A direct application of the shaft with a clearance fitting was used in these joints since the range of motion was very low (less than five degrees).

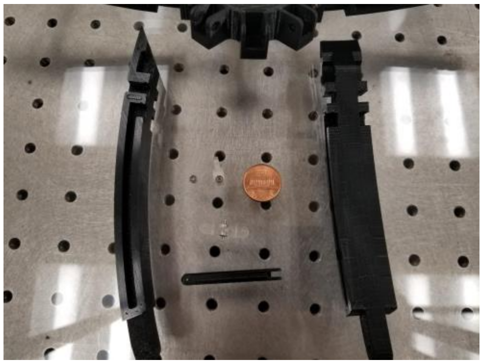

Figure 7. **3D printed and moving parts of the radial folding deployment mechanism (a penny is used for scaling purposes).**

After the assembly was completed, the inner surfaces of the ribs were treated with acetone vapor. The nature of the 3D printing process created steps on the inner surface ribs, even though they were printed side to side. These steps were smoothened by applying acetone vapor for a short period of time. Acetone vapor dissolves the ABS material of the print, smoothening the surface by melting/settling the thin outer layer of the part. Acetone vapor treatment was preferred because it treats the large areas easily and evenly which gives a more consistent result.

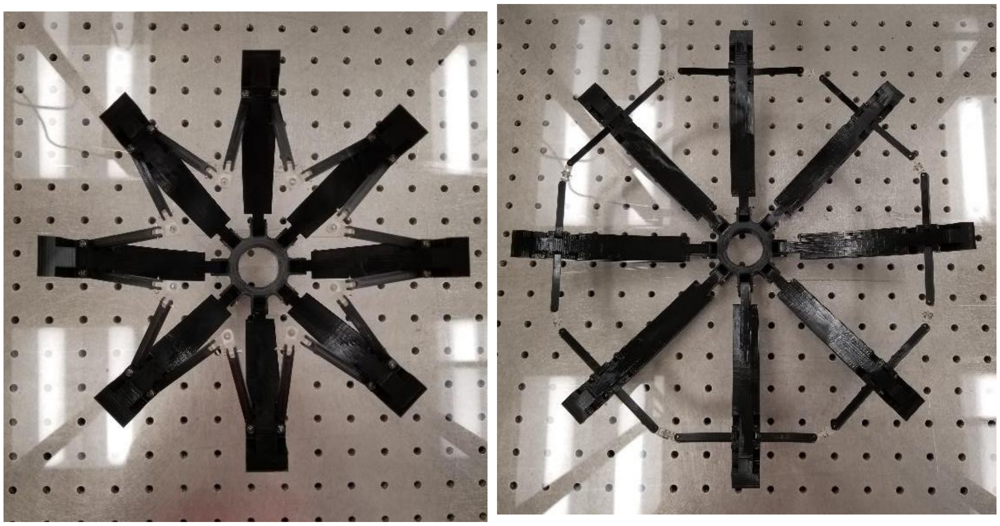

Figure 8. Assembled formation of the 3D printed radial folding deployment mechanism in the stowed (left side) and deployed (right side) configuration.

Fig. 8 shows the final assembly of the radial folding deployment mechanism prototype in stowed (left side) and deployed (right side) configurations. The mechanism works smoothly and can be deployed by gravity alone. Therefore, no spring back action was required in the design.

D. Preparation of Membranes

Another major component of the APERTURE deployment mechanism design was the preparation of the membranes. The preparation process includes tasks like obtaining samples, taking measurement, forming the membrane and putting the membrane and deployment mechanism together.

Since coating the MSM material is expensive and time consuming, membranes that consists of substrates and reflective surface only was used in the deployment research of APERTURE project. Additionally, the MSM coating can be neglected for now given that it's a very thin layer (10 microns) of coating compared to 5 mils of the substrate. Therefore, various membrane vendors were contacted which supplies membranes with different materials on substrates and reflective surfaces. While Mylar^{TM}, PET and Kapton^{TM} were the candidates for substrate material; silver, gold and aluminum were considered for the reflective surface. Another parameter in the membrane sample selection was the thickness of the membrane which varied between 1 and 5 mils.

After the membrane samples were obtained from various vendors, a surface roughness measurement procedure was conducted because the information was not provided by the vendors and it plays an important role in the overall surface accuracy. All measurements were done at Northwestern University using a Zygo New View^{TM} 7300 White Light Interferometer (WLI) which has a 0.1nm resolution in the z-direction and 2.21 microns in the x- and y-directions. The samples were placed in an aluminum fixture which has a 5 cm diameter opening at the center. The sample was secured by an O-ring on a guiding groove (depth of 0.3mm) in the top plate of the fixture. The plates were held together by four bolts, one at each corner. The bolts were screwed in evenly using a torque wrench. Table 1 shows the results of the measurements for various samples. While the left column lists the results of full scale membrane sample measurements (5 cm diameter) by stitching images together, the right column represents the results of single image measurements (1.12x0.83 mm). The images were taken in an area of 1.12 x 0.83 mm for a single image. The full sample area measurements were taken by stitching images together using a 25% overlap.

As seen in Table 1, CSHyde-PET-48-2F-1M, Dunmore Kapton^{TM} 200, Dunmore PET 300 and CSHyde-PET-48-5F-1M-13 are found promising due to their surface roughness of below 0.1 microns in RMS. In Chapter 2-A, the deflection goal was set by 1 micron. Therefore, membrane samples which has better surface accuracy will be required in the future. The CSHyde-PET-48-5F-1M-13 sample is selected to be used in current tests due to its higher thickness value (5 mils) than other candidates. It's a PET substrate oriented polyester film which is coated with aluminum that is vacuum deposited on to the surface of the film.

Table 1. Surface roughness measurements of various reflective membrane samples.

Surface Roughness Measurements		
Image Size	5x5	Single Image (averaged over 3 measurements)
Dimensions (mm)	5.65 x 4.24	1.12x0.83
Sample	**RMS (µm)**	**RMS (µm)**
Vivosun Horticulture Mylar	0.167	0.082
Apollo Horticulture Mylar	0.159	0.074
CSHyde-ESR-49-2RF	0.394	0.187
CSHyde-PET-48-1F-1M	0.093	0.047
CSHyde-PET-48-2F-1M	0.062	0.052
CSHyde-PET-48-5F-1M-13	0.087	0.028
Dunmore Kapton 500	0.205	0.075
Dunmore Kapton 300	0.337	0.051
Dunmore Kapton 200	0.063	0.047
Dunmore Kapton 100	0.112	0.076
Dunmore PET 300	0.064	0.009
Dunmore PET 200	0.273	0.119
Dunmore PET 92	0.035	0.014

Another process in the membrane preparation task was forming the membranes. All the membrane samples were received as flat film sheets in a rolled form or cut into rectangles. It is impossible to generate a perfect spherical surface out of a flat piece of membrane without stretching it. Thus, there are two ways to proceed: (1) to create approximate patches of the spherical surface, and (2) to stretch the flat membrane into a perfect spherical shape.

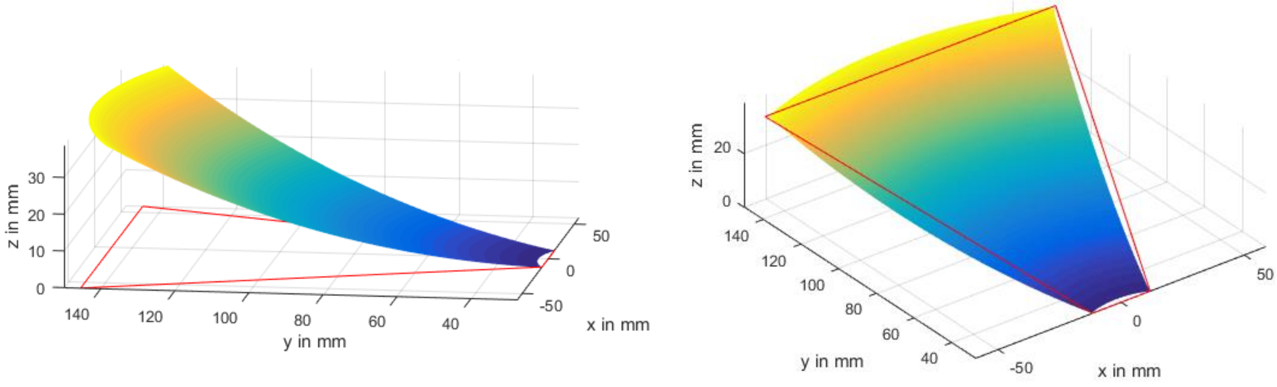

Figure 9. Straight line shape approximation of a patch projected (left) and overlapped (right) with desired spherical surface.

The patch approximation technique was chosen for the prototyped radial folding deployment mechanism as an initial attempt to complete the first full prototype. A patch size of one-eighth of the 30 cm diameter prototype was chosen as the prototype has eight ribs. A MATLAB code was written to generate the patch surfaces and compare the patch surfaces and that of a perfect spherical shape. The area of the desired (reference) 1/8 spherical patch is 9116 mm^3. Fig. 9 shows the first iteration of the patch approximation which consists of only straight lines. The colorful surface represents the desired spherical shape and the trapezoid created by the red lines is the first order approximation. The surface area of the trapezoid is 8338 mm^3. Therefore the percentage error of the fitting is calculated as 91.5%.

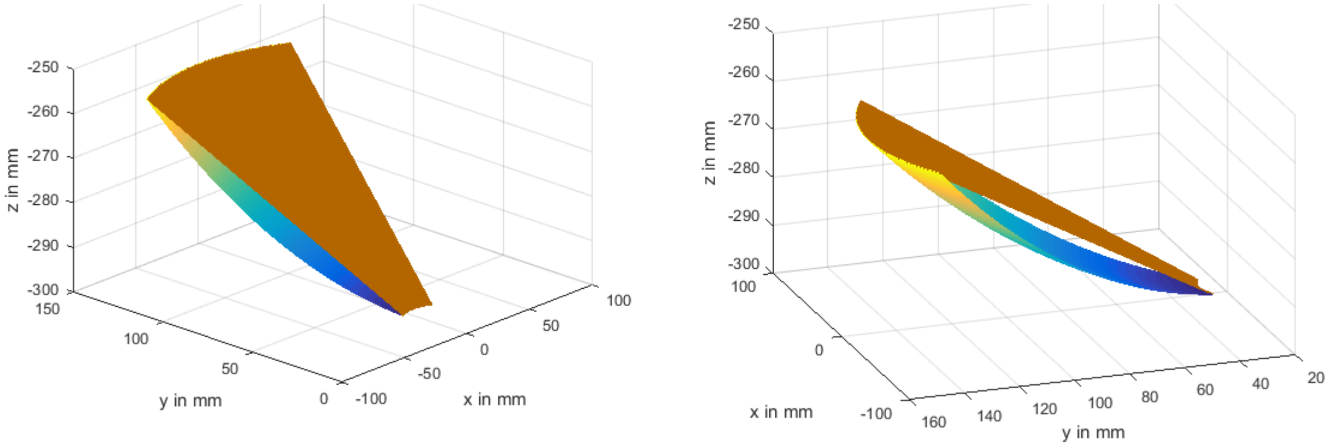

Figure 10. **Conical shape approximation patch overlapped with desired spherical surface.**

In the next attempt of the patch generation, conical surface approximation approach was used. The overlapped representation of the conical and desired surface is demonstrated in Fig. 10. The surface area of the conical patch is 8794 mm^3 which gives a fitting percentage of 96.5% over the desired spherical area of 9116 mm^3.

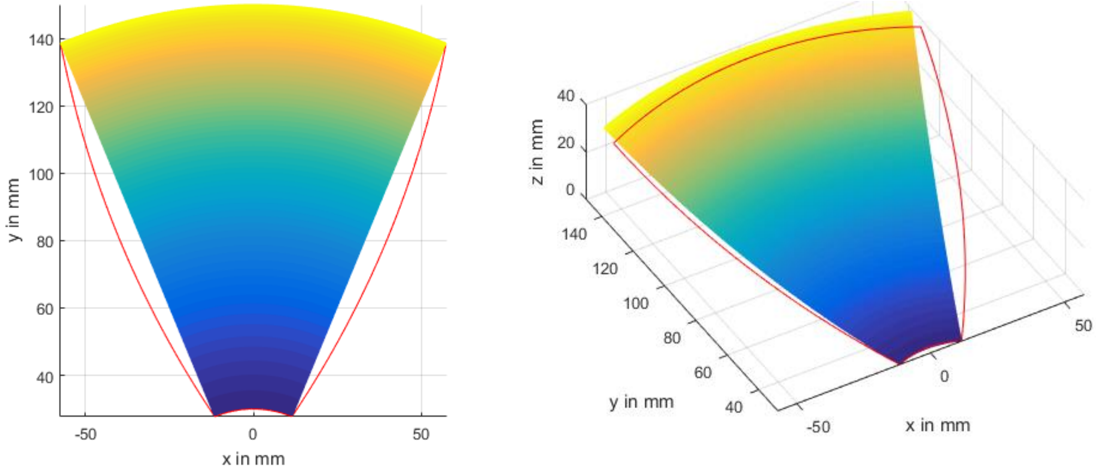

Figure 11. **All curved lines trapezoid shape approximation patch projected (left) and overlapped (right) with desired spherical surface.**

Even though the fitting percentage of the conical surface was not bad, a better patch approximation can be achieved by curving the patch not only side to side as in the conical approach, but also leaving a margin of length by increasing the length of the patch. Therefore, a patch design, which consists of curved lines on all sides was generated. The projected view on the right side and overlapped view on the left side are shown in Fig. 11. While the curves on the bottom and the top side of the patch was designed to match with the desired spherical surface, the side curves were designed to match with the lateral curved lines of the desired spherical surface, when they are folded inside through the spherical surface. The surface area of this patch is 9611 mm^3 which is bigger than the desired spherical surface by a fitting percentage of 105.4%. Therefore, this patch design was abandoned since it's much harder to control a loose membrane.

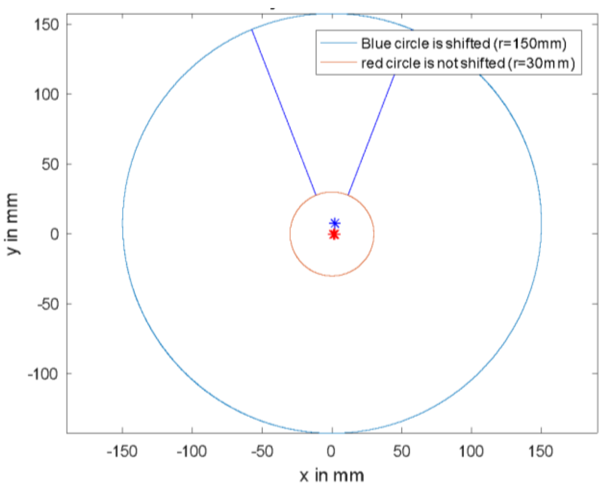

Figure 12. **Representation of the shifted center circles patch approximation.**

The concept of increasing the length of the patch to achieve a better fitting percentage was used to generate a patch which consists of two shifted center circles. The center of one circle is shifted from the other by the length difference between the side curve of the desired spherical shape and a straight line from bottom to top corner of that side curve. Fig. 12 explains the idea of a shifted center circles patch, as seen the diameters of the circles kept the same to be match with desired spherical surface's top and bottom curved edges (see right side of Fig. 13). The star shapes represent the centers of the blue and red circles. Additionally, corner of these curved lines were connected through straight lines (the dark blue lines in Fig. 12). These straight lines are longer than overlapped circle's radius, so they increase the surface area for better fitting percentage.

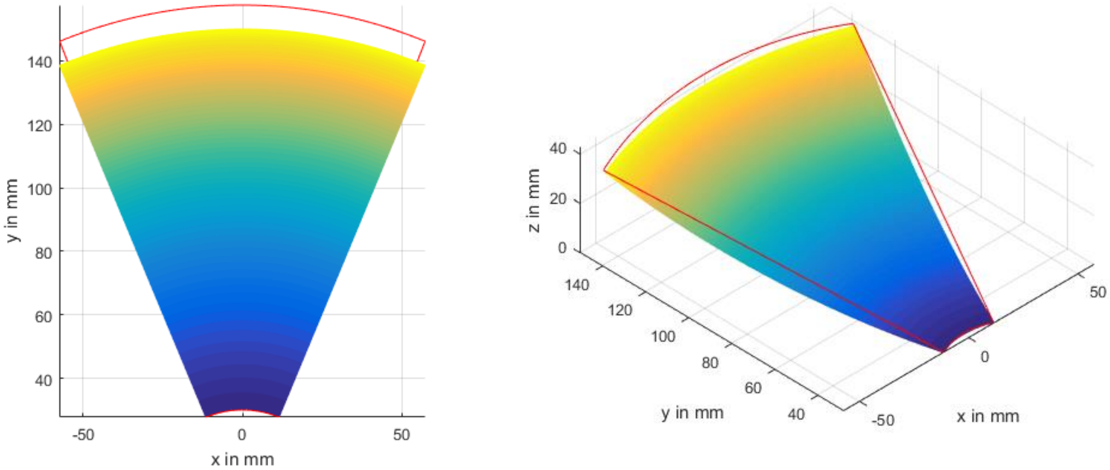

Figure 13. **Shifted center circles approximation patch projected (left) and overlapped (right) with the desired spherical surface.**

The left side of Fig. 13 shows the projected view of the generated patch and the desired spherical surface from the top side, on the right side the overlapped configuration in isometric view is shown. The surface area is 9004 mm^3 with a fitting percentage of 98.8%. This patch approximation is the closest to the desired spherical surface and only requires the membrane to be stretched by 1.2%. As a result, the membrane patches were cut using this generated shape out of CSHyde-PET-48-5F-1M-13 rolled film.

III. Results & Discussion

Two of the prepared membrane patches were fixed on quarter of the 3D printed radial folding deployment mechanism (see Fig. 14) and figure accuracy measured using the experimental setup. CSHyde-PET-48-5F-1M-13 rolled film was selected as the membrane due to its surface accuracy and thickness for better handling. The inner surface accuracy of the deployment mechanism ribs were not good enough, despite the acetone treatment. The membrane patches prepared by shifted center method, applied to only quarter of the mechanism since it is an axisymmetric geometry.

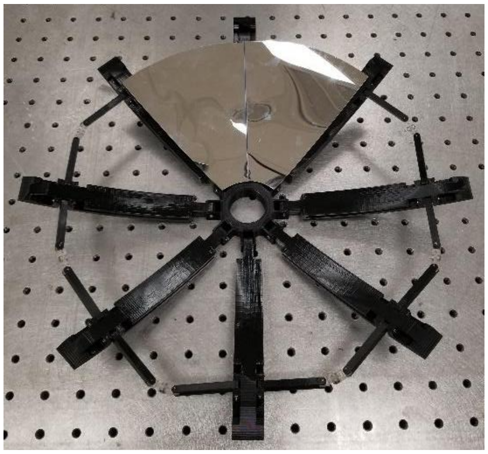

Figure 14. Quarter assembly of the prepared membrane patch and the radial folding deployment mechanism.

Unfortunately, the surface accuracy measurement was out of the dynamic range of the shack-hartmann sensor which points out that the deflections were in mm level. A better surface accuracy can be achieved by using (1) precision machined parts on the deployment mechanism, (2) membranes with better surface roughness, and (3) stretch forming the membrane to a perfect spherical shape during the membrane preparation phase.

Optical grade quality film membranes with much smoother surface are found in the market. These optical quality films are developed primarily to minimize wavefront distortion through the material for imaging applications. To address other two issues and finding out a solution pathway for next deployment designs, precision machining of the deployment mechanism parts and accurate membrane forming into spherical shape are essential. On this manner, a new deployment design is created which has much narrower ribs. Narrow ribs enables the precision manufacturing of the ribs out of metals using a CNC machine. In the previous designs, precision machining was very costly and difficult to do, because of having two different curves in two directions (side-side, top-bottom). Therefore, the ribs were produced by using a 3D printer but the surface accuracy was not enough. Therefore the ribs are narrowed down to a thickness, in which side to side (azimuth direction) curve is no longer significant. So that, we can neglect that curve and high tolerance machine the ribs out of metals. Fig. 15 shows the next generation deployment mechanism design. Another important change in the design is simplifying it by cancelling out the outer ring reference surfaces. It is considered that these references will be provided by using strip coating of a spring back or shape memory alloy material, so it can be embedded to the membrane. This new approach significantly simplifies the design of the deployment mechanism.

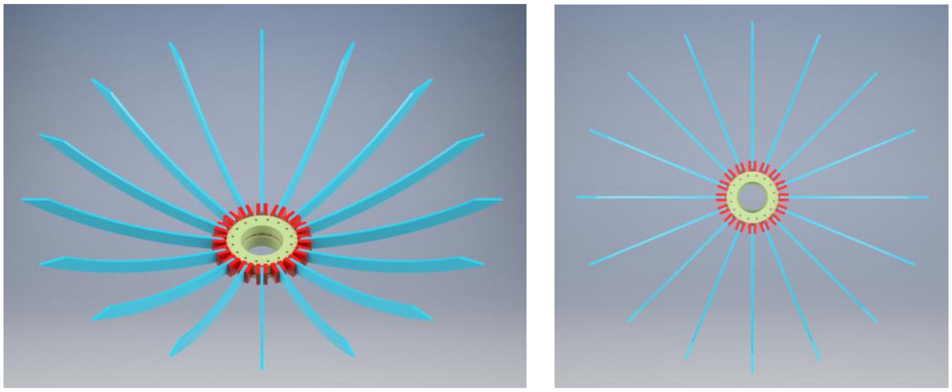

Figure 15. Final iteration deployment mechanism design of APERTURE project.

Although a surface area match of 98.8% is achieved by using a shifted center circles approximation patch, it is still a significant difference when working in the micron level. Therefore, a membrane stretch forming method was needed to obtain a perfect spherical geometry out of a flat film sheet. A wide literature review was conducted to find a suitable method. Based on this, we decided to use vacuum forming to shape the membrane. A vacuum chamber will be developed and will be integrated in the current surface profiling experimental setup. Thus, a real-time membrane figure accuracy feedback control system can be developed by giving feedback from the shack-hartmann surface profiler to an automated vacuum pressure regulator.

IV. Conclusion

The design process of the deployment mechanism, experimental setup for surface profiling, and initial results of the first deployment prototype of the APERTURE project is described in this paper. A micro-yielding study was conducted and a maximum deformation limit of 1 micron was used. To reach this goal, two main tasks of the project was identified as (1) deployment mechanism design and (2) membrane forming/preparation. Both of these tasks were investigated and the process is presented. In task 1 we developed less complex and precise prototypes of a deployment mechanism and refined the design of the mechanism. In task 2 we found a cost efficient method of precision forming the membrane and accurately attaching the membrane to the deployment mechanism. The issues that were identified during the two tasks were addressed, used to improve subsequent designs and a pathway to a final design was developed. In addition, the designed and developed surface profiling experimental setup was verified.

13. Acknowledgments

This work was supported primarily by NASA NIAC grant number NNX15AL89G as well as synergistic work for adaptive X-ray optics supported NASA (Grant NNX16AL31G). The authors would like to thank to Dr. Ron Shiri for his valuable advice and support. We thank Giovanni Pareschi for suggesting working with MSM films in the first place. We thank to undergraduate students Jacob Hinojos, Kevin Norman, Kyle Condron and Remi Madelon for their support and help.

14. References

[1]"Delta IV, Payload Planners Guide," tech. rep., United Launch Alliance, 2007.

[2]Lillie, C. F., Polidan, R. S., and Dailey, D. R., "Key enabling technologies for the next generation of space telescopes," *Space Telescopes and Instrumentation 2010: Optical, Infrared, and Millimeter Wave*, Vol. 7731, SPIE, 2010, pp. 773102-773104.

[3]"Replicated diffractive optics, moire." http://www.ballaerospace.com/page.jsp?page=259. Accessed: 2017-02-17.

[4]Lan, L., Jiang, S., Zhou, Y., Fang, H., Wu, Z., & Du, J., "An experimental study on reflector wave-front error correction using PZT actuators," *SPIE Smart Structures and Materials Nondestructive Evaluation and Health Monitoring*, 2016, pp. 97990G-97990G.

[5]Liu, C., & Shi, Y., "Comprehensive structural analysis and optimization of the electrostatic forming membrane reflector deployable antenna," *Aerospace Science and Technology*, Vol. 53, 2016, pp. 267-279.

[6]Center, N. G., "Three newly designed tracking and data relay satellites to help replenish existing on-orbit fleet," Tech. Rep. FS-2001-9-025-GSFC, NASA Goddard Space Flight Center, 2001.

[7]Thomson, M. W., "Astromesh deployable reflectors for Ku-and Ka-band commercial satellites," *20th AIAA International Communication Satellite Systems Conference and Exhibit*, Vol. 12, AIAA, Reston, VA, 2002, p. 15.

[8] Ulmer, M.P., Coverstone, V.L., Cao, J., Chung, Y.W., Corbineau, M.C., Case, A., Murchison, B., Lorenz, C., Luo, G., Pekosh, J. and Sepulveda, J., "APERTURE: a precise extremely large reflective telescope using re-configurable elements," *SPIE Astronomical Telescopes and Instrumentation*, SPIE, 2016, pp. 99041I-99041I

[9] Domber, J. and Peterson, L., "Implications of material microyield for gossamer optical reflectors," *43rd AIAA/ASME/ASCE/AHS/ASC Structures, Structural Dynamics, and Materials Conference*, AIAA, 2002, p. 1503..

[10] Enders, J., Kas-Danouche, S., Liao, W., Rasmussen, B., Vo, T.A., Yokley, K., Robertson, L. and Smith, R.C., "Design of a membrane aperture deployable structure," *44th AIAA/ASME/ASCE/AHS Structures, Structural Dynamics, and Materials Conference*, AIAA, AIAA Paper No AIAA-2003-1494 , 2003.

[11] Li, J. H., Gao, X. X., Zhu, J., Bao, X. Q., Xia, T., and Zhang, M. C., "Ductility, texture and large magnetostriction of fe-ga-based sheets," *Scripta Materialia*, Vol. 63, No. 2, 2010, pp. 246-249.

APERTURE: a precise extremely large reflective telescope using re-configurable elements

M. P. Ulmer[a], V. L. Coverstone[b], J. Cao[a], Y.-W. Chung[a], M.-C. Corbineau[b], A. Case[b], B. Murchison[b], C. Lorenz[b], G. Luo[b], J. Pekosh[b], J. Sepulveda[b], A. Schneider[a], X. Yan[a], and S. Ye[a]

[a]Northwestern University, 633 Clark St, Evanston, IL, USA, 60208
[b]University of Illinois at Urbana-Champaign, 104 S Wright St, Urbana, IL, USA, 61801

ABSTRACT

One of the pressing needs for the UV-Vis is a design to allow even larger mirrors than the JWST primary at an affordable cost. We report here the results of a NASA Innovative Advanced Concepts phase 1 study. Our project is called A Precise Extremely large Reflective Telescope Using Reconfigurable Elements (APERTURE). The idea is to deploy a continuous membrane-like mirror. The mirror figure will be corrected after deployment to bring it into better or equal lambda/20 deviations from the prescribed mirror shape. The basic concept is not new. What is new is to use a different approach from the classical piezoelectric-patch technology. Instead, our concept is based on a contiguous coating of a so called magnetic smart material (MSM). After deployment a magnetic write head will move on the non-reflecting side of the mirror and will generate a magnetic field that will produce a stress in the MSM that will correct the mirror deviations from the prescribed shape.

Keywords: Large telescope concept, magnetostriction, deployment, reflective membrane

1. INTRODUCTION

1.1 Need for the Concept

Twenty-six years after the launch of the ultraviolet-visible (UV-Vis) 2.4m-diameter Hubble Space Telescope, the desire for larger space telescopes is ever present. The near-infrared James Webb Space Telescope (JWST) and the Advanced Technology Large-Aperture Space Telescope (ATLAS-T) have a diameter of 6.5 m and 16 m[1] , respectively. In addition, after the cancellation of the Ares V heavy lift vehicle[2] , the ATLAS-T requires the future modified Space Launch System (SLS). Therefore, even if rocket fairings are made larger, the astronomers' desire for larger apertures will surely outstrip the ability of rocket fairings to accommodate these larger apertures.

In response to the desirable circumstance of wanting larger mirrors, using deployable mirrors is the logical choice. Within this category there are segmented mirrors, e.g. JWST. A preliminary conservative approach of scaling up JWST by unfolding rigid segments yields an about design with a maximum diameter of about 12 m[3] . Another approach to deployable space optics is the MOIRE[4] optic design supported by DARPA, which is based on diffraction, and hence is not competitive with a broad band mirror of the same size.

Thus, in order to achieve larger that 12-m diameter reflecting space mirrors, we investigated using deployable membrane optics. The problem with membrane-like mirror such as the Tracking and Data Relay Satellites (TDRS)[5] or the AstroMesh design[6], is that they have yet to achieve a better shape than the figure accuracy acceptable for S, Ku and Ka-band wavelengths (respectively 150 mm, 20 mm, 11 mm). If one assumes a Strelh ratio of 90%, then the Ka-band wavelength corresponds to a figure Root Mean Square (RMS) error of about 11 mm/20. Since APERTURE is meant to be used for UV-Vis observations, a similar Strelh ratio would lead to a RMS of (400 nm)/20 (or better for the deep UV). Therefore if a deployed membrane mirror is to be employed, post deployment corrections will need to be applied. What is novel about our concept is that the corrections will be applied to a *contiguous* film that has been deposited on a monolithic membrane.

Further author information: (Send correspondence to M. P. Ulmer)
M. P. Ulmer: E-mail: m-ulmer2@northwestern.edu, Telephone: 1 847-491-5633

Space Telescopes and Instrumentation 2016: Optical, Infrared, and Millimeter Wave, edited by
Howard A. MacEwen, Giovanni G. Fazio, Makenzie Lystrup, Proc. of SPIE Vol. 9904,

99041I · © 2016 SPIE · CCC code: 0277-786X/16/$18 · doi: 10.1117/12.2231679

1.2 The APERTURE Concept

1.2.1 Overview

This paper is based on a Phase I NIAC study, and the goal of which was not to solve all the many technical issues, but rather to demonstrate that the APERTURE concept is feasible enough to warrant further examination. The proposed concept uses Magnetic Smart Material (MSM) to apply figure corrections to extremely large (16-m diameter) deployable reflective optics. The first step of the deployment will utilize an umbrella-like structure to achieve a parabolic shape for the optics. The inside of the umbrella will be the reflective surface, while the outside will be coated with MSM. Several magnetic write heads will move to different locations on the MSM coated side to manipulate the MSM, changing the shape of the optics and eliminating any deviation from the desired final shape. Figure 1 depicts the concept of APERTURE: the write head (dark brown in the video illustrating the concept `www.youtube.com/watch?v=4j-Elbjvh78&feature=youtu.be`) moves along the curved arm, while the curved arm rotates about the center axis.

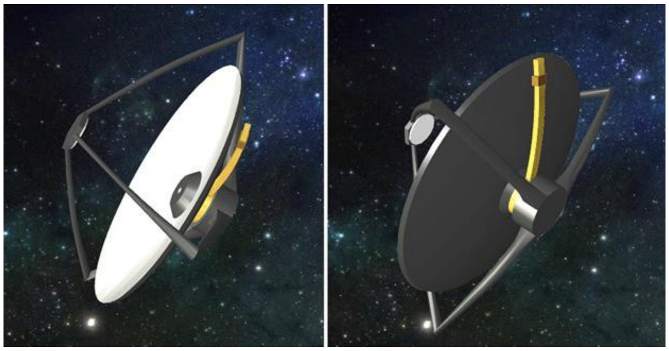

Figure 1. APERTURE concept. For simplicity only one boom and write head are shown here.

1.2.2 Alternative Approaches to correcting deployed membrane mirrors

For comparison with our concept, we briefly review previous work. To the best of our knowledge all previous work based on correcting membrane and deployable space mirrors has considered electrostatic or piezoelectric control. A big disadvantage is that wires must be attached to every point on the mirror for which actuator control is needed, and so far the ability to provide post deployment figure corrections to the level of $\lambda/20$ in the visible using membrane mirrors has eluded the space community. Furthermore, piezoelectric actuators intended for large membrane mirrors require thousands of actuators which reduces the stroke per actuator. Another specific disadvantage of PZT actuators is the relatively low positioning accuracy compared to other actuators (e.g. electrostatic).

Previous work has been done using polyvinylidene fluoride (PVDF) actuators for surface control on a flexible Kapton™ reflector by Hill, *et al.*[7] . Their experiment concluded that a feasible RMS surface error between 100 and 400 μm is obtainable depending on the initial configuration of the reflector. While a surface error of this scale is accurate enough for long (1 mm) wavelength reflectors, a reflector operating in the UV wavelength range requires a surface error of at most 10 nm. Thus, it can be seen a UV-Vis space reflector requires an alternate method from piezoelectric actuators to produce adequate post deployment correction to the figure of membrane mirrors. The APERTURE concept based moving magnetic write head to modify the mirror figure *without attachment* to the mirror, then, has the potential to overcome the difficulties encountered with actuators that are attached to the membrane.

2. FEASIBILITY STUDY OF THE DEPLOYMENT

2.1 Rocket Fairing and Constraints for the Stowed Configuration

To use a concrete example APERTUREs deployment design assumes a Delta IV Heavy rocket fairing which can carry a payload with a diameter up to 4.6 m and a height under 17 m. Given the dimensions of the desired rocket fairing, if the mirror is monolithic then it needs to be flexible. Moreover, the thinner a membrane is, the easier it is to make corrections with a magnetic write head. However, a thin membrane would not be able to hold a parabolic shape without stiffeners. Another parameter that needs to be taken into account in the calculation of the membrane thickness is its extreme susceptibility to micro-yields (microscopic plastic deformations). It is necessary to make sure that the membrane can be folded without being damaged.

2.2 Design of the Folded Membrane

The shape that has been considered is the umbrella design. In this article we present a variation of the method described by Enders *et al.*[8] ; instead of generating the section using circles we use these equations: θ=t+cos^4(pt) and r=r$_0$+ρ cos^4(pt) where *t* i the membrane thickness, 2*p* is the number of petals and $r_0 + \rho$ is the maximal radius of the stowed membrane. The corresponding results for 6.5-m and 16-m diameter mirrors are displayed on Figure 2; the diameter of the 16-m diameter folded mirror is 3.9 m which corresponds to a margin of 15% with respect to the rocket fairing inner diameter.

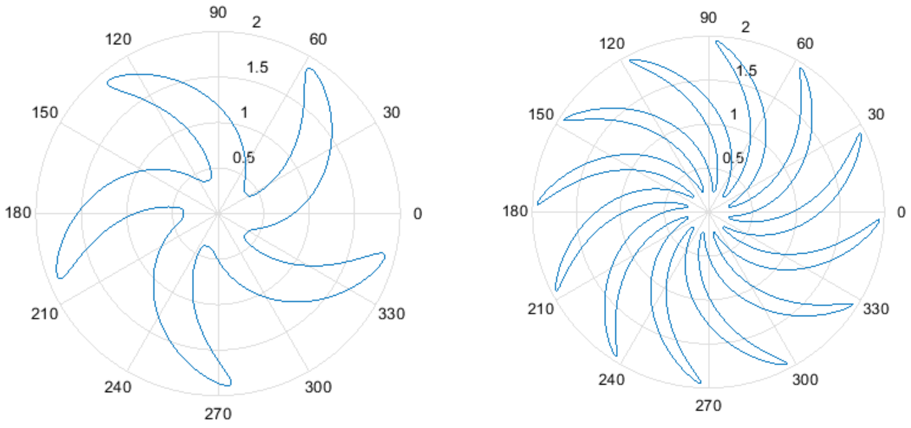

Figure 2. Top section of an umbrella-like folded mirror (a) 6.5-m diameter, (b) 16-m diameter.

2.3 Analysis of the Shape

As shown on Figure 3, the number of "petals" increases linearly with the diameter of the mirror, while the minimal radius of curvature decreases. Some points on the outer and inner edges exhibit very low radii of curvature, leading locally to a greater probability of micro-yield.

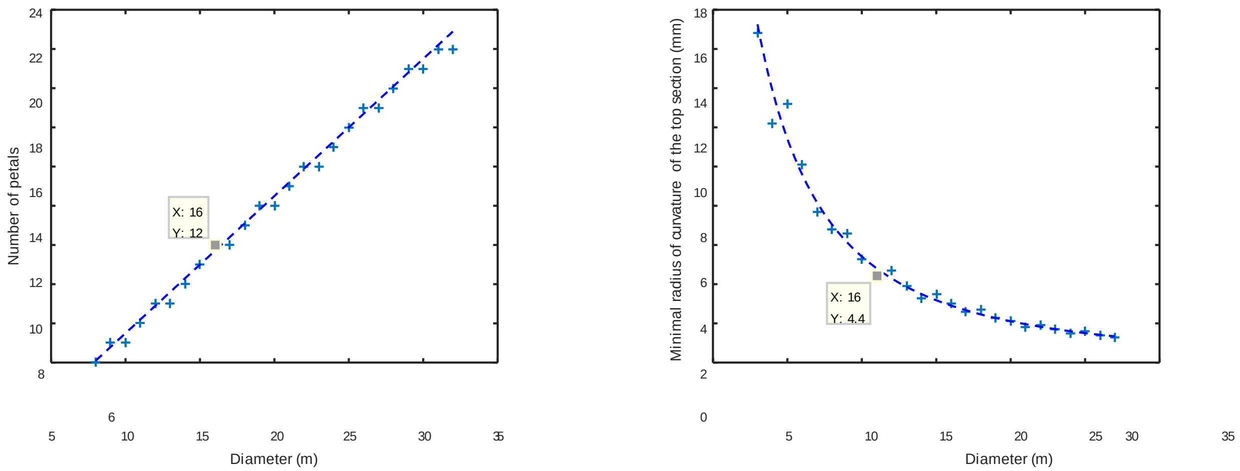

Figure 3. Left: Number of petals as a function of the mirror's diameter. Right: Minimal radius of curvature on the top section for different values of the mirror's diameter. Dotted lines are fits to the Matlab data, left: $y = 0.7x + 0.5$, right: $y = 800x^{-2}$.

To obtain the 3D shapes on Figure 4, the focal length is chosen equal to the diameter: $F/D = 1$; $D_{min}/D_{max} = 0.28$; the inner hole is approximately equal to the size of the secondary mirror: $D_{min} = 4.5$ m. Using this ratio, the collecting surface area represents about 92% of the total surface while. The JWST ratio is $D_{min}/D_{max} = 0.203$, yielding 96% effective primary mirror area. However, the risk of micro-yield is decreased with our design since the minimal radius of curvature is in our design is 1 mm for $D_{min}/D_{max} = 0.28$ versus 0.5 mm when $D_{min}/D_{max} = 0.203$ is chosen.

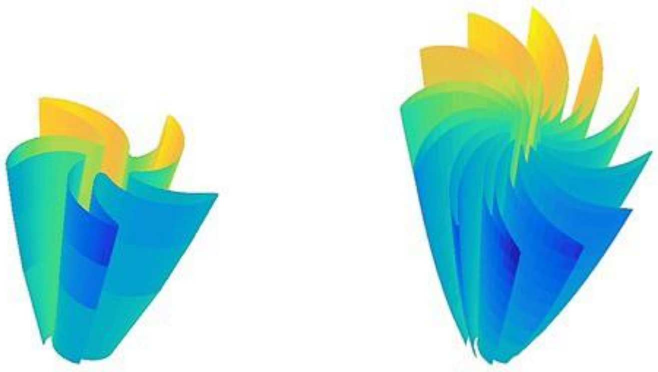

Figure 4. Folded mirror (a) 6.5-m diameter, (b) 16-m diameter (colors are not meaningful, used for visualization).

2.4 Determination of a Condition before Micro-Yield

2.4.1 Equations and Background

There is a minimal radius of curvature allowable before producing micro-yields in the structure; it depends on the materials that are used to make the membrane. The flexibility of a material, or allowable minimal radius of curvature R_F, can be computed according to the analytic approach of Domber and Peterson[9]. Usually, the criterion of the elastic "0.2%" yield stress is chosen, but for optical components even small residual strains must be considered. The calculation of R_F is given by Equation 1.

$$\frac{}{\omega t} \quad \frac{}{} \quad \frac{1}{} \quad \frac{n}{} \tag{1}$$

Here the variable ω is the allowable deflection, t is the thickness of the material, E is the Young's modulus of the material, H is the plasticity model constant, n is the strain hardening exponent. The length of the curved surface has been approximated by $2\pi R_F$,[8] which is true for localized curvature (true for the umbrella-like deployment). The main hypothesis behind this formula is that, for very small deformations, the plastic term in the Ramberg-Osgood model (Equation 2) can be neglected with regards to the elastic term.

$$E = \frac{}{E} + \frac{}{H}^{\frac{1}{n}} \tag{2}$$

The plastic parameter H and the exponent n can be found using the Ramberg-Osgood model for one-dimensional yield. The strain-stress curve of a material can be approximated by the model represented by Equation 2. A least-squares approximation, applied to the 23°C strain-stress curve for Kapton™, leads to $n_{Kapton} = 0.238$ and $H_{Kapton} = 0.249$ GPa (Figure 5 left). The same method is applied to Galfenol (see Figure 5 right). The exponent n takes its value between 0 and 1, and the smaller n is, the more plastic the material is. For aluminum Al 2014-T6, the value for H and n have been found in 9 : H = 0.68 GPa, n = 0.06.

To compute R_F using Equation 1, a value for the deflection ω must be chosen. Usually, the maximal deflection allowed for a mirror is expressed as a fraction of the shortest operating wavelength of the reflector[8] :

$$\omega_{max} \leq \alpha \lambda_{min}$$

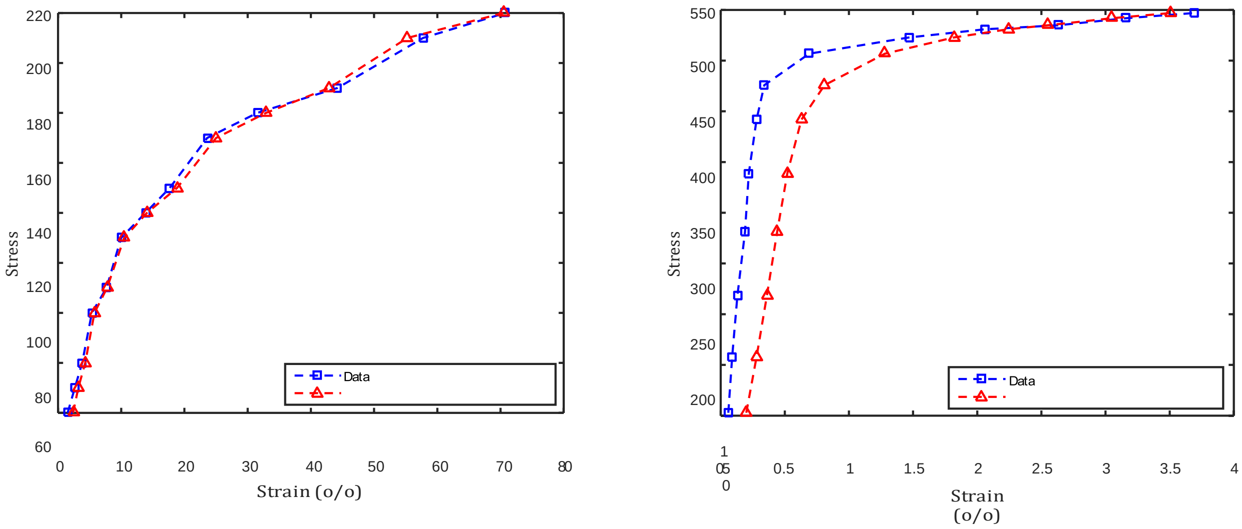

Figure 5. Left: strain-stress curve for Kapton™ (23° C), data (courtesy of Dupont) and approximation. Right: strain- stress curve for Galfenol ($Fe_{82.17}Ga_{16.83}B$), data[10] and approximation.

For APERTURE, λ_{min} is about 200 nm (UV). The value for α will be determined during Phase II of the NIAC program, but 1/20 is thought to be a lower limit. Thus, ω_{max} $10nm$. However, APERTURE will use post deployment corrections. Hence, it is reasonable to take a higher value for the maximal deflection, say $1\mu m$.

2.4.2 Results

The final composition of the membrane is not determined yet but preliminary results, summarized in Table 1, have been obtained for materials that are likely candidates. Aluminum, which has a high reflectance for UV, is a candidate for the reflective material, Kapton™ may be used as a substrate, and Galfenol is a magnetostrictive material similar to Terfenol-D, but more pliable and less subject to delamination.

Table 1. Radius of curvature before micro-yield, for different materials and various values of the thickness ($\omega = 1\mu m$)

Thickness (μm)	Al 2014-T6 (mm)	Kapton™ (mm)	Galfenol (mm)
10	1.2	1.7	1.2
25	3.3	6.6	3.1
50	6.9	18	6.3

2.5 Selection of Two Deployment Mechanisms

Now that the feasibility of stowing the mirror membrane in the Delta IV heavy rocket fairing has been demonstrated, the deployment mechanism needs to be devised. The two main criteria that have been used to characterize the different strategies are the ability to stow the primary mirror into a Delta IV Heavy rocket fairing without damaging the surface, and the possibility of deploying the mirror into space while assuring that the final shape is precise enough to be corrected by inserting a magnetic field into the MSM. Other relevant parameters are the stowed volume efficiency, the stability, and the launch weight. Based on those criteria two types of deployment have been selected to carry out experimental tests for Phase II. Figure 6 shows a conceptual view of the flexible primary mirror deployment. See also §1.2.1.

2.5.1 The Flexible Precision Reflector (FPR)

This design would be used for the umbrella deployment strategy described in section 2.2 is based on the use of a classic composite material combined with an elastic memory composite like TEMBO™. TEMBO™ was created by Composite Development Technology (CTD) and was used by Harris Corporation to study the deployment of a Flexible Precision Reflector (FPR)[11] . The FPR can operate at radio frequencies (40 GHz) and benefits from

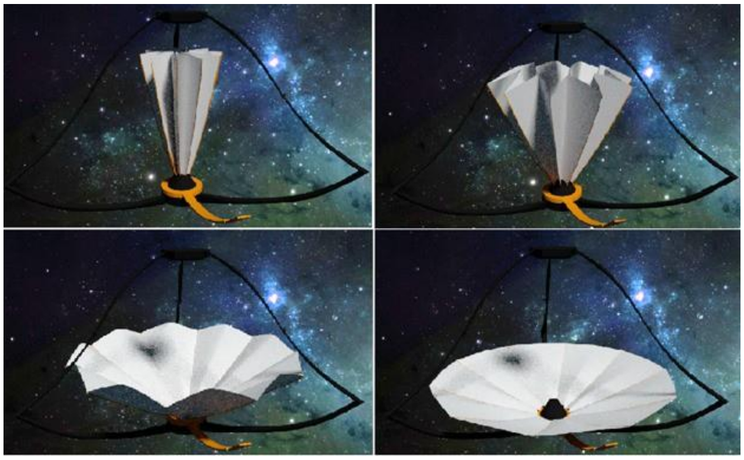

Figure 6. APERTURE deployment (conceptual view), see Figure 1 for the fully deployed telescope

a very-low-packaged volume, a potential diameter of 25 m and a very low areal mass density. The reflector is deployed by heating the stiffeners, leading to a gradual, controlled and predictable mechanism (Figure 7).

(a) Packaged

(b) Deployed

Figure 7. Flexible precision reflector before and after deployment[11]

2.5.2 Self-Deployable Shell Reflector (SDSR)

An alternative to the umbrella design and not detailed in the text due to its simplicity, is the self-deployable shell reflector recently developed by Soykasap *et al.*[12] . The deployment of a 1.5-m diameter reflector is illustrated on Figure 8. The material used is a Carbon Fiber Reinforced Polymer (CRFP). The deployment of this reflector requires no additional external energy. However, the sudden release of stored strain energy can create vibrations in the structure. These vibrations will need to be taken into account when considering this deployment design.

Figure 8. Deployment of the self-deployable shell reflector (duration: 1.4 s)[13]

2.5.3 Summary of prototypes

Table 2 summarizes the main characteristics of the prototypes that have been manufactured by Keller *etal.* and Soykasap *et al.* according to the two designs described above. The RMS error values can be compared to the magnitude of the maximal deflection that one can obtain using MSM as studied by the team at NU (see 3.4). The CRFP may prove too stiff, but the FRP has quite a low Young's modulus, measured in tens of kPa[14] .

Table 2. Characteristics of the two selected deployment designs

Design	Diameter	Thickness	Material	RMS error
FPR[11]	0.9 m	152 μm	TEMBO™, elastic memory composite	330 μm
SDSR[12]	1.5 m	220-880 μm	CRFP, plain weave	420 μm

3. USING MAGNETOSTRICTION FOR POST DEPLOYMENT SHAPE CORRECTIONS

3.1 Magnetostriction, General

The general effect is that any ferromagnetic material will expand or contract in the presence of a magnetic field. This effect is called magnetostriction and has been known since 1842 with work done by Joule and recently others[15, 16] . Both expansion and contraction are possible, see for example Ref. 16. Magnetostrictive thin films have been studied extensively for there properties. See, for example the references found in Refs. 17–19.

3.2 Magnetic Smart Materials and Applications

The magnetostrictive material Terfenol-D was invented in the 1960's by the Naval Ordnance Lab[20] and exhibited giant magnetostriction, on the order of $\delta L/L$ as high as 0.2%. The maximum saturation magnetic fields are about 0.5 T. Much research has been devoted to understanding the basic principles underlying the behavior of giant magnetostriction. There are now a range of materials to select from depending on parameters such as the optimal annealing temperature, applicable coating method (e.g. electroplate versus sputter deposit), and how much magnetostriction is desired. Besides Tefenol-D, other materials such as Tb-Fe or Fe-Ga (Galfenol) exhibit magnetostrictive properties[21, 22] , as do multilayers such as $Tb_{40}Fe_{60}/Fe_{50}Co_{50}$[23] and $BaFe_{12}O_{19}$-CoNiP[24] . A few of many applications are described in 25. They are mostly used for actuation but micro-electro mechanical systems (MEMS) have also been proposed, e.g. 24. The application that we are proposing is different from these, as an MSM film will instead be used to correct a deployed membrane optic, where "membrane" is defined to be flexible enough to be folded up in pre-deployment as well as thin enough to be correctable by the strains induced in MSMs via a magnetic field.

3.3 Selection of appropriate Magnetic Smart Materials (MSM)

Several options have been identified for the MSM: Terfenol-D, which requires a high magnetic remanence layer of say, NiCo; V-Permadur, which has a high remanence and thus holds very well the magnetic field; and Galfenol, which is similar to Terfenol-D, but more pliable. Table 3 summarizes some properties of the MSMs mentioned above along with information about the substrate and reflective material. Additional work can be done to check that the differences between the Coefficients of Thermal Expansion (CTE) of the membrane components do not lead to internal fractures.

Table 3. Properties of Candidate MSM and Membrane Materials

Material	Young's Modulus (GPa)	Poisson Ratio	CTE (ppm/°C)
Terfenol-D	216.9 (varies with magnetic field)	0.5	12
Vanadium-Permendur	207	-	9.50 (25 - 200°C)
Galfenol	75	0.3	11.7
Kapton™	2.5	0.34 (at 23°C)	20 (for -14 to 38°C)
Al-2014 T6	72.4	0.33	23

3.4 Magnets for Correction

The maximum required magnetic field is about 0.5 T as this is the saturation magnetic field. These fields can be produced either via permanent rare-earth magnets or electromagnets. Permanent magnets[26] of acceptable size (volumes of 2 cm^3) can produce the required field as can electromagnets of about 10 cm^3 with acceptably low power levels of less than a few Watts. Based on the experimental result from Wang *et al.*[18, 27], about 1 μm of deflection can be obtained from a 100 μm thick glass substrate (Young's modulus 80 GPa) over a 20 mm x 5 mm strip under a magnetic field of 0.1 T. Wang *et al.* have developed an analytic model which produced results that match closely with the experimental result. Using this model, it can be estimated that if a Kapton™ substrate is used under the same conditions, deflections of about 40 μm can be obtained. By reducing the thickness to 25 μm, the size of deformations possible rises inversely as the square of the thickness to a net deformation of over 600 μm. Furthermore the magnetic field strength can be raised to the saturation value to produce another factor of 0.5. Hence it is plausible that corrections of 300μm are possible in our candidate membrane materials.

4. OPERATIONS AND CHARACTERISTICS OF THE SHAPE CORRECTING SYSTEM

In order to avoid the risks of having a fixed wire attached to a moving component, the magnetic write head will be wireless and will be powered by a battery recharged thanks to a charging station. If the time during which the MSM holds its shape is shorter than the time needed to correct the shape using a single magnetic write head, then the single-magnetic write head APERTURE design would not be feasible. Thus, it is necessary to explore the relationship between the number of magnets and the time needed to make post deployment corrections. Other parameters like the size of the magnet's battery or the percentage of the spacecraft's main battery which is allocated to the magnetic write head can influence the duration of the correction process.

To carry out this analysis, a worst-case scenario is chosen, assuming that the entire back of the mirror needs to be corrected by the magnetic write head. A comprehensive calculation of the correction process duration, T_{tot}, has been produced. For simplicity, the baseline we used for the calculation was that of JWST but with a diameter of 16 m. The influence of different variables is studied by varying one parameter at a time. The list of the parameters that are used, along with their baseline value, can be found in Table 4. At the beginning of a calculation, each parameter is set equal to its baseline value except for the variable that is under study. Then the time needed to change the shape of the mirror is calculated assuming that the time required to correct a given surface area is fixed: there is no feedback nor control. The limited size of the batteries and the power produced by the solar panels are taken into account during the computation.

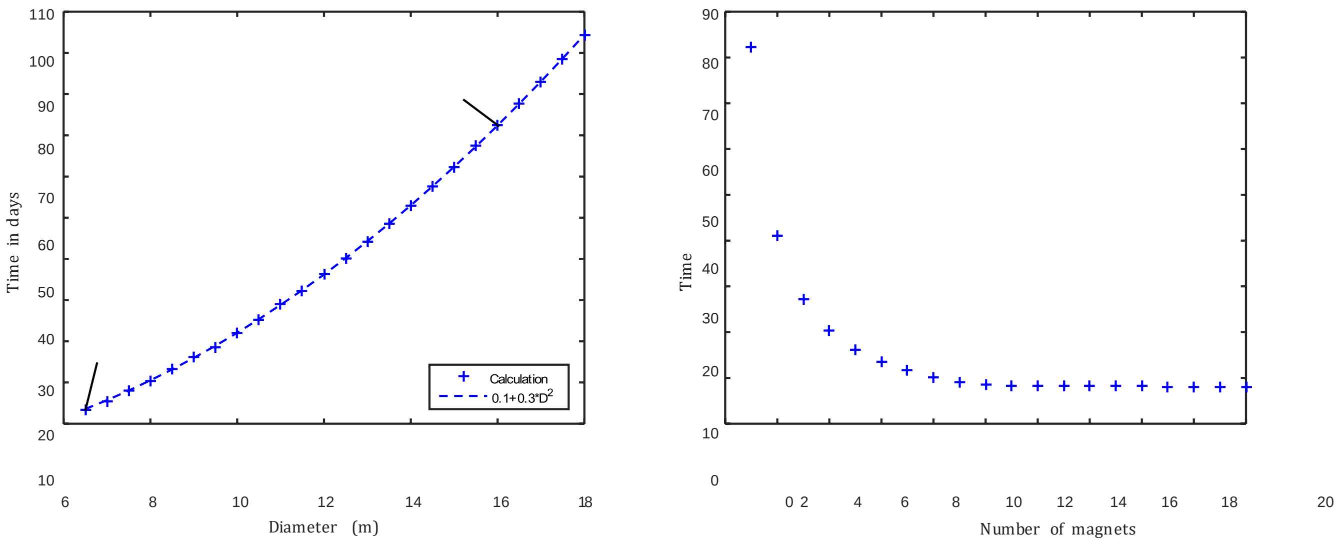

Figure 9. Left: Time spent to correct the entire membrane as a function of the mirror's diameter. Right: Time spent to correct the entire membrane as a function of the number of magnets.

As expected, T_{tot} increases with the diameter of the mirror; more precisely it is a linear function of the diameter squared (Figure 9 left). This parameter has a large impact on the duration of the figure correction process. It is not a free parameter of the design given that the baseline for the APERTURE concept is a 16-m diameter primary mirror, but this analysis shows that the size of the telescope is not only constrained by the rocket fairing but also by the time required to correct a very large mirror. The number of magnets also has a high impact on the time required to correct the primary mirror. However, the curve displays a horizontal asymptote (Figure 9 right). Hence, beyond a certain value, the benefits of adding more magnets, which are a diminution of T_{tot} and of the risk of failure (thanks to redundancy), do not compensate the drawbacks, which are the increased mass and complexity. For the preliminary design, 8 magnetic write heads are used.

Table 4 shows a summary of the study described above, including all the parameters that have been studied. The most driving parameters are: the size of the magnet's battery, the time allocated to each point, the mission lifetime, the number of daily cycles for the main battery, the number of magnets, and the surface of the magnet. Once choosing the diameter of the mirror, one can change those variables to meet the requirement in terms of time spent to correct the shape of the membrane and create an optimal design for APERTURE.

Table 4. Summary of the impact of different parameters over the time required to correct the mirror.

Parameter	Range	Baseline Value	Impact	Horizontal Asymptote
Diameter	6.25 - 18 m	16 m	High	No
Mission lifetime	6 - 15 yrs	10 yrs	Moderate	No
Daily Cycles (magnet)	4 - 40 cycles/day	4 cycles/day	Very low	No
Daily Cycles (main battery)	10 - 40 cycles/day	10 cycles/day	Moderate	Yes
Percentage of the main battery used to charge the magnet's battery	1.72 - 10 %	1.72 %	Moderate	Yes
Size of the magnet's battery	7×10^3 J (digital camera) - 2×10^5 J (laptop)	2×10^2 J	Very high	Yes
Size of the solar arrays	31 m^2 - 37 m^2 (Hubble) - 64 m^2 (Rosetta)	31 m^2	Very low	Yes for large values
Surface of the magnet	1 - 25 cm^2	1 cm^2	High	Yes
Time to treat each location	1 - 5 s	3 s	High	No
Number of magnets	1 - 20	1	High	Yes

5. PRELIMINARY DESIGN

5.1 Magnetic Smart Material and Substrate

There are a wide range of MSMs available. For simplicity we choose the strongest one, Terfenol-D, but Phase II funding would allow us to explore the approach of using a material that has both strong enough magnetostriction and high remanence, such as Vanadium-Permadur. Based on initial deflection studies on glass with an approximate 0.1 T field and a 4 μm Terenol-D film, we will baseline a 4 μm Terenol-D film, and < 1 μm NiCo film or FeCo film to hold in the magnetic field. We remark that preliminary results showing no measurable change over more that 70 hrs in the magnetically induced 2 μm deflection to the center of a 50 μm NiCo 5 cm 5 cm piece coated with a film Terfenol-D lends significant credence to our concept. For a membrane mirror, however, thinner substrates will be used.

The substrate could be as thin as 5 μm made up of a polyimide such as Kapton or CP-1. An alternative approach would be to use some shape memory composite whose front surface could be shiny electro-formed material such as Ni which is known to have a deployed shape good enough for the microwave regime[28] .

5.2 Magnetic Write-Head

The very tentative design would be a horseshoe geometry of soft magnetic material such as iron with a gap separation of 3 mm to 1 cm or even larger. With larger spacing, a stronger current and more windings would be needed, but conversely, the larger (no more than 10*cm*) the size of the "pixels" of the mirror that can be corrected, the better. It is true because a larger pixel size means fewer total pixels that will need correction. If the power requirement becomes too great, the fall back is to use permanent magnets whose gap strength can be controlled mechanically.

5.3 Stowed Configuration and Deployment Mechanism

The primary mirror membrane can be stowed in a Delta IV Heavy rocket fairing using the umbrella design introduced in section 2.2. The preliminary design assumes a focal length equal to the diameter of the primary mirror. The secondary mirror and the inner hole of the primary mirror have a diameter of 4.5 m, which corresponds to the utilization of 92% of the available light-collecting surface area. The height of the stowed membrane is about 8 m while its diameter is 3.9 m. This design exhibits very low local radii of curvature, the minimum being 1 mm. Hence, to avoid any risk of micro-yield, if aluminum is used as the reflective layer, Kapton^{TM} as the substrate and Galfenol as the magnetostrictive material, they have to be less than 8 μm, 7 μm and 9 μm respectively. The deployment of the umbrella membrane will be based on the flexible reflector which uses a memory composite material, leading to a slow and controlled deployment. An alternative design is the self-deployable shell reflector which can be used for reflectors up to 17 m for a Delta IV Heavy rocket fairing, while the umbrella design could be scaled-up. In all cases, the RMS figure accuracy will need to be improved from its deployed value in order to be effective for the UV-Vis wavelength range.

5.4 Post-Deployment Figure Assessment and Feedback

Two designs have been selected from a literature survey. The first design is that being used for JWST[29] which involves determining where a reference star is imaged from each segment in an out of focus image. Then, each segment is adjusted via a tip-tilt and push-pull until each star image is at its proper location. In the second approach, a standard Shack-Hartmann test is used to adjust the figure[30] .

5.5 Operations of the In-Space Shape Correcting System

The estimation of the time required to correct an entire 16-m mirror, with a single magnetic write head, and using the baseline values of Table 4, is about 82 days, but this number can be reduced by adding magnetic write heads and changing the other significant variables. An example of a modified design is proposed in Table 5 and corresponds to a total time of only **3.7 days**.

Table 5. Alternative design, reduced total time

Diameter	16 m
Mission lifetime	10 yrs
Daily cycles (magnet)	11 cycles/day
Daily cycles (main battery)	20 cycles/day
Percentage of the main battery used to charge the magnet	3%
Size of the magnet's battery	2×10^5 J
Size of the solar panels	31 m^2
Surface of the magnet	2 cm^2
Time allocated to each point	3 s
Number of magnets	8
Total time	3.7 days

6. SUMMARY AND CONCLUSION

In summary, space astronomical as well as space Earth observing applications of the future are counting on larger aperture telescopes than are currently available. Several groups have been working on the topic of enabling large (about 16-m diameter) UV-Vis telescopes for many years. The unique feature of the APERTURE concept is that magnetic films are used rather than electrostatic films or piezo-electrostatic pads. The preliminary work that has been described here was a study of the stowing, deployment, and post-deployment shape corrections. The results are very promising. We recognize there are still several unknowns, for brevity, we give just two examples: the initial accuracy of the deployed figure prior to the magnetic write head corrections; and, the length scale over which the corrections need to be applied. However, deployment strategies and the materials available continue to evolve, in particular shape memory composites (SMCs)[28] or alloys (SMAs)[31], such that at this time we see no show-stoppers for this concept. Furthermore, the ability to tune deformations down to much (factors of 10-100) smaller ($\sim\mu$m) scale opens the futuristic possibility of improving the figure well beyond Strehl values of 90%.

7. ACKNOWLEDGMENTS

This work was supported in part by a NASA NIAC grant number NNX15AL89G. We gratefully recognize many of the people who have given us input and support: Dr. G. Pareschi who introduced us to Dr. C. Joshi who introduced us to MSM films and their applications; Drs. X. Wang, Y. Yao, C. Liu who carried out MSM film coatings and the related measurements and modeling of deformation on glass; Drs. C. S. Arnold and D. Pappas for input on magnetic write heads, Dr. S. Padula regarding SMAs, Dr. R. Shiri for information on PZT plus the JWST actuator design, and Drs. Y. Yao and X. Wang for carrying out tests on producing magnetically induced changes in Terfenol-Dn coated NiCo.

REFERENCES

[1] Postman, M., Brown, T., Sembach, K., Giavalisco, M., Traub, W., Stapelfeldt, K., Calzetti, D., Oegerle, W., Michael Rich, R., Phillip Stahl, H., Tumlinson, J., Mountain, M., Soummer, R., and Hyde, T., "Ad- vanced Technology Large-Aperture Space Telescope: science drivers and technology developments," *Optical Engineering* **51**, 011007–011007 (Jan. 2012).

[2] Stahl, H. P., Thronson, H., Langhoff, S., Postman, M., Lester, D., and Lillie, C., "Potential astrophysics science missions enabled by NASA's planned Ares V," in [*UV/Optical/IR Space Telescopes: Innovative Technologies and Concepts IV*], *Society of Photo-Optical Instrumentation Engineers (SPIE) Conference Series* **7436**, 743607 (Aug. 2009).

[3] Lillie, C. F., Polidan, R. S., and Dailey, D. R., "Key enabling technologies for the next generation of space telescopes," in [*Space Telescopes and Instrumentation 2010: Optical, Infrared, and Millimeter Wave*], *Society of Photo-Optical Instrumentation Engineers (SPIE) Conference Series* **7731**, 773102 (July 2010).

[4] "Replicated diffractive optics, moire." http://www.ballaerospace.com/page.jsp?page=259. Accessed: 2015-01-26.

[5] "Three newly designedtracking and data relay satellites to help replenish existing on-orbit fleet," Tech. Rep. FS-2001-9-025-GSFC, NASA Goddard Space Flight Center (2001).

[6] Thomson, M. W., "Astromesh deployable reflectors for Ku-and Ka-band commercial satellites," in [*20th AIAA International Communication Satellite Systems Conference and Exhibit*], (May 2002).

[7] Hill, J. R., Wang, K. W., Fang, H., and Quijano, U., "Actuator grouping optimization on flexible space reflectors," in [*Proceedings of SPIE - The International Society for Optical Engineering*], **7977** (2011).

[8] Enders, J., Kas-Danouche, Liao, W., Rasmussen, B., Vo, T. A., Yokley, K., Robertson, L., and Smith., R., "Design of a membrane aperture deployable structure," in [*44th AIAA/ASME/ASCE/AHS Structures, Structural Dynamics, and Materials Conference*], *AIAA Conf. Proc.* (2003).

[9] Domber, J. and Peterson, L., "Implications of material microyield for gossamer optical reflectors," in [*43rd AIAA/ASME/ASCE/AHS/ASC Structures, Structural Dynamics, and Materials Conference*], American Institute of Aeronautics and Astronautics (AIAA) (apr 2002).

[10] Li, J. H., Gao, X. X., Zhu, J., Bao, X. Q., Xia, T., and Zhang, M. C., "Ductility, texture and large magnetostriction of fe-ga-based sheets," *Scripta Materialia* **63**(2), 246–249 (2010).

[11] Keller, P. N., Lake, M. S., Codell, D., Barrett, R., Taylor, R., and Schultz, M. R., "Development of elastic memory composite stiffeners for a flexible precision reflector," in [*Collection of Technical Papers - AIAA/ASME/ASCE/AHS/ASC Structures, Structural Dynamics and Materials Conference*], **10**, 6984–6994 (2006).

[12] Soykasap, O., Karakaya, S., and Kaplan, E., "Self-deploying composite shell reflector antenna for ku-band missions: 1.5 m diameter demonstrator," in [*RAST 2013 - Proceedings of 6th International Conference on Recent Advances in Space Technologies*], 631–636 (2013).

[13] Soykasap, O., Karakaya, S., Gayretli, A., and Akcin, Y., "Preliminary design of deployable flexible shell reflector of an x-band satellite payload," in [*2nd AIAA Spacecraft Structures Conference*], (2015).

[14] Hearon, K., Singhal, P., Horn, J., Small, W., Olsovsky, C., Maitland, K. C., Wilson, T. S., and Maitland,
D. J., "Porous Shape Memory Polymers," *Polymer reviews (Philadelphia, Pa.)* **53**, 41–75 (02 2013).

[15] Cullity, B. D. and Graham, C. D., [*Introduction to magnetic materials*], John Wiley & Sons, Inc., Hoboken, New Jersey (2009).

[16] Liu, J., Jiang, C., and Xu, H., "Giant magnetostrictive materials," *Science China Technological Sci- ences* **55**(5), 1319–1326 (2012).

[17] Ulmer, M. P., Wang, X., Knapp, P., Cao, J., Cao, Y., Karian, T., Grogans, S., Graham, M. E., Vaynman, S., and Yao, Y., "Comparisons of the deflections of magnetically smart films on alloy of NiCo and glass substrates," in [*Adaptive X-Ray Optics III*], *Society of Photo-Optical Instrumentation Engineers (SPIE) Conference Series* **9208**, 920808 (Sept. 2014).

[18] Wang, X., Knapp, P., Vaynman, S., Graham, M. E., Cao, J., and Ulmer, M. P., "Experimental study and analytical model of deformation of magnetostrictive films as applied to mirrors for x-ray space telescopes," *Appl. Opt.* **53**, 6256–6267 (Sep 2014).

[19] Wang, X., Yao, Y., Cao, J., Vaynman, S., Graham, M. E., Liu, T., and Ulmer, M. P., "Investigation of magnetically smart films applied to correct the surface profile of light weight X-ray optics in two directions," in [*Society of Photo-Optical Instrumentation Engineers (SPIE) Conference Series*], *Society of Photo-Optical Instrumentation Engineers (SPIE) Conference Series* **9603**, 960310 (Sept. 2015).

[20] Olabi, A.R. Grunwald, A., "Design and applications of magnetostrictive materials," *Materials and Design* **29**
(Dec. 2008).

[21] Ng, J. H.-G., Record, P. M., Shang, X., Wlodarczyk, K. L., Hand, D. P., Schiavone, G., Abraham, E., Cummins, G., and Desmulliez, M. P., "Optimised co-electrodeposition of fe???ga alloys for maximum mag- netostriction effect," *Sensors and Actuators A: Physical* **223**, 91 – 96 (2015).

[22] Mishra, R. and Podlaha, E. J., "Coupled Partial Current Density Behavior of Cobalt?Terbium Alloy Code- position," *Journal of The Electrochemical Society* **153** (2006).

[23] Ludwig, A. and Quandt, E., "Giant magnetostrictive thin films for applications in microelectromechanical systems (invited)," *Journal of Applied Physics* **87**, 4691–4695 (May 2000).

[24] Guan, S. and Nelson, B. J., "Magnetic composite electroplating for depositing micromagnets," *Journal of microelectromechanical systems* **15**, 330–337 (Apr. 2006).

[25] Engdahl, L., [*Handbook of giant magnetostrictive materials,*], Academic Press, San Diego (2000).

[26] McCaig, M., [*Permanent magnets in theory and practice / Malcolm McCaig*], Pentech Press London (1977).

[27] Wang, X., *Mechanics of Magnetostrictive Thin Film Deformation and its Application in Active X-Ray Optics*, PhD thesis, Northwestern University (2016). Submitted in 2016.

[28] Varlese, S. J., Ulmer, M. P., Hermiller, J., Young, K., Graham, M., Vaynman, S., and Snyder, B., "Per- formance characterization of a shape memory composite mirror," in [*UV/Optical/IR Space Telescopes: Innovative Technologies and Concepts II*], MacEwen, H. A., ed., *Society of Photo-Optical Instrumentation Engineers (SPIE) Conference Series* **5899**, 331–339 (Aug. 2005).

[29] Knight, J. S., Acton, D. S., Lightsey, P., Contos, A., and Barto, A., "Observatory alignment of the James Webb Space Telescope," in [*Space Telescopes and Instrumentation 2012: Optical, Infrared, and Millimeter Wave*], *Society of Photo-Optical Instrumentation Engineers (SPIE) Conference Series* **8442**, 84422C (Sept. 2012).

[30] Quadrelli, M. B., Wood, L. J., Riedel, J. E., McHenry, M. C., Aung, M., Cangahuala, L. A.,

Volpe, R. A., Beauchamp, P. M., and Cutts, J. A., “Guidance, Navigation, and Control Technology Assessment for Future Planetary Science Missions,” *Journal of Guidance Control Dynamics* **38**, 1165–1186 (July 2015).

[31] Padula, S., Qiu, S., Gaydosh, D., Noebe, R., Bigelow, G., Garg, A., and Vaidyanathan, R., “Effect of Upper-Cycle Temperature on the Load-Biased, Strain-Temperature Response of NiTi,” *Metallurgical and Materials Transactions A* **43**, 4610–4621 (Dec. 2012).